Earthquake Resilient Tall Reinforced Concrete Buildings at Near-Fault Sites Using Base Isolation and Rocking Core Walls

by

Vladimir Calugaru

A dissertation submitted in partial satisfaction of the
requirements for the degree of
Doctor of Philosophy
in
Engineering – Civil and Environmental Engineering
in the
Graduate Division
of the
University of California, Berkeley

Committee in charge:

Professor Marios A. Panagiotou, Chair
Professor Stephen A. Mahin
Professor James Demmel

Fall 2013

Earthquake Resilient Tall Reinforced Concrete Buildings at Near-Fault Sites
Using Base Isolation and Rocking Core Walls

Abstract

Earthquake Resilient Tall Reinforced Concrete Buildings at Near-Fault Sites
Using Base Isolation and Rocking Core Walls

Vladimir Calugaru
Doctor of Philosophy in Engineering – Civil and Environmental Engineering
University of California, Berkeley
Professor Marios A. Panagiotou, Chair

This dissertation pursues three main objectives: (1) to investigate the seismic response of tall reinforced concrete core wall buildings, designed following current building codes, subjected to pulse type near-fault ground motion, with special focus on the relation between the characteristics of the ground motion and the higher-modes of response; (2) to determine the characteristics of a base isolation system that results in nominally elastic response of the superstructure of a tall reinforced concrete core wall building at the maximum considered earthquake level of shaking; and (3) to demonstrate that the seismic performance, cost, and constructability of a base-isolated tall reinforced concrete core wall building can be significantly improved by incorporating a rocking core-wall in the design.

First, this dissertation investigates the seismic response of tall cantilever wall buildings subjected to pulse type ground motion, with special focus on the relation between the characteristics of ground motion and the higher-modes of response. Buildings 10, 20, and 40 stories high were designed such that inelastic deformation was concentrated at a single flexural plastic hinge at their base. Using nonlinear response history analysis, the buildings were subjected to near-fault seismic ground motions as well as simple close-form pulses, which represented distinct pulses within the ground motions. Euler-Bernoulli beam models with lumped mass and lumped plasticity were used to model the buildings. The response of the buildings to the close-form pulses fairly matched that of the near-fault records. Subsequently, a parametric study was conducted for the buildings subjected to three types of close-form pulses with a broad range of periods and amplitudes. The results of the parametric study demonstrate the importance of the ratio of the fundamental period of the structure to the period of the pulse to the excitation of higher modes. The study shows that if the modal response spectrum analysis approach is used—considering the first four modes with a uniform yield reduction factor for all modes and with the square root of sum of squares modal combination rule—it significantly underestimates bending moment and shear force responses. A response spectrum analysis method that uses different yield reduction factors for the first and the higher modes is presented.

Next, this dissertation investigates numerically the seismic response of six seismically base-isolated (BI) 20-story reinforced concrete buildings and compares their response to that of a fixed-base (FB) building with a similar structural system above ground. Located in Berkeley, California, 2 km from the Hayward fault, the buildings are designed with a core wall that provides most of the lateral force resistance above ground. For the BI buildings, the following are investigated: two isolation systems (both implemented below a three-story basement), isolation periods equal to 4, 5, and 6 s, and two levels of flexural strength of the wall. The first isolation system combines tension-resistant friction pendulum bearings and nonlinear fluid viscous dampers (NFVDs); the second combines low-friction tension-resistant cross-linear

bearings, lead-rubber bearings, and NFVDs. The designs of all buildings satisfy ASCE 7-10 requirements, except that one component of horizontal excitation is used in the two-dimensional nonlinear response history analysis. Analysis is performed for a set of ground motions scaled to the design earthquake (DE) and to the maximum considered earthquake (MCE). At both the DE and the MCE, the FB building develops large inelastic deformations and shear forces in the wall and large floor accelerations. At the MCE, four of the BI buildings experience nominally elastic response of the wall, with floor accelerations and shear forces being 0.25 to 0.55 times those experienced by the FB building. The response of the FB and four of the BI buildings to four unscaled historical pulse-like near-fault ground motions is also studied.

Finally, this dissertation investigates the seismic response of four 20-story buildings hypothetically located in the San Francisco Bay Area, 0.5 km from the San Andreas fault. One of the four studied buildings is fixed-base (FB), two are base-isolated (BI), and one uses a combination of base isolation and a rocking core wall (BIRW). Above the ground level, a reinforced concrete core wall provides the majority of the lateral force resistance in all four buildings. The FB and BI buildings satisfy requirements of ASCE 7-10. The BI and BIRW buildings use the same isolation system, which combines tension-resistant friction pendulum bearings and nonlinear fluid viscous dampers. The rocking core-wall includes post-tensioning steel, buckling-restrained devices, and at its base is encased in a steel shell to maximize confinement of the concrete core. The total amount of longitudinal steel in the wall of the BIRW building is 0.71 to 0.87 times that used in the BI buildings. Response history two-dimensional analysis is performed, including the vertical components of excitation, for a set of ground motions scaled to the design earthquake and to the maximum considered earthquake (MCE). While the FB building at MCE level of shaking develops inelastic deformations and shear stresses in the wall that may correspond to irreparable damage, the BI and the BIRW buildings experience nominally elastic response of the wall, with floor accelerations and shear forces which are 0.36 to 0.55 times those experienced by the FB building. The response of the four buildings to two historical and two simulated near-fault ground motions is also studied, demonstrating that the BIRW building has the largest deformation capacity at the onset of structural damage.

This dissertation is dedicated to my parents, who have inspired me to pursue both depth of understanding and breadth of interests in my professional work, as well as in life.

Contents

List of Figures iv
List of Tables viii
Acknowledgements ix
Chapter 1: Introduction 1
1.1 Seismic Design and Performance of Tall Buildings 1
1.2 Objectives of Research 4
1.3 Organization of Dissertation 5
Chapter 1 References 6
Chapter 2: Response of Tall Reinforced Concrete Core-Wall Buildings to Strong Pulse-Type Seismic Excitation 9
2.1 Introduction 9
2.2 Near-Fault Ground Motions and Their Closed-Form Representation 11
2.3 Description and Modeling of Buildings 14
2.4 Design of Buildings 17
2.5 Numerical Analyses Results 19
2.5.1 Modal analysis 19
2.5.2 Building response to near-fault ground motions and their pulse approximations 21
2.5.3 Building response to close-form pulses and comparison of NDRHA and MRSA 23
2.5.4 Effect of Damping Model 33
2.6 A Modified Modal Response Spectrum Analysis Method for RC Cantilever Walls with Base Inelasticity 35
2.7 Summary and Conclusions 37
Chapter 2 References 38
Chapter 3: Seismic Response of 20-Story Base-Isolated and Fixed-Base RC Core Wall Buildings at a Near-Fault Site 41
3.1 Introduction 41
3.2 Site and Ground Motions 44
3.3 Description and Design of Buildings 47
3.3.1 Fixed-base (FB) building 48
3.3.2 Base-isolated (BI) buildings 48
3.4 Numerical Modeling 51
3.5 Results of Numerical Analysis 53
3.5.1 Modal Analysis 53
3.5.2 Response History Analysis using Sets of Motions Scaled to the DE and MCE 53
3.5.3 Effect of Vertical Ground Motion Component Excitation 58

3.5.4 Response History Analysis to Unscaled Near-Fault Pulse-Type Ground Motions 59
3.6 Summary and Conclusions 64
Chapter 3 References 66
Chapter 4: Earthquake Protection of Tall RC Buildings near the San Andreas Fault Using Base Isolation or Combination of Base Isolation and Rocking Core Walls 69
4.1 Introduction 69
4.2 Site and Ground Motions 71
4.3 Description and Design of Buildings 74
4.3.1 Fixed-base (FB) building 74
4.3.2 Base-isolated (BI) buildings 74
4.3.3 Base-isolated and rocking core-wall (BIRW) building 77
4.4 Numerical Modeling 79
4.5 Results of Numerical Analysis 81
4.5.1 Modal Analysis 81
4.5.2 Response History Analysis using Sets of Motions Scaled to the DE and 81
4.5.3 Response History Analysis 87
4.6 Summary and Conclusions 91
Chapter 4 References 93
Chapter 5: Conclusions and Recommendations 95
5.1 Summary and Conclusions 95
5.1.1 Pulse-Type Excitation and Higher Mode Effects 95
5.1.2 Base Isolation of Tall RC Core Wall Buildings 96
5.1.3 Combination of Base Isolation and a Rocking Core Wall 98
5.2 Recommendations for Further Research 100
5.2.1 3-D Modeling and Analysis 100
5.2.2 Experimental Verification of Numerical Analysis 100

List of Figures

Figure 2-1. (a) Acceleration, velocity, and displacement time histories; (b) absolute acceleration; and (c) relative displacement response spectra of the three close-form pulses considered, $\zeta = 2\%$. 12

Figure 2-2. (a) Acceleration; (b) velocity time histories of ground motions considered and their close-form pulse approximation; and (c) elastic SDOF absolute acceleration response spectra of ground motions and their close-form pulse representation. 12

Figure 2-3. Response spectra for the considered ground motions compared to DBE and MCE spectra, based on ASCE-7, at the station locations of the records. 13

Figure 2-4. Floor plan-view of the 10-, 20-, and 40-story buildings. 14

Figure 2-5. (a) Flexural plastic hinge definition; (b) mass distribution of the lumped-mass Euler-Bernoulli cantilevers; (c) idealized moment-curvature hysteretic response. 16

Figure 2-6. Acceleration and displacement design spectra for a site in downtown Pasadena, CA. 17

Figure 2-7. Design bending moment and shear force envelopes based on MRSA. 18

Figure 2-8. Normalized modal characteristics of the buildings. 20

Figure 2-9. Comparison of the NDRHA results using near-fault ground motions and their close-form pulse approximations. Time histories of (a) ground acceleration, (b) mid-height bending moment, (c) base bending moment, (d) base shear force, and (e) roof absolute acceleration. 22

Figure 2-10. Response envelopes of NDRHA, MRSA, and MMRSA using the near-fault ground motions, and of NDRHA using close-form pulse representations. 23

Figure 2-11. Acceleration amplitude a_p of close-form Pulses A, B, and C versus T_1 / T_p computed with MRSA and a uniform R to all modes, resulting in a base bending moment equal to $M_{b,y}$. 24

Figure 2-12. ASCE design basis and maximum considered earthquake and pulse response spectra for the 10-story building. 25

Figure 2-13. ASCE design basis and maximum considered earthquake and pulse response spectra for the 20-story building. 26

Figure 2-14. ASCE design basis and maximum considered earthquake and pulse response spectra for the 40-story building. 26

Figure 2-15. Peak base curvature ductility $\mu_{\varphi,b}$ computed with NDRHA. 27

Figure 2-16. Ratio of peak mid-height bending moments computed with NDRHA and MRSA. 28

Figure 2-17. Ratio of peak base shear forces computed with NDRHA and MRSA. 29

Figure 2-18. Bending moment envelopes for the 20-story building subjected to pulses A, B, and C for four T_1 / T_p ratios computed with (a) MRSA and NDRHA; (b) R = 2; and (c) R = 6. 30

Figure 2-19. Effect of effective flexural rigidity value on the ratio of responses computed with NDRHA and MRSA for the 20-story building and Pulse B. 31

Figure 2-20. Effect of effective flexural rigidity value, on the ratio of peak mid-height to yield base bending moment computed with NDRHA for the 20-story building subjected to Pulse B. 32

Figure 2-21. Peak shear force at 75% of the 20-story building's height computed with NDRHA. 32

Figure 2-22. Caughey and Rayleigh damping comparison for the 20-story building. 33

Figure 2-23. Damping sensitivity study for the 20-story building for pulse B and R = 4. 34

Figure 2-24. Yield reduction factor R_H for higher modes computed based on: (a) mid-height bending moment and (b) base shear force obtained from NDRHA of the 20-story building. 36

Figure 3-1. Mean linear acceleration and displacement response spectra of the FN, FP, principal, normal to principal, and vertical (only *Sa*) components for two sets of ground motions scaled to the MCE; DE, and MCE design spectra. 46

Figure 3-2. (a) Elevation of the 20-story buildings; (b) Floor plan-view above ground; (c) Plan-view of isolation system 1; and (d) Plan-view of isolation system 2. 47

Figure 3-3. (a) Idealization of horizontal force (static) versus horizontal displacement of the two isolation systems; (b) schematic of the numerical model of the BI buildings. 52

Figure 3-4. Mean responses along the building height at DE and MCE hazard level using the principal direction horizontal components of Set 1 and Set 2 ground motions. 57

Figure 3-5. Ground velocity time history of the four near-fault ground motions in the principal horizontal direction. 60

Figure 3-6. Acceleration and displacement linear response spectra for FN, FP, principal, normal to principal, and vertical (*Sa* only) components of the four near-fault historical records compared to the design spectra for the Berkeley, California, site; ζ=5%. 62

Figure 3-7. Response of the FB building and the four BI buildings to the four historical near-fault ground motions. 63

Figure 4-1. Mean linear acceleration and displacement response spectra of the FN, FP, principal, normal to principal, and vertical (only *Sa*) components for two sets of ground motions scaled to the MCE; DE and MCE design spectra. 73

Figure 4-2. (a) elevation view of the FB, BI, and BIRW buildings; (b) plan view of the BIRW building above ground; (c) plan view of isolation system (BI and BIRW); (d) elevation view at deformed state of the bottom part of the BIRW building; (e) Plan

view of the rocking plane of the BIRW building; reinforcement embedded in the section is not show for clarity. 76

Figure 4-3. (a) Idealization of horizontal force (static) versus horizontal displacement of the two isolation systems; (b) Schematic of the numerical model of the BIRW buildings; (c) Schematic detail of isolation and rocking planes, not to scale. 80

Figure 4-4. Mean response envelopes along the height of the buildings at the DE and MCE levels of shaking. 85

Figure 4-5. Ground velocity time history of the four near-fault ground motions in the principal horizontal direction. 88

Figure 4-6. Acceleration and displacement linear response spectra for FN, FP, principal, normal to principal, and vertical (Sa only) components of the two near-fault historical records compared to the design spectra for the Berkeley, California, site; ζ=5%. 89

Figure 4-7. Response of the FB, BI-1, BI-2, and BIRW buildings to two historical and two simulated near-fault ground motions. 90

List of Tables

Table 2-1. Building characteristics. 15

Table 2-2. Main modal characteristics of the buildings. 21

Table 2-3. Caughey and Rayleigh damping comparison. 33

Table 3-1. Ground motions and scale factors at the DE- and MCE-levels of shaking. 45

Table 3-2. Characteristics of the seven buildings. 48

Table 3-3. Modal properties and mean response quantities computed using nonlinear response history analysis (NRHA). 56

Table 3-4. Coefficients of variation of mean responses for the MCE-level of shaking. 58

Table 3-5. Mean response quantities for analysis with and without vertical ground motions components scaled at the MCE-level. 58

Table 3-6. Available near-fault records with R_{rup}<10 km for earthquakes with $M \geq 7.0$. 59

Table 3-7. Characteristics of the four near-fault ground motions used. 60

Table 4-1. Ground motions and scale factors at the DE- and MCE-levels of shaking. 72

Table 4-2. Characteristics of the four studied buildings. 75

Table 4-3 Mean response quantities computed using nonlinear response history analysis (NRHA). 84

Table 4-4 Coefficients of variation and mean plus one standard deviation responses for the MCE-level of shaking. 86

Table 4-5. Characteristics of the four near-fault ground motions used. 87

Acknowledgements

First and foremost, I would like to express gratitude to my research advisor, Professor Marios A. Panagiotou. This dissertation would not be possible without his encouragement, technical guidance, and a comprehensive vision of the research direction, particularly at times when it was easy to lose focus, while dealing with numerical issues with the building models or going through yet another set of building design iterations.

I am greatly thankful to Professor Stephen A. Mahin, a member of the dissertation committee, for his guidance during our collaboration on an extensive shaking table experimental program, studying seismic isolation of liquid storage tanks, a project that formed my M.S. Thesis four years ago. It was the success of that research project that lead to my decision to pursue a Ph.D. degree.

I appreciate the participation of Professor James Demmel as a member of the dissertation committee and as a phenomenal instructor and researcher in numerical linear algebra, a subject that became the foundation for the numerical analysis necessary to complete this dissertation.

Keeping the best for last, I cannot overstate the importance of the inspiration and support from my parents, Margarita Bulgakova and Serguei Calugaru, and my wife, Catherine, to the completion of this dissertation.

Chapter 1: Introduction

1.1 Seismic Design and Performance of Tall Buildings

Construction of buildings exceeding 50 m in height, referred herein as "tall" buildings, is increasing in earthquake-prone regions of the U.S. and worldwide. Common structural systems used in the seismic design of these buildings are reinforced concrete (RC) structural walls (for brevity referred to herein as "walls"), including non-planar core walls [1].

Considerable damage of tall RC wall buildings in past earthquakes has been reported, including the 1985 magnitude 8 (M8.0) Mexico earthquake [2], the 2010 M8.8 Chile earthquake [3], and the 2011 M6.3 Christchurch, New Zealand, earthquake [4]. These buildings were not designed according to the provisions considered here. In the 1999 M7.6 Chi-Chi, Taiwan, earthquake [5], tall RC frame buildings—the most common type of RC tall buildings close to the fault rupture (less than 10 km)—suffered severe damage or collapsed. In the Mexico and Chile subduction-zone earthquakes severe damage and collapse of tall RC wall buildings occurred far from the fault rupture, 400 km [6] and 35 km [7], respectively, due partly to amplification of the long-period content of the ground motions at soft-soil sites. Following the 2011 M6.3 Christchurch, New Zealand, earthquake out of the 50 tallest buildings taller than 35 m, 36 have been demolished or slated for demolition, 4 severely damaged with their fate still undecided at the time of this publication, and only 10 have reopened to occupants, most after 2 or more years of repair work [8]. Out of the 40 buildings demolished, slated for demolition, or severely damaged, 7 were built after year 2000.

Conventional tall RC wall buildings in the U.S. are designed to develop the majority of expected deformations in a single flexural plastic hinge, usually located near ground level [1, 9–12]. Design forces are typically calculated using the code-prescribed design earthquake (DE) spectra with modal response spectrum analysis (MRSA) as prescribed in ASCE 7-10 [13], using a response modification factor, R, equal to 5; RC structural members are designed according to ACI 318-11 code provisions [14].

Research on RC cantilever wall buildings has shown that flexural yielding at the base reduces mainly the first-mode response [11, 15–20]; therefore, the relative contribution of the higher modes to response quantities increases with increasing ground motion intensity. Using MRSA, results in non-conservative estimates of seismic demand in nonlinear cantilever walls.

A simplified modal superposition method proposed by Eibl [15] considers only the first two modes of response, with a response modification factor applied only at the first mode, i.e., the second mode of response is considered elastic. For the case of near-fault ground motions, Panagiotou and Restrepo [17] proposed a method that considers only the first two modes of response with different response modification factors in each of them. Researchers demonstrated that applying MRSA using the SRSS combination method—where the higher modes are considered to be elastic—provide a satisfactory estimate of acceleration [20] and force [18, 19] response parameters. There are no published studies investigating the use of different yield reduction factors in more than 2 modes of response.

Although previous research has investigated the effects of near-fault ground motions on the inelastic response of wall buildings [11, 17, 21], none of these studies focusing on RC walls have investigated this effect for a broad range of pulse waveform, period, and amplitude. This type of ground motions can cause significant inelastic deformation demands with concurrent strong excitation of the higher than the first modes of response. Furthermore, the said studies did not investigate this effect on a broad range of inelastic response quantities, i.e. section curvatures, floor accelerations, story shear forces, and story bending moments.

Numerical studies have investigated the seismic response to DE, MCE, and higher levels of shaking of 40- to 42-story tall RC core wall buildings both located hypothetically in downtown Los Angeles, California with S_{D1} = 0.73 g [1, 9, 10]. There are no published studies on the seismic response of a tall RC wall building located at less than 5 km from the San Andreas fault or the Hayward fault.

Seismic base isolation has been used as a design strategy for tall buildings to reduce accelerations, forces, and inelastic deformations in the superstructure (structure above the isolation system) and thus earthquake-induced structural and non-structural damage. This is achieved by concentrating the majority of deformations in robust isolation systems and by reducing higher mode response. A variety of seismic isolation devices are now available that have the force and displacement capacities required to seismically isolate tall buildings. These devices include large (1.5 m-diameter) rubber bearings [22], large friction pendulum bearings [23], and large cross-linear bearings [24]. Friction pendulum bearings and cross-linear bearings with strength in tension up to 9 MN are also available [23–25]. Rubber bearings, linear bearings, friction pendulums, and fluid viscous dampers with more than 1 m horizontal displacement capacity are available and have been experimentally tested [22–29].

Japan is the leading proponent of using seismic isolation technology in tall buildings [30, 31]. Between 1990 and 2002, one-third of all the approved base-isolated (BI) buildings in Japan were taller than 40 m, and 40% of all BI buildings built in Japan after 1995 had a height-to-length ratio larger than two [30]. In the U.S., ASCE 7-10 permits the design of the structure above the isolation system of BI buildings for forces smaller than that required for elastic response at the DE; the isolation system is required to have force and displacement capacity larger than the expected demand at the MCE. Numerical studies have investigated the response of BI RC or steel frames using two degree-of-freedom (2DOF) models [32], or modeling 6 stories [33], 9 stories [34], 15 [35], 20 [36], 18 or 40 stories [28] of the superstructure. These studies show that the level of inelastic response of the superstructure depends on both the relative characteristics of the superstructure and isolation system, and ground motion characteristics. Oakland City Hall [37] is the only currently available study of the seismic response of a tall BI building with structural walls designed to resist most of the seismic forces along a part of the building height.

Another strategy to reduce post-earthquake damage due to plastic hinging in tall RC wall buildings, which have been presented in literature, is to use rocking walls without [38], or with unbonded steel and post-tensioning tendons [39]. The latter study proposed a design including multiple rocking planes along the height of a wall to reduce the contribution of second and higher modes of response. There has been no experimental study on rocking RC core (non-planar) walls. The behavior or rocking structures using un-bonded reinforcement and post-tensioning strands or bars has been studied numerically and experimentally extensively for low- and medium-rise structures [40–46], including designs where energy dissipation devices are externally attached to the RC rocking walls [44, 45]. The combination of base isolation and rocking has been investigated numerically for a rigid block subjected to

pulse-type ground excitations [47]. The present study is the first to consider the combination of base isolation and a rocking core-wall for a tall building.

1.2 Objectives of Research

The main objectives of this dissertation are to:

1) Investigate the seismic response of tall RC core wall buildings subjected to pulse type near-fault ground motion, with special focus on the relation between the characteristics of the ground motion and the higher-modes of response.
2) Determine the characteristics of a base isolation system that results in nominally elastic response of the superstructure of a tall RC core wall building at the maximum considered earthquake level of shaking.
3) Demonstrate that the seismic performance, cost, and constructability of a base-isolated tall RC building can be significantly improved by incorporating a rocking core-wall in the design.

While reaching these objectives, the following questions are addressed in this dissertation:

1) What is the accuracy of simplified close-form representations of pulse-type near-fault ground motions in computing the inelastic response.
2) How accurate is modal response spectrum analysis, as prescribed in current building codes, in predicting inelastic response of tall reinforced concrete buildings.
3) How efficient is the modification to the modal response spectrum analysis that uses different yield reduction factors in the first and higher-modes.
4) What is the level of response (and possible damage of the structural and non-structural components) of a fixed-base building designed according to ASCE 7-10 at the design earthquake and maximum considered earthquake levels of shaking.
5) What are the characteristics of the base-isolated designs that result in nominally elastic response of the superstructure at the MCE level of shaking.
6) For these base-isolated designs, what is the level of reduction of floor accelerations and interstory drifts compared to that of the FB building.
7) What is the relation between the flexural strength of the isolated superstructure, the characteristics of the isolation system, and the level of inelastic deformations the isolated superstructure develops at the DE and MCE.
8) What is the effect of the vertical component of the ground motion excitation.
9) What is the level of the response of the FB and BI buildings when subjected to four unscaled historical ground motion records with the largest linear spectral demands for periods longer than 5 s among all the historical records available.
10) How does a 20-story fixed-base building designed according to ASCE 7-10 at a site 0.5 km from the San Andreas fault perform at the DE and MCE levels of excitation.
11) What are the base-isolation designs that can result in nominally elastic response of the superstructure at the MCE level of shaking, and what is the level of reduction of shear forces and floor accelerations compared to those of the FB building.
12) How and to what extent, can the performance, cost, and constructability of a base-isolated building be improved by incorporating a rocking core-wall in the design.

1.3 Organization of Dissertation

This dissertation is organized into five chapters. Chapter 2 presents a numerical investigation of the seismic response of tall fixed-base core wall buildings of 10-, 20-, and 40-story height subjected to pulse type ground motion, with special focus on the relation between the characteristics of ground motion and the higher-modes of response. The importance of the ratio of the fundamental period of the structure to the period of the pulse to the excitation of higher modes is demonstrated. Significant underestimation of bending moment and shear force response is identified for modal response spectrum analysis with a uniform yield reduction factor for all modes. A response spectrum analysis method that uses different yield reduction factors for the first and the higher modes is presented.

Chapter 3 presents a numerical investigation of the seismic response of six base-isolated 20-story reinforced concrete buildings (varying in type of isolation system, isolation period, and level of flexural strength of the wall) and compares their response to that of a fixed-base building with a similar structural system above ground. The response of the fixed-base building and four of the base-isolated buildings to four unscaled historical pulse-like near-fault ground is also studied.

Chapter 4 introduces a design of a 20-story building that combines base isolation and a rocking core wall and numerically compares its seismic performance to a fixed-base building and two base-isolated buildings. Mean structural response to sets of ground motions scaled to design earthquake and maximum considered earthquake levels is presented. Chapter 4 also discusses the response of the four buildings to two historical and two simulated near-fault ground motions, demonstrating that the base-isolated and rocking core wall building has the largest deformation capacity at the onset of structural damage.

Chapter 5 summarizes the main results and conclusions of this dissertation and presents a list of possible directions for further research. A separate list of references for Chapters 1, 2, 3, and 4 immediately follows each of these chapters.

Chapter 1 References

1. Klemencic R, Fry A, Hooper JD, Morgen BG. Performance-based design of ductile concrete core wall buildings – issues to consider before detailed analysis. *Structural Design of Tall and Special Buildings* 2007; **16**:599–614.
2. Aguilar J, et al. The Mexico earthquake of September 19, 1985 – statistics of damage and of retrofitting techniques in reinforced concrete buildings affected by the 1985 earthquake. *Earthquake Spectra* 1989; **5**(1):145-151.
3. Westenenk B, et al. Response of reinforced concrete buildings in Concepcion during the Maule earthquake. *Earthquake Spectra* 2012; **28**(S1):S257-S280.
4. Elwood, K. J., Pampanin, S., and Kam, W.Y., 2012. NZ 22 February 2011 Christchurch Earthquake and Implications for the Design of Concrete Structures, in *Proceedings, International Symposium on Engineering Lessons Learned from the 2011 Great East Japan Earthquake,* Tokyo, Japan, pp.1157-1158.
5. Tsai KC, Hsiao CP, Bruneau M. Overview of building damages in 921 Chi-Chi earthquake. *Earth. Engineering and Engineering Seismology* 2000; **2**(1):93–108.
6. Seed HB, Romo MP, Sun JI, Jaime A, Lysmer J. The Mexico earthquake of September 19, 1985 – relationships between soil conditions and earthquake ground motions. *Earthquake Spectra* 1988; **4**(4):687-729.
7. Boroschek RL, Contreras V, Kwak DY, Stewart JP. Strong ground motion attributes of the 2010 Mw 8.8 Maule, Chile, earthquake. *Earthquake Spectra* 2012; **28**(S1):S19-S38.
8. List of tallest buildings in Christchurch. http://en.wikipedia.org/wiki/List_of_tallest_ buildings_in_Christchurch [accessed September 2013].
9. Moehle J, Bozorgnia Y, et al. Case studies of the seismic performance of tall buildings designed by alternative means. Task 12 Report for the Tall Buildings Initiative. *PEER Report 2011/05*, University of California, Berkeley, CA, 2011.
10. Yang TY, Moehle JP, Bozorgnia Y, Zareian F, Wallace JW. Performance assessment of tall concrete core-wall building designed using two alternative approaches. *Earthquake Engineering and Structural Dynamics* 2012; **41**(11):1515–1531
11. Panagiotou M, Restrepo JI. Dual-plastic hinge design concept for reducing higher-mode effects on high-rise cantilever wall buildings. *Earthquake Engineering and Structural Dynamics* 2009; **38**(12):1359–1380.
12. Calugaru V, Panagiotou M. Response of tall cantilever wall buildings to strong pulse-type seismic excitation. *Earthquake Engineering and Structural Dynamics* 2012; 41(9):1301-1318.
13. American Society of Civil Engineers. *Minimum Design Loads for Buildings and Other Structures*. ASCE 7-10, Reston, VA, 2010.
14. American Concrete Institute. *Building Code Requirements for Structural Concrete (ACI 318-11) and Commentary*. ACI 318-11, ACI Committee 318, Farmington Hills, 2011.
15. Eibl J, Keintzel F. Seismic shear forces in RC cantilever shear walls. *Proceedings, 9th World Conference on Earthquake Engineering*, Tokyo/Kyoto, Japan 1988, Report 9-1-1.
16. Panagiotou, M., Restrepo, J.I., and Conte J.P. Shake Table Test of a 7-Story Full Scale Reinforced Concrete Wall Building Slice, Phase I: Rectangular Wall. *ASCE Journal of Structural Engineering*, Vol. 137, No. 6, 2011.
17. Panagiotou M. Seismic design, testing, and analysis of reinforced concrete wall buildings. Ph.D. Dissertation, University of California, San Diego, 2008.
18. Priestley MJN, Calvi GM, Kowalsky MJ. *Displacement Based Seismic Design of Structures*. IUSS Press, Pavia, Italy. 2007.
19. Sullivan TJ, Priestley MJN, Calvi GM, Estimating the Higher-Mode Response of Ductile Structures. *Journal of Earthquake Engineering,* 2008; 12(4):456-472.

20. Rodríguez ME, Restrepo JI, Carr AJ. Earthquake-induced floor horizontal accelerations in buildings. *Earthquake Engineering and Structural Dynamics* 2002; 31:693-718.
21. Panagiotou M, Calugaru V, Visnjic T. Higher mode effects on the seismic response of tall cantilever wall buildings subjected to near fault ground motions. *Proceedings, Structural Engineers Association of California Convention*, San Diego, CA 2009; 345–357.
22. Dynamic Isolation Systems (DIS). http://www.dis-inc.com/index.html [accessed June 2013].
23. Earthquake Protection Systems. http://www.earthquakeprotection.com/ [accessed June 2013].
24. THK. http://www.thk.com/?q=eng/node/260 [accessed June 2013].
25. Roussis PC, Constantinou MC. Experimental and analytical studies of structures seismically isolated with an uplift-restraining friction pendulum system. *Earthquake Engineering and Structural Dynamics*, 2006; **35**(5):595–611.
26. Taylor Devices Inc. http://www.taylordevices.com/dampers-seismic-protection.html [accessed September 2012].
27. Fujita T. Seismic isolation rubber bearings for nuclear facilities. *Nuclear Engineering Design*, 1991; **127**:379-391.
28. Komuro T, Nishikawa Y, Kimura Y, Isshiki Y. Development and realization of base isolation system for high-rise buildings. *Journal of Advanced Concrete Technology,* 2005; **3**(2):233–239.
29. Ryan KL, Dao ND, Sato E, Sasaki T, Okazaki T. Aspects of isolation device behavior observed from full-scale testing of an isolated building at E-Defense. *Proceedings, 20th Analysis & Computation Specialty Conference*, 2012; p. 25-36.
30. Pan P, Zamfirescu D, Nakashima M, Nakayasu N, Kashiwa H. Base-isolation design practice in Japan: introduction to the post-Kobe approach. *Journal of Earthquake Engineering*, 2005*;* **9**(1):147–171.
31. Kani N. Current state of seismic-isolation design. *Journal of Disaster Research*, 2009*;* **4**(3):175–181.
32. Sayani PJ, Ryan KL. Comparative evaluation of base-isolated and fixed-base buildings using a comprehensive response index. *ASCE Journal of Structural Engineering*, 2009; **135**(6):2952-2968.
33. Hall JF, Ryan KL, Isolated buildings and the 1997 UBC Near-Source Factors, *Earthquake Spectra*, 2000; **16**(2):393-411.
34. Morgan TA, Mahin SA. The use of base isolation systems to achieve complex seismic performance objectives. *Pacific Earthquake Engineering Research Center*, PEER Report 2011/06.
35. Kikuchi M, Black CJ, Aiken ID. On the response of yielding seismically isolated structures. *Earthquake Engineering and Structural Dynamics*, 2008; **37**(5):659-679.
36. Calugaru V, Panagiotou M. Seismic responses of 20-story base-isolated and fixed-base RC structural wall buildings at a near-fault site. *Earthquake Engineering and Structural Dynamics*, 2013, in review.
37. Walters M. The seismic retrofit of the Oakland City Hall. *Proceedings, SMIP03 Seminar on Utilization of Strong-Motion Data,* 2003*;* p. 149-163.
38. Nielsen GM. Performance of rocking core walls in tall buildings subjected to severe seismic demands. *Master's Thesis*, University of California, Berkeley, CA, 2009.
39. Wiebe L, Christopoulos C. Mitigation of higher mode effects in base-rocking systems by using multiple rocking sections. *Journal of Earthquake Engineering* 2009; **13**(1):83–108.
40. Kurama Y, Sause R, Pessiki S, Lu LW. Lateral load behavior and seismic design of unbonded post-tensioned precast concrete walls. *American Concrete Institute, ACI Structural Journal* 1999; **96**:622-632.

41. Nakaki SD, Stanton JF, Sritharan S. An overview of the PRESSS five-story precast test building. *PCI Journal* 1999; **44**:26-39.
42. Seo C, Sause R. Ductility demands of self-centering systems under earthquake loading. *American Concrete Institute, ACI Structural Journal* 2005; **102**(2):275-285.
43. Restrepo JI, Rahman A. Seismic performance of self-centering structural walls incorporating energy dissipators. *Journal of Structural Engineering* 2007; **11**:1560-1570.
44. Marriott DJ, Pampanin S, Bull DK, Palermo A. Dynamic testing of precast, post-tensioned rocking wall systems with alternative dissipating solutions. *Bulletin of the New Zealand Society of Earthquake Engineering* 2008; **41**(2):90-102.
45. Marriot DJ, Pampanin S, Palermo A, Bull DK. Shake-table testing of hybrid post-tensioned precast wall systems with alternative dissipating solutions. *Proceedings of the 14th World Conference on Earthquake Engineering, Beijing, China,* 2008.
46. Kurama Y, Qiang S. Seismic design and response evaluation of unbonded post-tensioned hybrid coupled wall structures. *Earthquake Engineering and Structural Dynamics* 2008; **37**(14):1677-1702.
47. Vassiliou MF, Makris N. Analysis of the rocking response of rigid blocks standing free on a seismically isolated base. *Earthquake Engineering and Structural Dynamics* 2011; **41**(2):177-196.

.

Chapter 2: Response of Tall Reinforced Concrete Core-Wall Buildings to Strong Pulse-Type Seismic Excitation

2.1 Introduction

The inelastic response of tall reinforced concrete wall buildings is greatly affected by higher-mode effects. This phenomenon was first demonstrated by the pioneering analytical work of Blakeley *et al.* [1] and has been corroborated by various analytical [2–8], small-scale [9] experimental, and large-scale [10, 11] experimental studies. The higher modes significantly affect the acceleration, force, and displacement inelastic seismic response of reinforced concrete wall buildings.

Seismic design of buildings for a code-prescribed design level earthquake recommends using reduced design lateral forces as opposed to the elastic ones, accepting the possibility of nonlinear deformations occurring in parts of the structural system. Current design procedures include methods consistent with traditional capacity design concepts [12], where parts of a structure are intended to remain elastic, and nonlinear deformations are restricted to regions defined as plastic hinges. Building codes [13] include prescriptive requirements to ensure the withstanding of deformation demands in plastic hinge regions. In reinforced concrete (RC) wall buildings, a single plastic hinge is selected to develop at the base of walls in vertically regular buildings [4, 10, 13–18]. Capacity design of wall regions other than the plastic hinges, assuming an essentially elastic response, requires estimating the bending moment and shear force demands.

To ensure elastic response in regions other than the plastic hinges, several seismic design codes [15–17] account for higher-mode effects by proposing a design bending moment envelope that varies linearly from the expected flexural over-strength at the wall base to zero at the top. Studies have found that such a linear envelope does not always preclude the spread of plasticity into regions above the bottom plastic hinge [7, 18–21]. For the shear design envelope, the NZS 3101 code [16] uses an empirical factor that accounts for flexural over-strength and higher-mode response by amplifying the first mode design shear forces. The EC8 [15] proposes that design shear forces be taken at least 50% larger than the shear forces obtained from analysis, with the design shear force at any point along the height of the building to be taken as larger than 50% of the amplified base shear force. According to EC8, the magnification factor of shear forces can be as large as the behavior factor, q, used in the design.

The design force envelopes in tall RC wall buildings are commonly estimated by modal response spectrum analysis (MRSA), using an accepted modal combination method such as the square root of sum of squares (SRSS). Elastic forces obtained from the modal combination are reduced by a response modification factor, R, to obtain the design forces. Performing MRSA using SRSS and an R, uniform to all the modes, will be termed MRSA throughout this dissertation.

Research on RC cantilever wall buildings has shown that flexural yielding at the base reduces mainly the first-mode response [3, 10, 11, 19–22]; therefore, the relative contribution of the higher modes to response quantities increases with increasing ground motion intensity. Using MRSA, results in non-conservative estimates of seismic demand in nonlinear cantilever walls. For frame structures it has been also shown that nonlinear response reduces more the first than the higher modes of response [23, 24].

A simplified modal superposition method proposed by Eibl [3] considers only the first two modes of response, with a response modification factor applied only at the first mode, i.e., the second mode of response is considered elastic. For the case of near-fault ground motions, Panagiotou and Restrepo [11] proposed a method that considers only the first two modes of response with different response modification factors in each of them. Researchers demonstrated that applying MRSA using the SRSS combination method—where the higher modes are considered to be elastic—provide a satisfactory estimate of acceleration [22] and force [19, 21] response parameters. Chopra and Goel [24] proposed a similar approach for frames, which was evaluated in terms of story drifts, not forces.

Although previous research has investigated the effects of near-fault ground motions on the inelastic response of steel frame [25–31], RC frame [32, 33], and wall [11, 20, 34] buildings, none of these studies focusing on RC walls have investigated this effect for a broad range of pulse waveform, period, and amplitude. This type of ground motions can cause significant inelastic deformation demands with concurrent strong excitation of the higher than the first modes of response. Nor have these studies investigated this effect on a broad range of inelastic response quantities, i.e. section curvatures, floor accelerations, story shear forces, and story bending moments.

This study investigates the inelastic response of tall reinforced concrete cantilever wall buildings subjected to strong pulse-type ground motion. Emphasis is given to the relationship between the ground motion characteristics and higher-mode response. The study explores the accuracy of simplified close-form representations of pulse-type near-fault ground motions to compute the inelastic response. The response parameters considered are base section curvature, floor accelerations, bending moments, and shear forces. Three types of close-form pulses with a broad range of periods and amplitudes are considered. In order to evaluate the efficiency of MRSA, this study compared the response obtained using MRSA and nonlinear dynamic response history analysis (NDRHA). This study then goes on to develop a modified modal response spectrum analysis (MMRSA) approach that considers only the first three modes of response using different yield reduction factors in the first and higher-modes.

2.2 Near-Fault Ground Motions and Their Closed-Form Representation

Near-fault ground motion records may contain high amplitude acceleration, velocity, and displacement pulses [35]. High amplitude low frequency pulses are contained in far field ground motions affected mostly by site effects. The waveform, number of cycles, predominant period, and amplitude of the pulses determine the motion's damage potential for different structures [20, 25-34, 36–42]. For near fault ground motions these pulse characteristics depend roughly on the fault type and orientation, as well as the direction of rupture propagation [35].

Several approaches use close-form mathematical pulses or waveforms [37–44] that approximate the distinct pulses observed in the displacement, velocity, and acceleration time histories of strong near-fault ground motions. Such approximations capture many of the characteristics of the corresponding ground motions and allow for parametric numerical studies of structures where the relationship between the structural period and the pulse period can be explored.

This study reported herein uses the close-form representation of near-fault ground motions as described by Makris [38]. Figure 2-1(a) shows the displacement, velocity, and acceleration histories of three close-form pulses. Pulses A and B are described by a one-sine and one-cosine acceleration time history, respectively. Pulses A and B have a duration equal to their period, T_p, while the duration of Pulse C is equal to $1.43T_p$. Figure 2-1(b) and (c) depict the elastic single degree of freedom (SDOF) oscillator acceleration and displacement response spectra, respectively, of the pulses for viscous damping ratio ζ = 2%. The spectra are presented in terms of T / T_p, where T is the period of the oscillator. Spectral acceleration S_a is normalized by the peak pulse acceleration amplitude, a_p, while the spectral relative displacement S_d is normalized by $a_p \cdot T_p^2$.

Figure 2-2(a) depicts the ground acceleration time histories of three strong near-fault ground motions. The RRS228 and JFA292 records are from the Mw 6.7 1994 Northridge earthquake, and the PCD164 record is from the Mw 6.6 1971 San Fernando earthquake. Figure 2-2(b) shows the velocity time histories of the ground motions, and Figure 2-2(c) plots the absolute acceleration response spectra for ζ = 2%. Pulses A, B, and C approximate distinct pulses observed in the time histories of the RRS228, JFA292, and PCD164 records, respectively. The pulse parameters were selected to provide a fit of the strong pulses recorded in the velocity time histories. The velocity pulse amplitudes, v_p, used to represent the RRS228, JFA292, and PCD164 records are 1.66, 0.73, and 0.82 m/sec, respectively, while the corresponding values of T_p are equal to 0.78, 0.99, and 1.24 sec. For the JFA292 record, pulse B was used to approximate only the first of the two distinct pulses contained in the velocity record.

Figure 2-2(c) depicts the elastic acceleration response spectra of the close-form pulses. For the RRS228 record, the pulse approximation resulted in a fair estimation of the spectral acceleration. Underestimation of the spectral acceleration is observed for T smaller than 1.6 sec. For the JFA292 record, the pulse approximation did not adequately estimate spectral accelerations, especially in the period range between T = 1 to 2.5 sec. This is due to the lack of representation of the second distinct pulse observed in the velocity and acceleration time histories of the JFA292 record. For the PCD164 record, the close-form pulse estimated spectral accelerations with high accuracy for cases where T was longer than 0.8 sec and shorter than 4.0 sec. Pulse C in this case could not estimate spectral accelerations when T was less than 0.8 sec. This is because the spectral acceleration in this period range was due to the strong high-frequency spikes observed in the time, t, history after t = 4 sec.

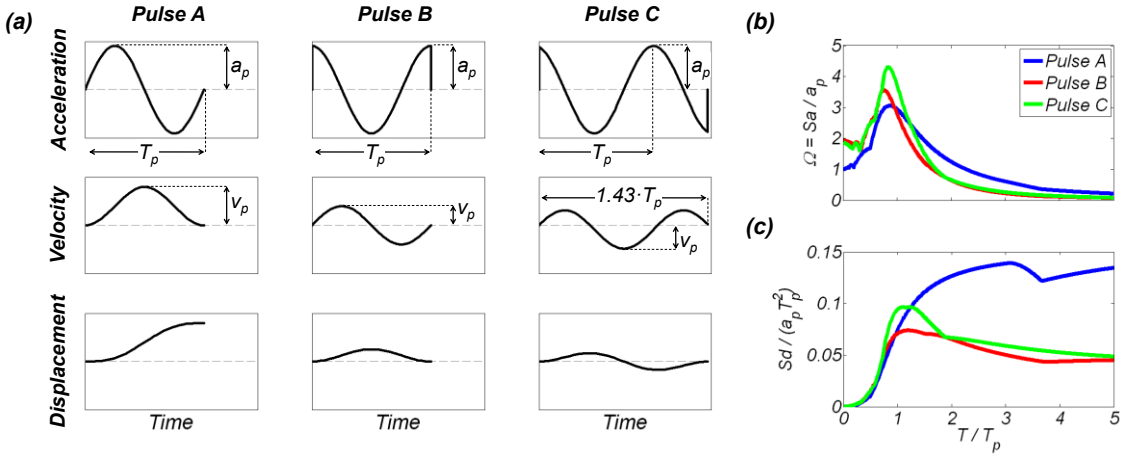

Figure 2-1. (a) Acceleration, velocity, and displacement time histories; (b) absolute acceleration; and (c) relative displacement response spectra of the three close-form pulses considered, $\zeta = 2\%$.

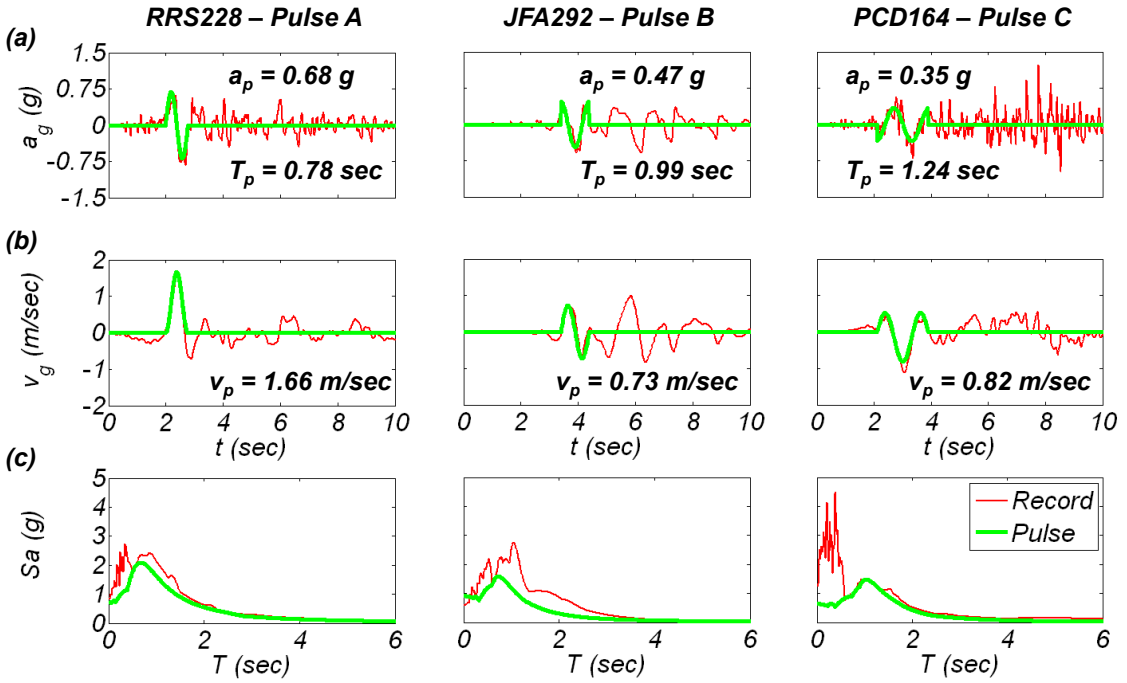

Figure 2-2. (a) Acceleration; (b) velocity time histories of ground motions considered and their close-form pulse approximation; and (c) elastic SDOF absolute acceleration response spectra of ground motions and their close-form pulse representation, $\zeta = 2\%$.

Figure 2-3 compares the response spectra for the considered RRS228, JFA292 and PCD164 recorded ground motions to the design base earthquake (DBE) and maximum considered earthquake (MCE) spectra, based on ASCE-7 [14], for the corresponding station locations, where the motions were recorded. For all the three ground motions considered the spectral accelerations around the predominant period, T_p, as defined above, significantly exceed the spectral accelerations of the MCE spectra. For the JFA292 this is true in the period range of the second distinct velocity pulse with T_p of about 1.58 sec that exists in this record and is not approximated in this study. The spectral accelerations at T_p are 1.76, 1.63, and 1.60 times the MCE spectral acceleration for the RRS228, JFA292 and PCD164 records, respectively.

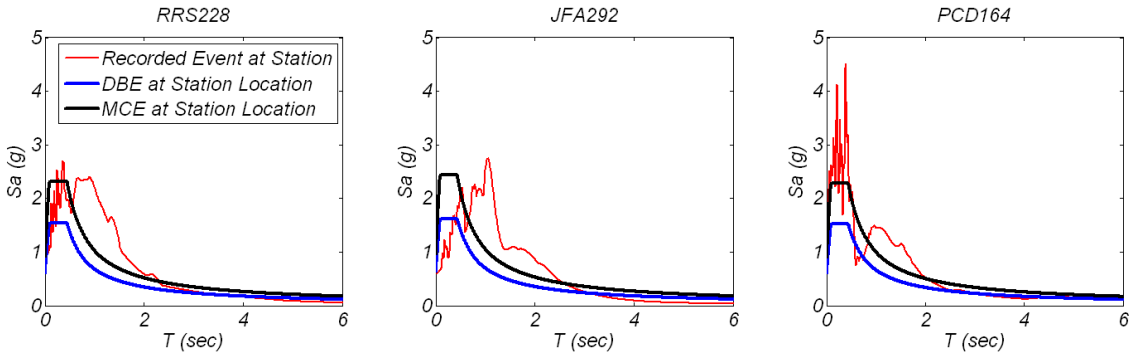

Figure 2-3. Response spectra for the considered ground motions compared to DBE and MCE spectra, based on ASCE-7, at the station locations of the records.

2.3 Description and Modeling of Buildings

Reinforced concrete core-walls provide all the lateral force resistance for these buildings. Figure 2-4 shows the floor, core wall, and gravity column dimensions and layout for the three buildings. Table 2-1 lists the main characteristics of these buildings, including the floor height h, the building height H, the seismic weight per floor w, the axial load per floor ΔP_W and ΔP_C acting on the wall and the gravity columns, respectively, as well as the main characteristics of the core-wall and gravity columns. P_{bw} and P_{bc} are the axial loads at the base of the core walls and gravity columns with the highest axial load, respectively. The nominal compressive strength of concrete is $f_c^{'}$ = 41.4 MPa for the 10-story building, and $f_c^{'}$ = 55.2 MPa for the 20- and 40-story buildings.

The buildings are designed to allow the formation of a single flexural plastic hinge extending over the bottom 10% of the building height; see Figure 2-5(a). The design of the buildings based on ASCE-7 [14] is discussed in the Section 2.3.2. The reinforcing steel ratio in the plastic hinge region $\rho_{l,b}$ is equal to 1.27%, 1.32%, and 0.81% for the 10-, 20-, and 40-story buildings, respectively. The remaining portion of the wall is considered essentially elastic, assuming adequate amount of longitudinal reinforcement is provided. Expected flexural strengths, $M_{b,y}$, and the corresponding yield curvatures, φ_y, were calculated by moment-curvature analysis using the provided reinforcement and axial loads; see Table 2-1. The total seismic weight of the building is W_t.

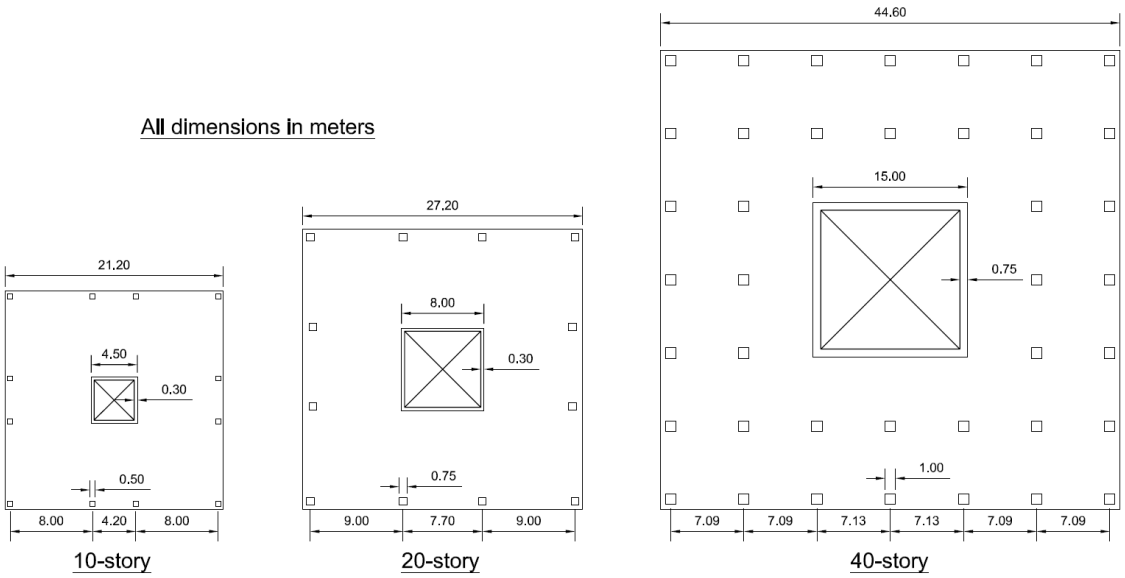

Figure 2-4. Floor plan-view of the 10-, 20-, and 40-story buildings.

All floors had identical lumped mass, m; see Figure 2-5(b). One-component Giberson beam elements [45] were used to model the walls. One such beam element represents a core-wall segment between two consecutive floors. The plastic hinge length at each end was assumed to be half the element length. The moment-curvature hysteretic response in the plastic hinges was represented by the Clough [45] hysteretic rule; see Figure 2-5(c). Using expected yield flexural strength M_y and the yield curvature φ_y, the effective flexural rigidity of the beam element was given by $EI_e = M_y / \varphi_y$. A post-yield flexural rigidity ratio r equal to 0.02 was computed from moment-curvature analysis. The elastic portions of the walls were modeled with elastic elements, with $EI_e = 0.4EI_g$, where I_g is the gross-section moment of inertia and E the initial concrete modulus. The effect of EI_e value was investigated below, considering also the cases of EI_e equal to $0.2EI_g$ and $0.6EI_g$. In this model, the flexural rigidity ignored completely the tension stiffening effect. Tension stiffening affects the initial period of the buildings and can also affect the response, especially in cases of limited nonlinear response or lightly reinforced walls. The stiffness and strength of the gravity load system was not considered, and all walls were fixed at their base. The cumulative flexural strength of the gravity columns at their base was calculated to be less than 9% of the corresponding strength of the core walls for all three buildings; see Table 2-1. The longitudinal steel ratio of the gravity columns was $\rho_{gc} = 1.5\%$. This study ignored the effect of shear deformations. The lumped-plasticity model used did not consider the effect of axial force–bending moment–shear force interaction in the nonlinear hysteretic behavior of the walls. The computer program Ruaumoko [45] was used to perform the NDRHA, and large displacement theory was selected for the analyses. Caughey constant 2% viscous damping ratio was used in all the modes [45, 46]. The effect of the damping model is investigated in the *Effect of Damping Model* section.

Table 2-1. Building characteristics.

Building	10-story	20-story	40-story
Floor height, h (m)	3.35	3.35	3.35
Building height, H (m)	33.5	67.1	134
Seismic weight / floor, w (kN)	4827	6829	19195
Axial load / floor in core wall, ΔP_W (kN)	1813	2754	8135
Axial load / floor in gravity columns, ΔP_C (kN)	3014	4075	11060
Length of core wall, L_w (m)	4.5	8	15
Core wall thickness, t_w (m)	0.3	0.3	0.75
Core wall base axial load ratio $P_{bw} / (f_c' A_{gw})$	0.09	0.11	0.14
Longitudinal reinforcement steel ratio at core wall's base, $\rho_{l,b}$ (%)	1.27	1.32	0.81
Base expected yield flexural strength of core wall, $M_{b,y}$ (kN·m)	94582	405030	3305770
Base expected yield curvature of core wall, φ_y (Rad/m)	7.49E-4	4.50E-4	2.36E-4
EI_e / EI_g for plastic hinge region of core wall	0.31	0.36	0.35
Design Shear Stress of Core Walls based on $1.25M_{b,y}$ (MPa)	1.59	2.31	2.33
Curvature Ductility at 5% tensile strain of steel, $\mu_{\varphi,5\%}$	16.3	14.8	15.2
Side dimension of square gravity columns (m)	0.50	0.75	1.0
Gravity columns base axial load ratio, $P_{bc} / (f_c' A_{gc})$	0.24	0.22	0.20
Sum of expected flexural strength of gravity columns / $M_{b,y}$	0.086	0.082	0.078
Normalized design base moment, $M_u / W_t H$	0.042	0.027	0.0237
Normalized design base shear corresponding to M_u, V_u / W_t	0.088	0.074	0.074

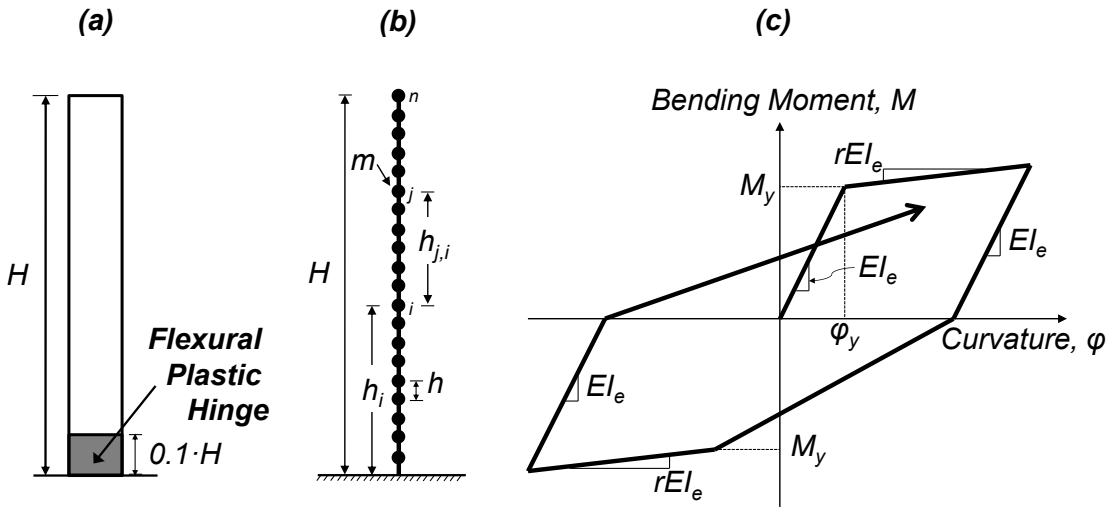

Figure 2-5. (a) Flexural plastic hinge definition; (b) mass distribution of the lumped-mass Euler-Bernoulli cantilevers; and (c) idealized moment-curvature hysteretic response.

2.4 Design of Buildings

The buildings were designed according to the ASCE 7 [14] seismic design requirements for a site in downtown Pasadena, CA, for soil type C, corresponding to very dense soil and soft rock. Figure 2-6 depicts the DBE and MCE acceleration and displacement spectra for the site considered. For the specific site S_S = 2.53 g, S_1 = 0.87 g, S_{DS} = 1.68g, and S_{D1} = 0.75g.

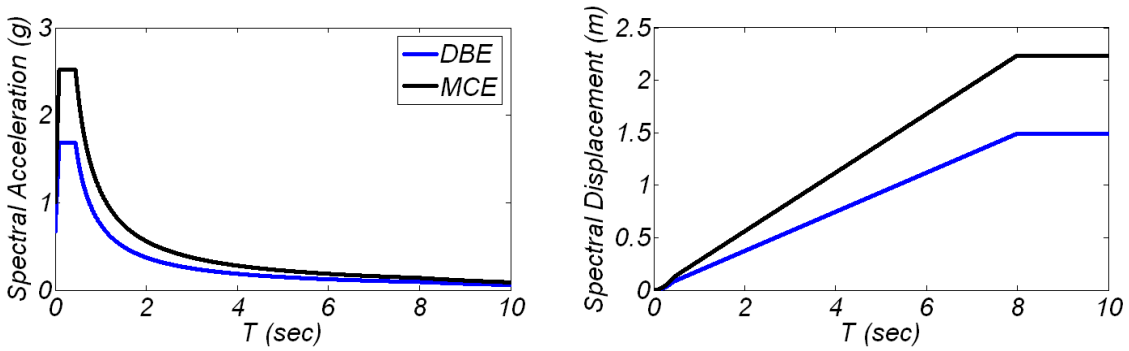

Figure 2-6. Acceleration and displacement design spectra for a site in downtown Pasadena, CA.

Modal response spectrum analysis (MRSA), based on the requirements of ASCE-7, with a response modification factor of R = 5 was used to obtain design forces. The design bending moment, M_u, and shear force, V_u, envelopes are shown in Figure 2-7 and are also reported in Table 2-1. An effective section moment of inertia $I_e = 0.5I_g$ was used for the core-walls along their entire height elements for the MRSA. In Figure 2-7, the MRSA bending moment and shear force envelopes for this design model are labeled *MRSA*. Based on section 12.9.4 of ASCE-7 the design base shear force can't be less than 85% of the base shear force, $V_{b,ELFP}$, required based on the equivalent lateral force procedure (ELFP). This requirement controlled the design shear forces for the 20-, and 40-story buildings. The envelopes, termed $MRSA_{VELFP}$ in Figure 2-7, are the MRSA envelopes scaled up by $0.85\frac{V_{b,ELFP}}{V_{b,MRSA}}$, where $V_{b,MRSA}$ is the base shear force computed with MRSA. The $MRSA_{Mb,o}$ envelopes, shown also in Figure 2-7, are the *MRSA* envelopes scaled by $1.25\frac{M_{b,y}}{M_{b,MRSA}}$, where 1.25 is the base flexural over-strength factor, and $M_{b,MRSA}$ is the *MRSA* base bending moment.

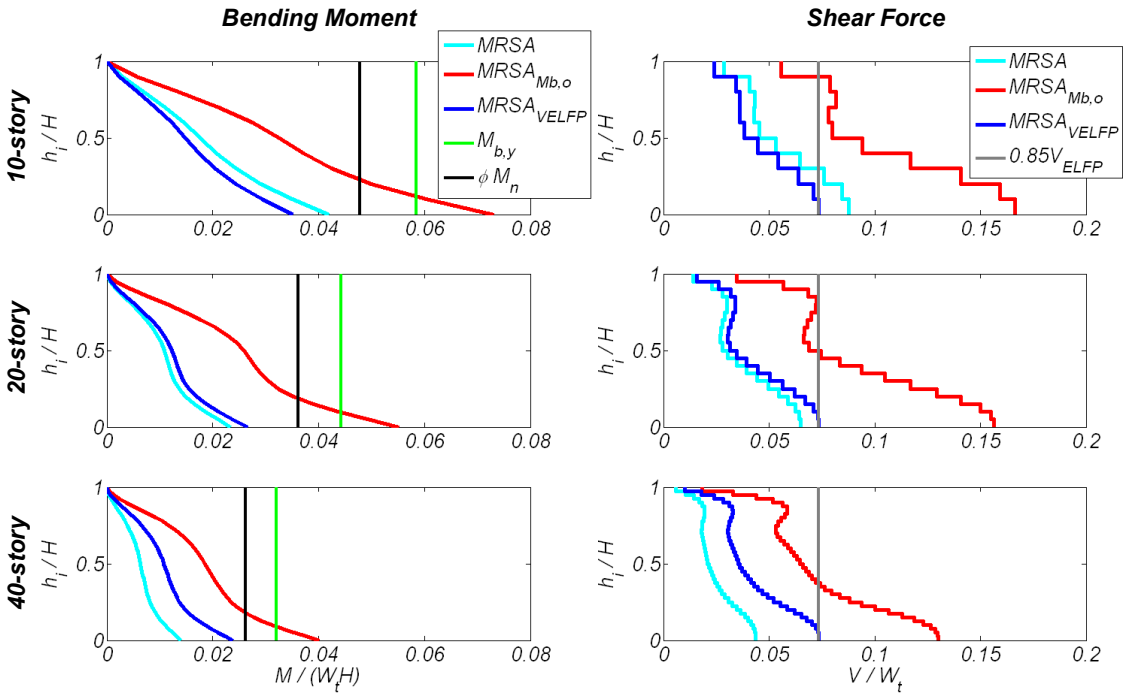

Figure 2-7. Design bending moment and shear force envelopes based on MRSA.

2.5 Numerical Analyses Results

The results of numerical analyses of the 10-, 20-, and 40-story buildings are presented next. First, modal analysis of the buildings is performed and then, NDRHA of the buildings subjected to the near-fault ground motions and to their pulse approximations, described above, is conducted. Finally, the results of the parametric NDRHA study of the buildings subjected to the three close-form pulses of various amplitudes a_p and periods T_p are presented, and the efficiency of MRSA is evaluated.

2.5.1 Modal analysis

Figure 2-8 and Table 2-2 present the main modal characteristics of the first three modes of the buildings considered. The buildings termed 10-, 20-, and 40-story are these with $EI_e = 0.4EI_g$ for the elastic parts of the walls. Figure 2-8 also includes the modal characteristics of the 20-story building using the reduced flexural rigidity (RFR), rEI_e, defined in Figure 2-5(c), for the plastic hinge elements. The modal characteristics of the 20-story building with EI_e = 0.2 EI_g used for the elastic portions of the wall, termed 20-story-0.2EI_g, are also presented in Figure 2-8.

The normalized modal characteristics presented are: (a) modal lateral force; (b) modal bending moment; and (c) modal shear force diagrams for the first three modes. The normalized modal lateral force of mode q at floor i, $r_{F,q,i} = F_{q,i} / (m \cdot A_q)$, is equal to the ratio of lateral force due to mode q, $F_{q,i}$, to the product of the modal acceleration, A_q, and the floor seismic mass, m [46]. Equation 2.1 relates $F_{q,i}$ to the product of $\Gamma_q \Phi_{q,i}$, where Γ_q is the modal participation factor and $\Phi_{q,i}$ is the value of the modal vector of mode q at floor i. The normalized modal shear force, $r_{V,q,i} = V_{q,i} / (m_t \cdot A_q)$, is equal to the ratio of the shear force at floor i due to mode q, $V_{q,i}$, to the product of the total seismic mass, m_t, times A_q. $V_{q,i}$ is calculated using Equation 2.2. The normalized modal base shear force is equal to the effective modal mass m_q [46] normalized by m_t. The normalized modal bending moment, $r_{M,q,i} = M_{q,i} / (m_t \cdot H \cdot A_q)$, is equal to the ratio of the bending moment at floor i due to mode q, $M_{q,i}$, to m_t times the height, H, of the building times A_q. $M_{q,i}$ is calculated using Equation 2.3. The term $h_{j,i}$ is defined in Figure 2-5(b).

$$F_{q,i} = \Gamma_q \cdot \Phi_{q,i} \cdot m \cdot A_q \tag{2.1}$$

$$V_{q,i} = \sum_{j=i}^{n} \Gamma_q \cdot \Phi_{q,j} \cdot m \cdot A_q \tag{2.2}$$

$$M_{q,i} = \sum_{j=i}^{n} \Gamma_q \cdot \Phi_{q,j} \cdot m \cdot h_{j,i} \cdot A_q \tag{2.3}$$

The normalized modal characteristics of the 10-, 20- and 40- story buildings, with EI_e = 0.4 EI_g for the walls' regions above the base plastic hinge, were practically identical, indicating insensitivity to the number of floors. For these three buildings, the peak normalized first and second mode bending moment occurred at their base. The absolute value of the second mode bending moment at mid-height was close to the corresponding value at the base of the wall. The values of the normalized third mode bending moment along the building heights were small. Same sign of first and second mode accelerations resulted in modal bending moments and shear forces at the base of same sign, while they resulted in

mid-height modal bending moments of different sign. Reduction of flexural rigidity at the base (see Figure 2-8 for the 20-story-RFR building) resulted in a straighter first-mode lateral force diagram without any significant change in its value at the top of the building, resulting in an increase of the normalized effective first modal mass.

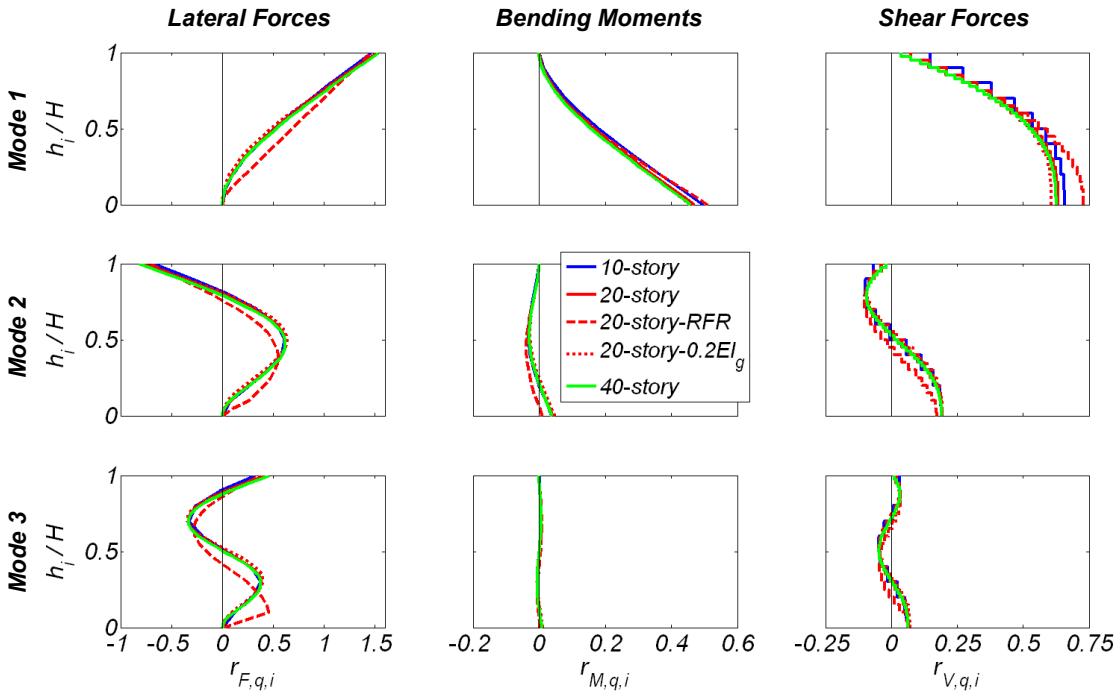

Figure 2-8. Normalized modal characteristics of the buildings.

Table 2-2 summarizes the main modal characteristics of four of the buildings considered. For the buildings with $EI_e = 0.4EI_g$, the ratios T_1 / T_2 and T_1 / T_3 of the first modal period T_1 to the second and third mode, respectively, were essentially insensitive to the number of stories. The absolute values of the normalized second mode base bending moment were less than one tenth of the corresponding first-mode values for all buildings studied. Thus, inelastic response at the base of the walls should be expected to reduce the first mode of response more than the second. The reduction of flexural rigidity at the base affected mainly the first modal period, elongating it 8.8 times, while the second-mode period was elongated only 1.5 times. The cumulative normalized effective modal mass of the first three modes increased from 0.89 for the 20-story building to 0.97 for the 20-story-RFR building. The 20-story-RFR building had a nearly zero normalized second-mode base bending moment. In this case, base inelasticity is expected to have a limited effect in reducing the second mode of response. Changing EI_e / EI_g from 0.2 to 0.4 caused only minor changes of the normalized modal characteristics.

The effect of the gravity system on the stiffness of the buildings was investigated. The columns, and the slabs were modeled using Euler-Bernoulli beam elements with effective flexural rigidities at yield, EI_e, based on moment-curvature analysis. The full width of the slabs and the framing between the core walls, the slabs, and the gravity columns were considered. This reduced the first mode period by less than 9% for all three buildings. The corresponding reduction of the second mode period was less than 2%.

Table 2-2. Main modal characteristics of the buildings.

Mode	Building	10-story	20-story	20-story-RFR	40-story
1	Modal period T_q (sec)	2.2	4.0	35	6.6
2		0.3	0.6	0.9	1.0
3		0.1	0.2	0.3	0.4
2	Modal period ratio T_1 / T_q	6.5	6.4	41	6.5
3		18	18	110	18
1	Normalized modal base shear force (equal to normalized effective modal mass) $r_{V,q,b} = m_q / m_t$	0.66	0.63	0.73	0.63
2		0.19	0.20	0.17	0.19
3		0.07	0.06	0.07	0.06
1	Normalized modal base moment $r_{M,q,b} = M_{q,b} / (m_t \cdot H \cdot A_q)$	0.497	0.470	0.511	0.459
2		0.039	0.040	0.010	0.039
3		0.008	0.008	0.003	0.008
1	Normalized modal mid-height moment $r_{M,q,0.5H} = M_{q,0.5H} / (m_t \cdot H \cdot A_q)$	0.181	0.166	0.170	0.159
2		-0.032	-0.030	-0.038	-0.029
3		-5.8E-4	-2.7E-4	0.005	1.8E-5

2.5.2 Building response to near-fault ground motions and their pulse approximations

Figure 2-9 presents the NDRHA results for the three buildings, each subjected to one of the near-fault ground motions and its pulse approximation as described above. The base bending moment, M_b, mid-height bending moment, $M_{0.5H}$, base shear force, V_b, and roof absolute acceleration, A_r, response histories are presented. The response quantities are normalized by the maximum of the peak values computed using the near-fault record and its pulse representation. The 10-, 20-, and 40-story buildings were subjected to the JFA292, RRS228, and PCD164 records, respectively. The base curvature ductility, μ_φ, calculated as the peak curvature in the first-story inelastic beam element divided by the yield curvature, φ_y, for the 10-, 20-, and 40-story buildings computed equal to 8.1, 14.1, and 11.6, respectively, indicated highly nonlinear response. Table 2-1 lists the curvature ductility $\mu_{\varphi,5\%}$ at a tensile strain ε_s = 5% of the extreme section fiber at the base of the wall sections. For all case studies for the duration of the pulse approximation, the computed response using the pulse approximation satisfactorily matched those computed using the near-fault ground motions, except in the case of the base shear force for the 10-story building. For the 20-story building subjected to the RRS228 record, Pulse A provided a satisfactory estimation of peak response quantities. For the 10-story building subjected to the JFA292 record, Pulse B computed satisfactorily the bending moment and roof acceleration response quantities up to the end of the close-form pulse. For the 40-story building subjected to the PCD164 record, Pulse C computed quite well the different response quantities, even after the end of the close-form pulse and up to t = 6 sec. After t = 6 sec, the response to the near-fault record was dominated by the strong high-frequency excitation, which is not represented by the close-form pulse.

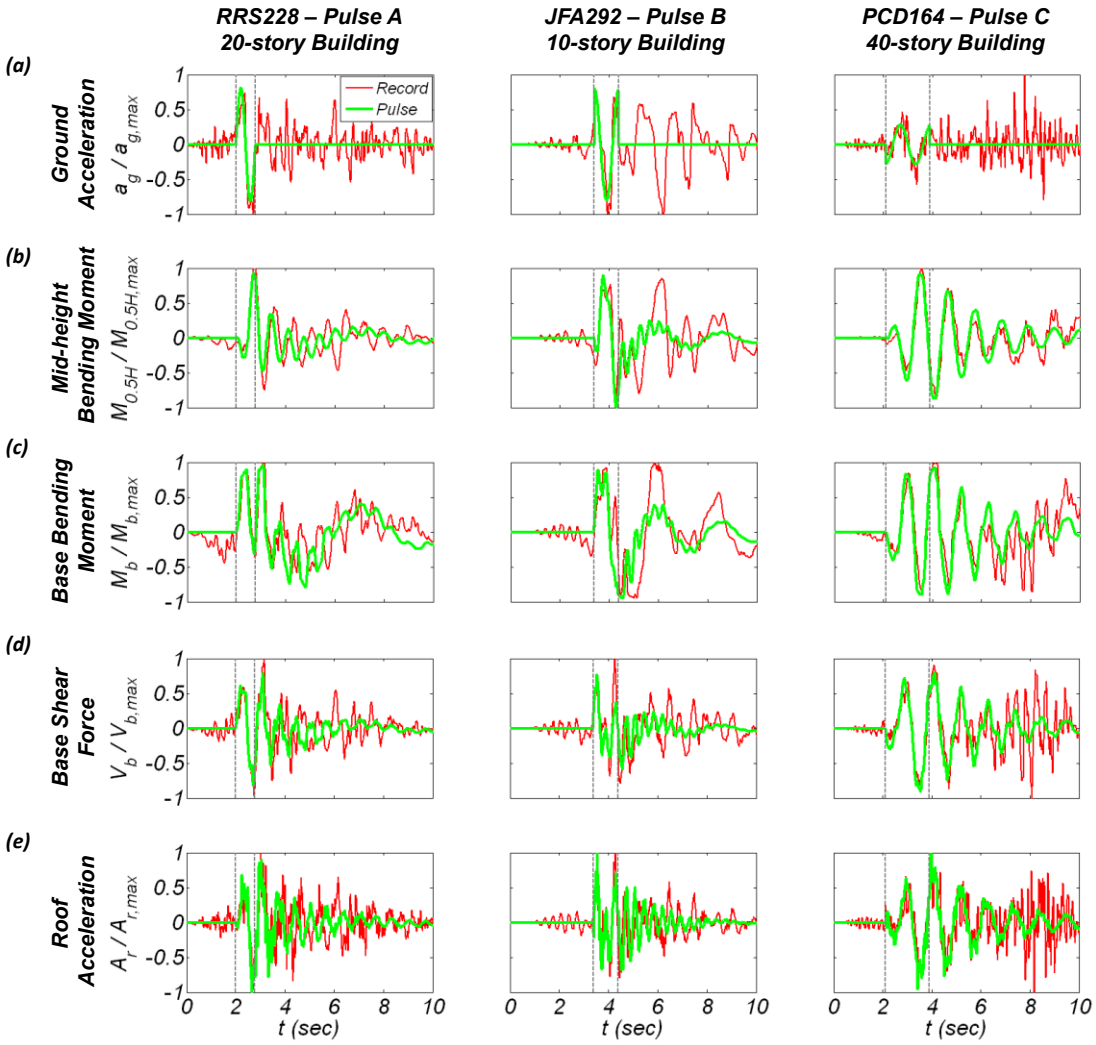

Figure 2-9. Comparison of the NDRHA results using near-fault ground motions and their close-form pulse approximations. Time histories of (a) ground acceleration, (b) mid-height bending moment, (c) base bending moment, (d) base shear force, and (e) roof absolute acceleration.

For the 20- and 40-story buildings considered, the close-form pulse period was closer to the second modal period of the buildings than to the first-mode period. The T_1 / T_p ratios for the 10-, 20-, and 40- story building case studies are 2.3, 5.1, and 5.3, respectively. The corresponding T_2 / T_p ratios are 0.4, 0.8, and 0.8. Since the pulse period is close to the second modal period of the buildings, significant contribution of the second mode of response is expected, especially for the 20- and 40-story buildings, as shown in Figure 2-10 for the bending moment, shear force, and acceleration response envelopes computed with NDRHA. The significant effect of the higher modes, especially the second mode, can be seen in all the response quantities for all motions. The peak bending moment around mid-height approached or even exceeded the peak base bending moment for all buildings. The effect of the second mode of response is seen in the shear force envelopes as well, where a local peak was observed close to 80% of the height. This local peak characterizes the normalized second mode shear force diagram, as shown in Figure 2-8.

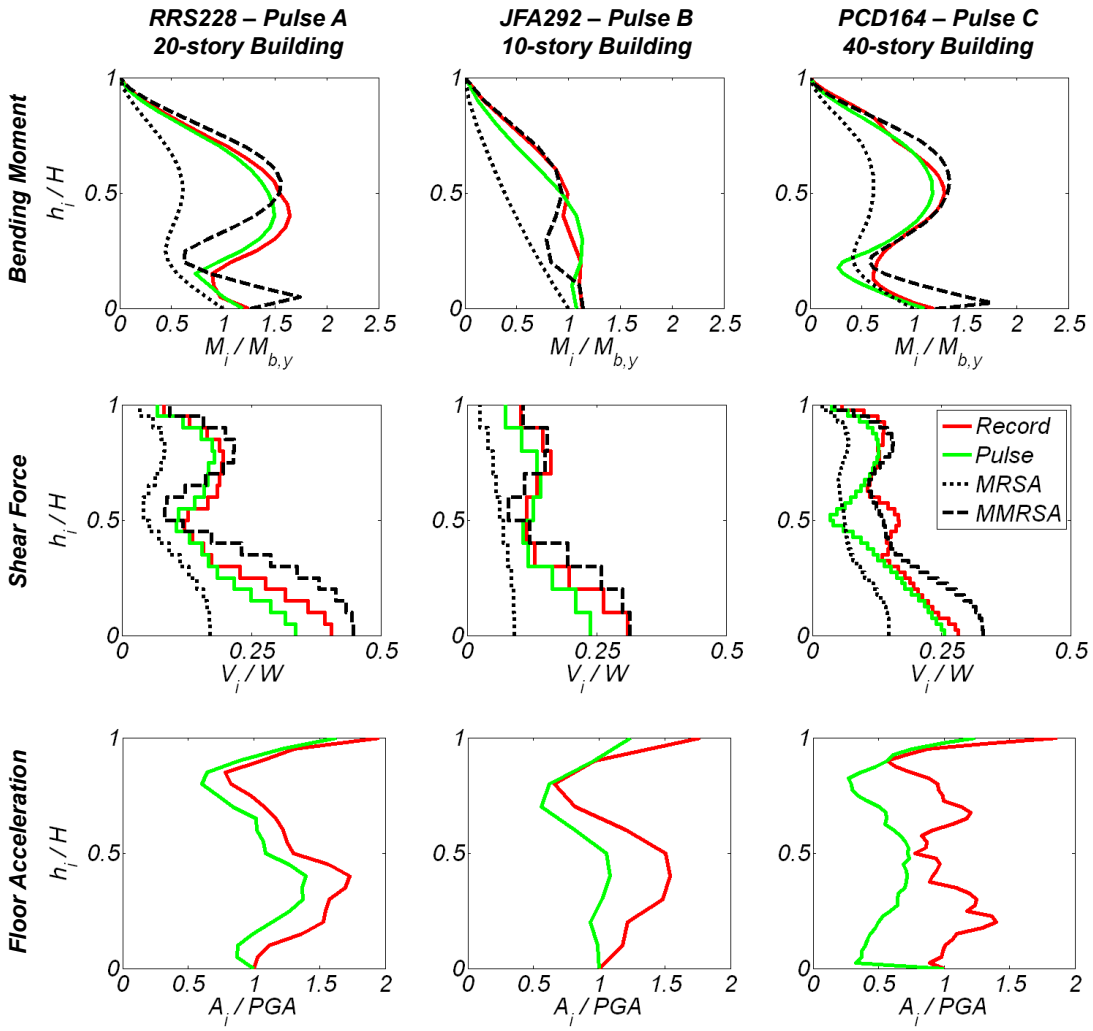

Figure 2-10. Response envelopes of NDRHA, MRSA, and MMRSA using the near-fault ground motions, and of NDRHA using close-form pulse representations.

The response envelopes computed using the close-form pulses are comparable to those computed with the near-fault records, indicating that the distinct pulses contained in the ground motions determined the response to a large extent. The bending moment and shear force response envelopes computed with the close-form pulses adequately represent those of the near-fault ground motions for the three buildings. Relatively good agreement was also observed in the computed acceleration response for the 20-story building. The largest differences between the responses computed with the near-fault records and their pulse representation is seen in the floor acceleration response, especially for the 40-story building. For this case, floor acceleration response was greatly affected by the higher frequency excitation observed beyond $t = 6$ sec in the PCD164 record after the end of the approximated pulse; see Figure 2-9. For this record, a local peak was observed in the shear force envelope around the mid-height of the 40-story building. Here, the high-frequency excitation observed after $t = 6$ sec significantly excited the third mode of response. Shown in Figure 2-8, the third mode shear force diagram has a local peak around mid-height. The acceleration spikes of the PCD164 record after $t = 6$ sec, see Figure 2-2(a), resulted in significant spectral accelerations at $T = 0.4$ sec, see Figure 2-2(c), which was equal to the third modal period of the building.

2.5.3 Building response to close-form pulses and comparison of NDRHA and MRSA

Results of the NDRHA of the three buildings subjected to the close-form Pulses A, B, and C are presented below. Pulse periods T_p corresponding to T_1 / T_p ratios 0.25, 0.50, 0.75, and 1.0 through 20.0, with a step of 1.0, are considered to cover a range extending from low- to high-frequency of excitation. To investigate different levels of inelasticity on the response, different amplitudes a_p for each pulse of period T_p were investigated. For each T_p, the amplitude a_p was determined from the MRSA considering the first four modes. Once the modal characteristics of the buildings were determined, the SRSS combination method was used and a uniform reduction factor R was applied to all modes. By setting the moment demand at the base of the wall equal to the yield base moment strength $M_{b,y}$, the required pulse amplitude was calculated as:

$$a_p = \frac{R \cdot M_{b,y}}{m_t \cdot H \cdot \sqrt{\sum_{q=1}^{4} \left[r_{M,q,b} \cdot \Omega_q \right]^2}} \tag{2.4}$$

where $r_{M,q,b}$ is the normalized base modal bending moment, see Table 2-2, and $\Omega_q = Sa(T_q) / a_p$, see Figure 2-1(b), where $Sa(T_q)$ is the q^{th} mode elastic SDOF spectral acceleration. The cumulative normalized effective modal mass of the first four modes considered was more than 0.9 for all buildings.

Figure 2-11 plots the calculated values of a_p for the three buildings versus T_1 / T_p for Pulses A, B, and C; values of a_p are normalized by R times the acceleration of gravity g. The secondary (top) x-axis shows also the points that correspond to T_2 / T_p and T_3 / T_p ratios equal to one. In general, a_p increased with increasing T_1 / T_p ratio for all three pulses. For the specific buildings considered in this study for a given T_1 / T_p and R, the required a_p decreased with an increase in the building height. For the 20-story building with $T_1 = 4.0$ sec for $T_1 / T_p = 5$ and pulse A, $a_p / R = 0.28$g. In this case, $T_p = 0.8$ sec and $R = 2.4$, $a_p = 0.68$g. This might represent the case of the 20-story building subjected to the pulse approximation of the RRS228 record with $a_p = 0.68$g and $T_p = 0.78$ sec; see Figure 2-2. For the three buildings, high values of T_1 / T_p and R resulted in very large values of a_p, which are not found in existing near-fault records. That said, these cases are still worth considering for exploring the effect of decrease of T_p (increase of T_1 / T_p) and the effect of increase of a_p.

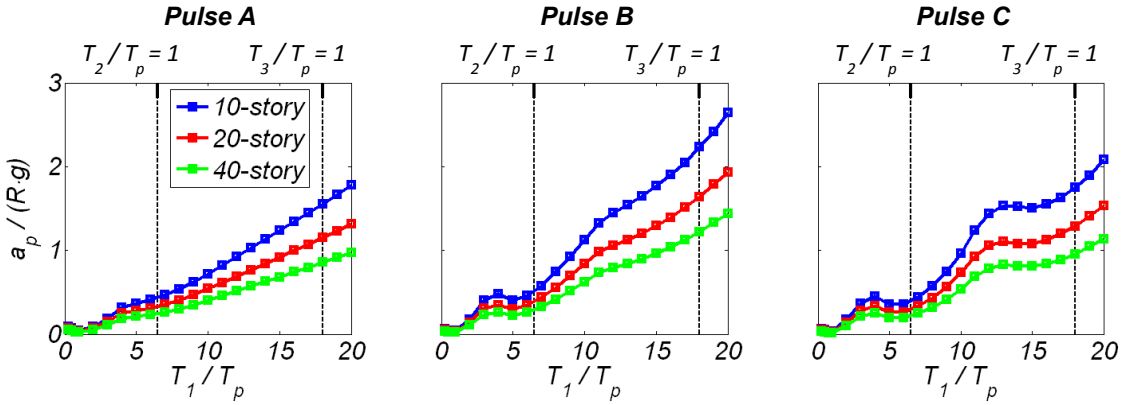

Figure 2-11. Acceleration amplitude a_p of close-form Pulses A, B, and C versus T_1 / T_p computed with MRSA and a uniform R to all modes, resulting in a base bending moment equal to $M_{b,y}$.

Figure 2-12 through Figure 2-14 compare the DBE and MCE design spectra to the spectra of pulses A, B, and C, with a_p computed based on Equation 2.4, for three values of R and three values of T_p. The design spectra are compared to the pulse excitation spectra for the 10-story building in Figure 2-12. The corresponding comparisons for the 20-, and 40-story buildings are depicted in Figure 2-13 and Figure 2-14, respectively. For the 10-story building, $T_p = T_2$, and $R = 2$, the spectral accelerations are close to the corresponding values of the MCE spectrum in the constant acceleration region. For $T_p = T_2$, and R equal to 4 and 6, the spectral accelerations for the pulse motion far exceed the corresponding values of the MCE spectrum in the constant acceleration region. For $T_p = T_2$, all R values, and T larger than 1.0 sec, the spectral accelerations of the pulse motions are smaller than the corresponding magnitude of the MCE spectra, except for pulse A and $R = 6$. For $T_p = 0.5T_1$, $R = 2$, the pulse spectral accelerations are below the MCE for all pulses and periods, except pulse C around $T = T_p = 1.1$ sec. For $T_p = 0.5T_1$ and $R = 4$ the spectral acceleration for the pulse motions exceed the corresponding MCE values for pulses B and C, and T between 0.7 and 2 sec. The same is true for $T_p = 0.5T_1$ and $R = 6$ for all pulses and T between 0.7 and 2.5 sec. For $T_p = T_1$, R equal to 2 and 4, the spectral accelerations for all pulses are lower than the corresponding MCE values. For $T_p = T_1$, and $R = 6$, the spectral accelerations for all the pulse motions exceed the corresponding MCE values for T around $T_p = 2.2$ sec. Observations similar to those for the 10-story building, can be made for the 20-, and 40-story buildings, with noticeable differences due to the increase of T_1 and T_2 with number of building stories.

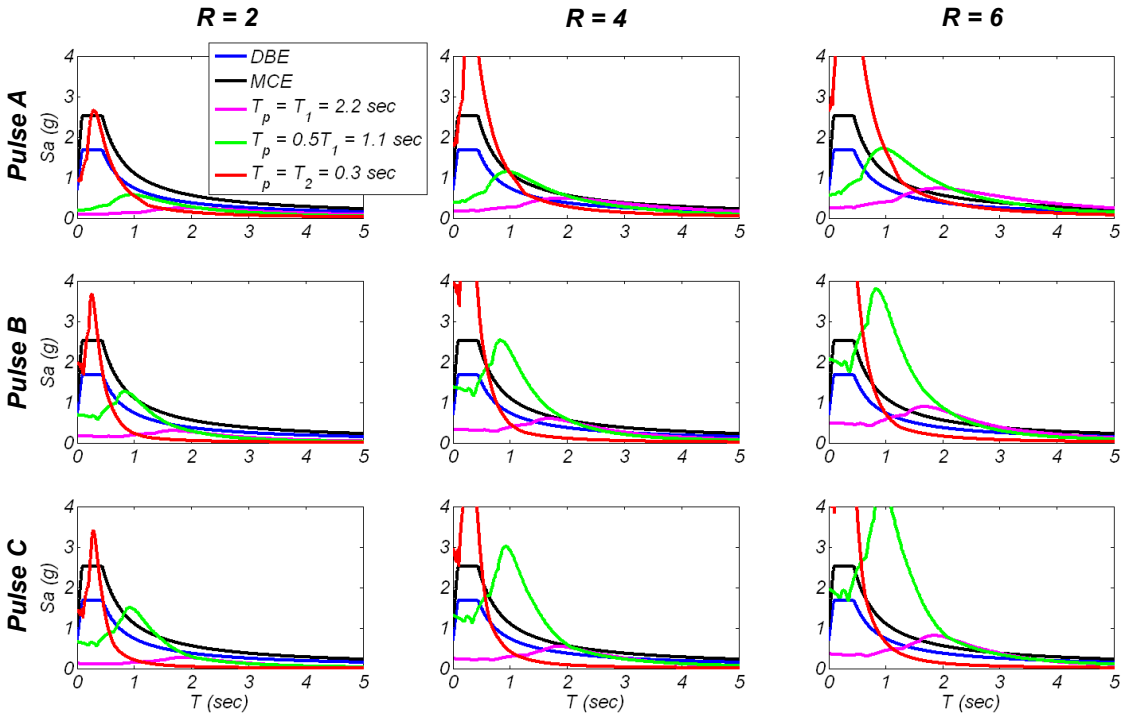

Figure 2-12. ASCE design basis and maximum considered earthquake and pulse response spectra for the 10-story building.

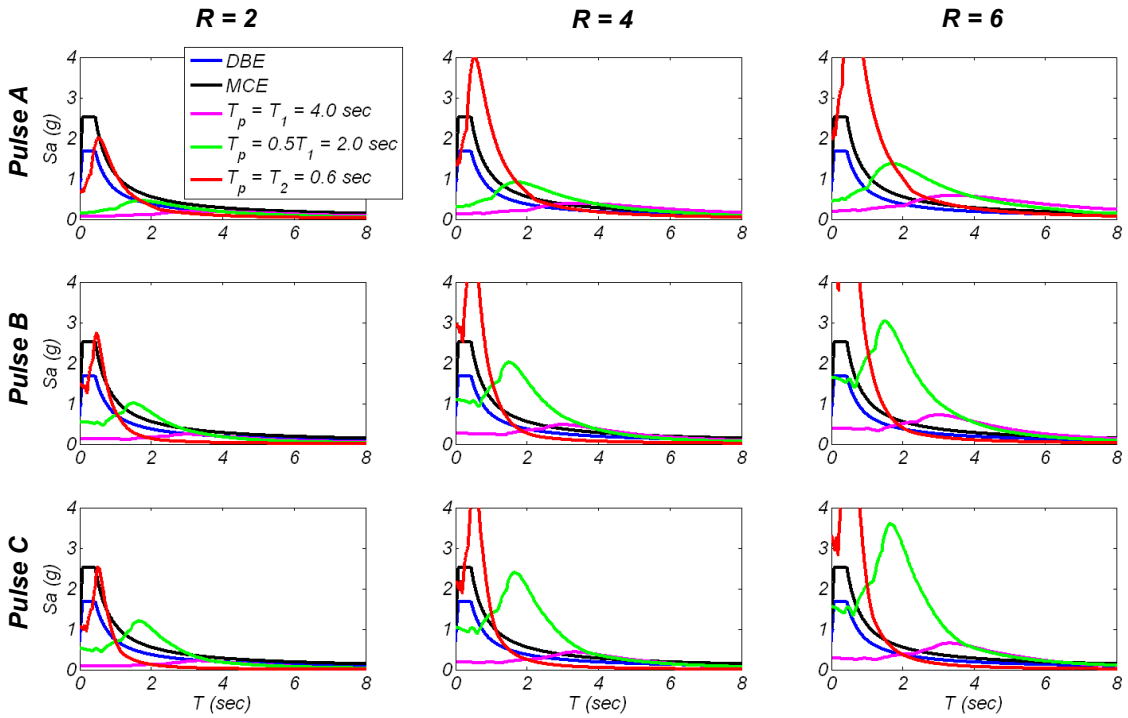

Figure 2-13. ASCE design basis and maximum considered earthquake and pulse response spectra for the 20-story building.

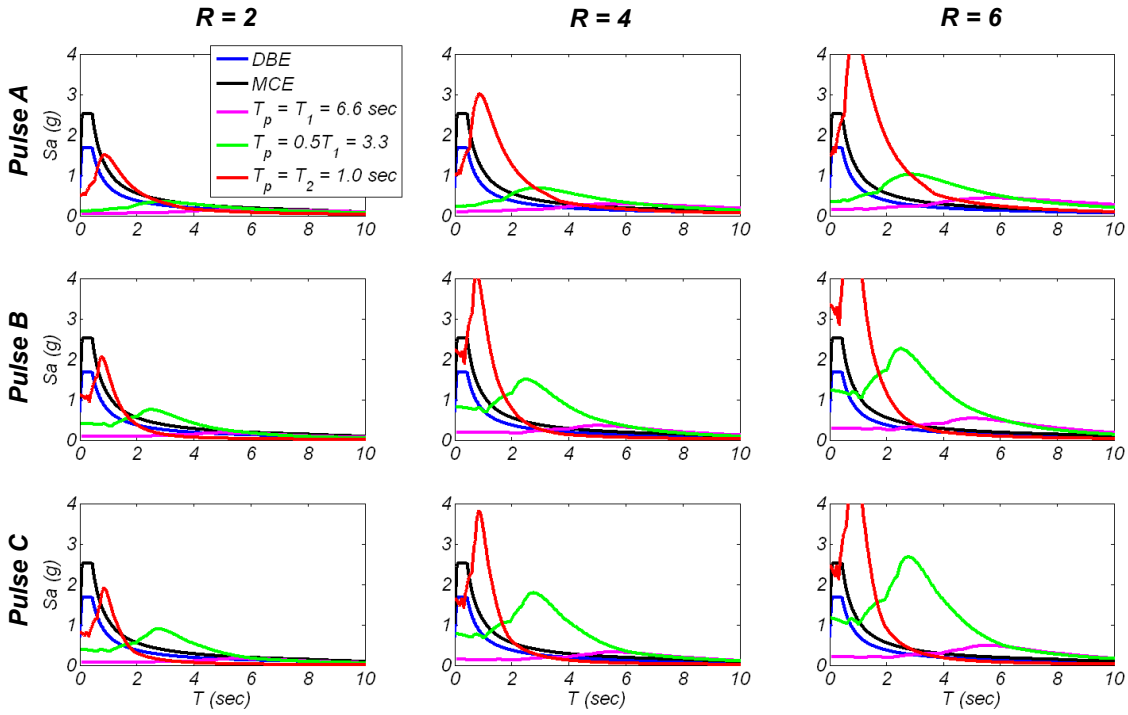

Figure 2-14. ASCE design basis and maximum considered earthquake and pulse response spectra for the 40-story building.

Figure 2-15 presents the results of the NDRHA for the three buildings in terms of base curvature ductility $\mu_{\varphi,b}$ calculated as the peak curvature computed at the base of the buildings divided by the yield curvature, φ_y, to Pulses A, B, and C for R = 2, 4, and 6 versus T_1 / T_p. The response parameter $\mu_{\varphi,b}$ indicates the level of inelastic response. As expected for all pulses and buildings, $\mu_{\varphi,b}$ generally increased with increasing R. For T_1 / T_p smaller than 1.0, $\mu_{\varphi,b}$ increased very rapidly with a corresponding decrease of T_1 / T_p. For T_1 / T_p equal to 0.25 or 0.5, the computed values of $\mu_{\varphi,b}$ were virtually unattainable. For T_1 / T_p ratios higher than 1, curvature ductility demands of up to 45 were computed. Excessive and practically unattainable levels of inelastic response computed for some T / T_p ratios, especially for R = 4 and 6, are worth exploring theoretically. Interestingly, $\mu_{\varphi,b}$ attains a local maximum for T_1 / T_p = 4, corresponding to T_2 / T_p = 0.6, for both R = 4 and 6.

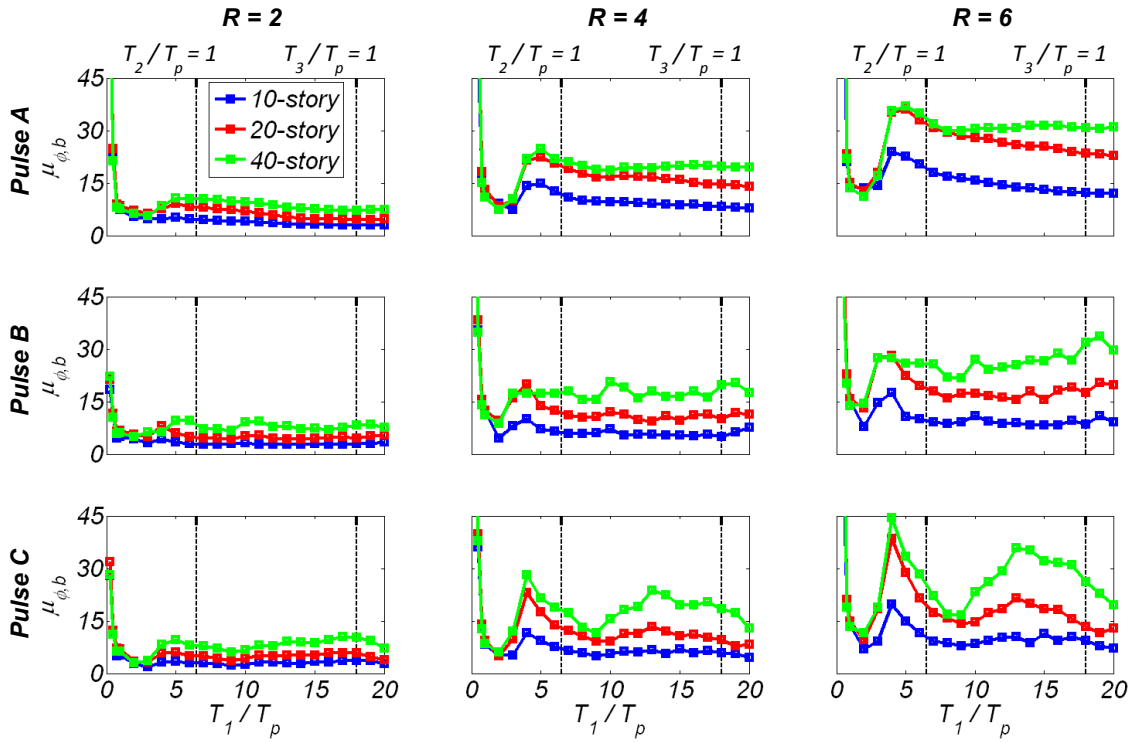

Figure 2-15. Peak base curvature ductility $\mu_{\varphi,b}$ computed with NDRHA.

Figure 2-16 and Figure 2-17 present the results of the NDRHA in terms of the mid-height bending moment $M_{0.5H}$ and base shear force V_b for the three buildings to Pulses A, B, and C, for R = 2, 4, and 6, and for the twenty-three distinct ratios of T_1 / T_p. These response quantities are normalized by those computed by MRSA using a uniform R factor in the four modes.

Figure 2-16 plots the computed mid-height bending moment in terms of the ratio $\Psi_{M,0.5H} = M_{0.5H,NDRHA} / M_{0.5H,MRSA}$, where $M_{0.5H,NDRHA}$ and $M_{0.5H,MRSA}$ are the peak mid-height bending moments computed by NDRHA and MRSA, respectively. For T_1 / T_p lower than one, corresponding to low-frequency excitation and R equal to 4 and 6, $\Psi_{M,0.5H}$ was much higher than one due to the excessive post-yield section hardening at the base of the walls. Section hardening is not accounted for in MRSA; see Equation 2.4. For T_1 / T_p higher than one, MRSA significantly underestimated $M_{0.5H}$ for all buildings, all pulses, and all R factors. For all pulses and all R factors, $\Psi_{M,0.5H}$ was more or less independent of the building height and was dependent only on the ratio of T_1 / T_p. For R equal to 4 and 6 and for T_1 / T_p ratios higher than one, maximum values of $\Psi_{M,0.5H}$ occurred at T_1 / T_p = 4 for all pulses, except for the 40-story building for Pulse B. For T_1 / T_p = 4, corresponding to T_2 / T_p = 0.6, significant excitation of the second mode of response occurred. For all the three pulses and for R equal to 4 and 6, $\Psi_{M,0.5H}$ increased rapidly for T_1 / T_p, increasing between 1 and 4. For T_1 / T_p larger than 4, values of $\Psi_{M0.5H}$ were high and of the order of $\frac{2}{3}R$. For R = 2, $\Psi_{M,0.5H}$ was nearly uniform and equal to R.

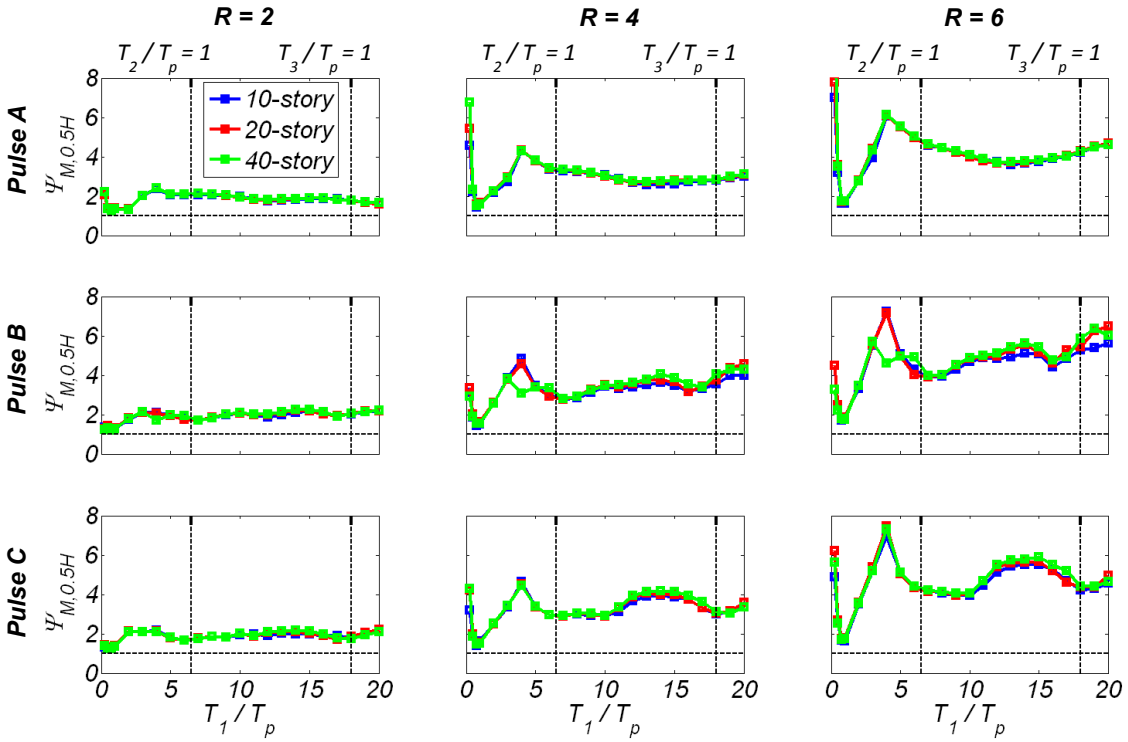

Figure 2-16. Ratio of peak mid-height bending moments computed with NDRHA and MRSA.

The computed ratio $\Psi_{V,b} = V_{b,NDRHA} / V_{b,MRSA}$, where $V_{b,NDRHA}$ and $V_{b,MRSA}$ are the peak base shear forces computed by NDRHA and MRSA with a uniform R factor in all the modes, respectively, is shown in Figure 2-17. The variation of $\Psi_{V,b}$ with T_1 / T_p—similar to that of $\Psi_{M,0.5H}$—was essentially independent of the number of stories, depending mainly on the R factor with a minor sensitivity to the pulse type. For T_1 / T_p lower than one and R equal to 4 and 6, $\Psi_{V,b}$ was much higher than one due to the excessive post-yield base section hardening as explained above. For R equal to 4 and 6, $\Psi_{V,b}$ increased rapidly for T_1 / T_p between 1 and 3 or 4. For R = 4 and 6, and T_1 / T_p larger than one, $\Psi_{V,b}$ attained a maximum value at T_1 / T_p equal to 3 or 4. For R equal to 4 and 6 and for T_1 / T_p larger than 3, $\Psi_{V,b}$ was larger than 0.4R. For R equal to 2, $\Psi_{V,b}$ was nearly constant and equal to R.

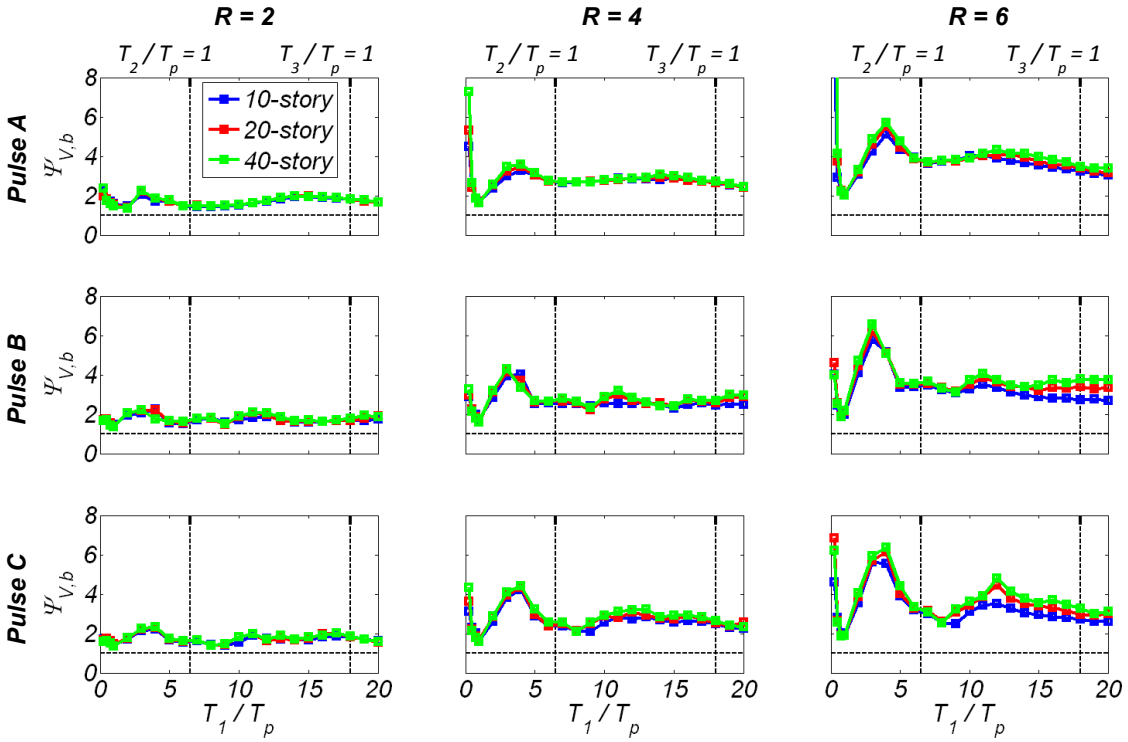

Figure 2-17. Ratio of peak base shear forces computed with NDRHA and MRSA.

Figure 2-18 plots the bending moment envelopes computed by MRSA and NDRHA for R equal to 2 and 6, for four values of T_1 / T_p. The bending moment at floor i, M_i, was normalized by $M_{b,y}$. The envelope computed with MRSA is independent of the value of R since the relative contribution of the modes is independent of R. Values of $M_i / M_{b,y}$ at the base computed with NDRHA were larger than one due to post-yield base section hardening. Compared to NDRHA, MRSA significantly underestimated the bending moment demands in the upper part of the wall. The level of underestimation increased with increasing R.

The amplitude of peak normalized bending moment and the height at which this occurs strongly depends on T / T_p. For values of T_1 / T_p equal to and larger than 3, the bending moment on the upper part of the wall reaches or exceeds the base bending moment yield capacity $M_{b,y}$ in all cases; see Figure 2-18. For example, for $T_1 / T_p = 6$, Pulse A, and for $R = 2$ and 6, the bending moment at 40% of the height is 1.4 and 3.4 times $M_{b,y}$, respectively, which causes a practical difficulty when trying to ensure elastic response of these regions. If this wall were required to remain elastic, the required longitudinal reinforcement ratio at the eighth story (40% of the height) for Pulse A, $T_1 / T_p = 6$ and $R = 2$ would be 2.8%, an excessively large value. In comparison to the base, the larger bending moment combined with the reduction of axial force resulted in a significant increase in the required longitudinal reinforcement. For $T_1 / T_p = 20$, corresponding to $T_3 / T_p = 1.1$, the peak moment based on NDRHA occurred close to 75% of the height, indicating significant contribution of the third mode of response.

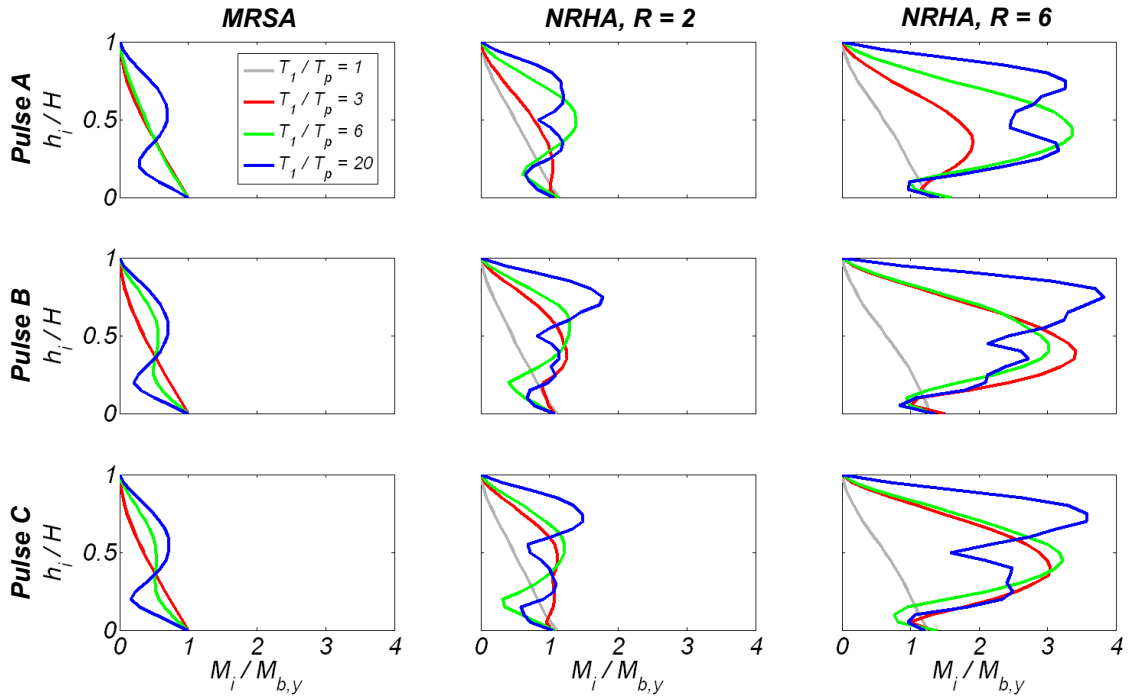

Figure 2-18. Bending moment envelopes for the 20-story building subjected to pulses A, B, and C for four T_1 / T_p ratios computed with (a) MRSA and NDRHA; (b) $R = 2$; and (c) $R = 6$.

Next, the effect of EI_e, used to model the elastic wall regions on the computed ratios $\Psi_{M,0.5H}$ and $\Psi_{V,b}$ for the 20-story building subjected to Pulse B was investigated. Two values of the yield reduction factor, R = 2 and R = 6, and three values of EI_e / EI_g = 0.2, 0.4 and 0.6 were considered. For each value of T_1 / T_p, a_p was recomputed using Equation 2.4 and accounting for the change in modal characteristics with the corresponding change of EI_e. Figure 2-19 shows that $\Psi_{M,0.5H}$ and $\Psi_{V,b}$ are practically independent of the EI_e considered.

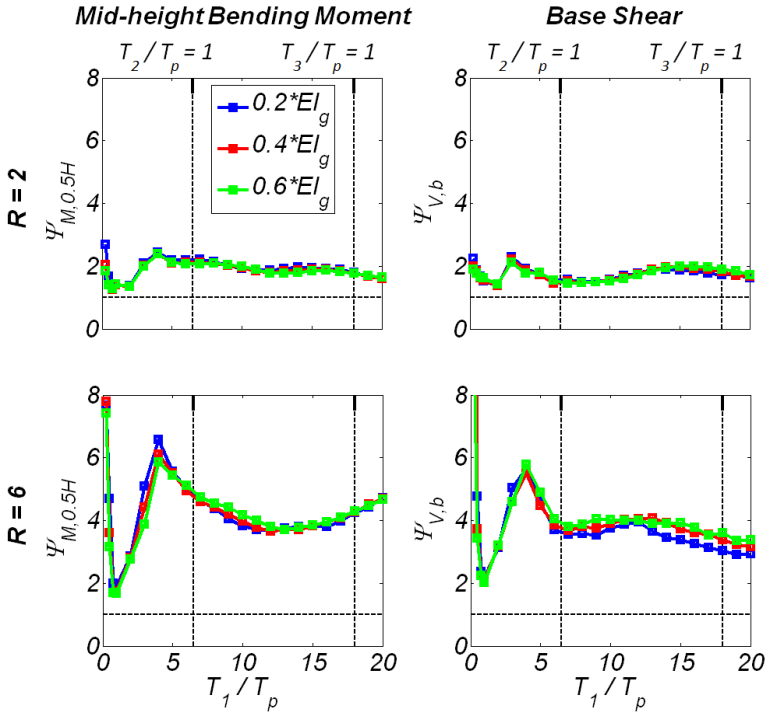

Figure 2-19. Effect of effective flexural rigidity value on the ratio of responses computed with NDRHA and MRSA for the 20-story building and Pulse B.

The ratio of peak mid-height bending moment $M_{0.5H,max}$ to yield base bending moment $M_{b,y}$ was also investigated (see Figure 2-20) for EI_e / EI_g equal to 0.2, 0.4, and 0.6, for the 20-story building subjected to Pulse B. For T_1 / T_p lower than one, and R =4 and 6, the ratio $M_{0.5H,max}$ / $M_{b,y}$ was much higher than one because of the excessive post-yield hardening of the base sections. The ratio $M_{0.5H,max}$ / $M_{b,y}$ increased rapidly for values of T_1 / T_p between 1 and 4, reaching a peak at T_1 / T_p between 4 and 8, a period range with significant contribution of the second mode to response. For T_1 / T_p larger than 4, $M_{0.5H,max}$ / $M_{b,y}$ increased with increasing R and increasing EI_e. For EI_e = 0.4EI_g, the peak $M_{0.5H,max}$ / $M_{b,y}$ was 1.4, 2.3, and 3.4 for R equal to 2, 4, and 6, respectively.

Finally, the effect of T_1 / T_p on the shear force that developed on the upper part of the buildings was explored. Figure 2-21 shows the ratio of the peak shear force at three quarters of the wall height, $V_{0.75H,max}$, to the peak base shear force, $V_{b,max}$. Results for the 20-story building for R = 2, 4, and 6 and for all pulses A, B, and C are presented. Small sensitivity of $V_{0.75H,max}$ / $V_{b,max}$ to the pulse type was observed. At T_1 / T_p = 3 corresponding to T_2 / T_p = 0.5 for all R and pulses, the ratio $V_{0.75H,max}$ / $V_{b,max}$ reached its peak value. For all cases except for R = 4 and Pulse A, this peak value was very close or exceeded one. The results presented in Figure 2-21 indicate that the design shear force at three quarters of the wall height should be at least half of the corresponding value at its base independent of pulse period and R factor.

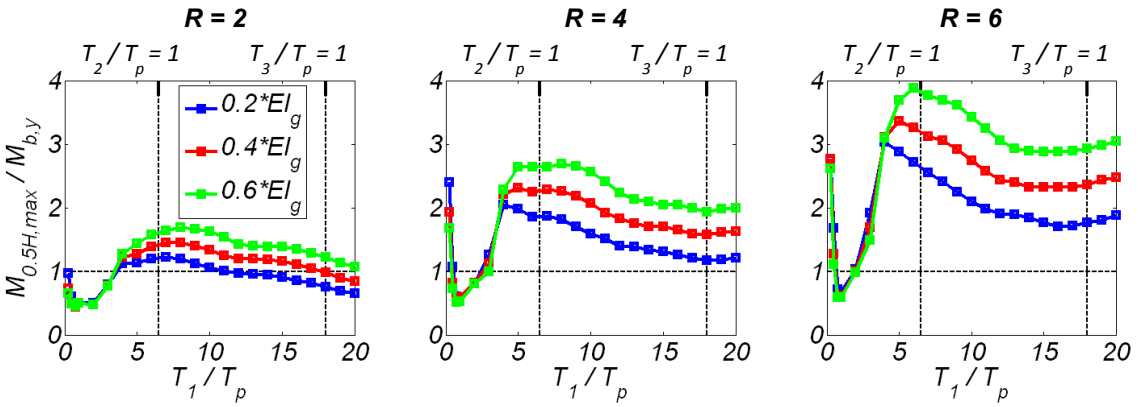

Figure 2-20. Effect of effective flexural rigidity value, on the ratio of peak mid-height to yield base bending moment computed with NDRHA for the 20-story building subjected to Pulse B.

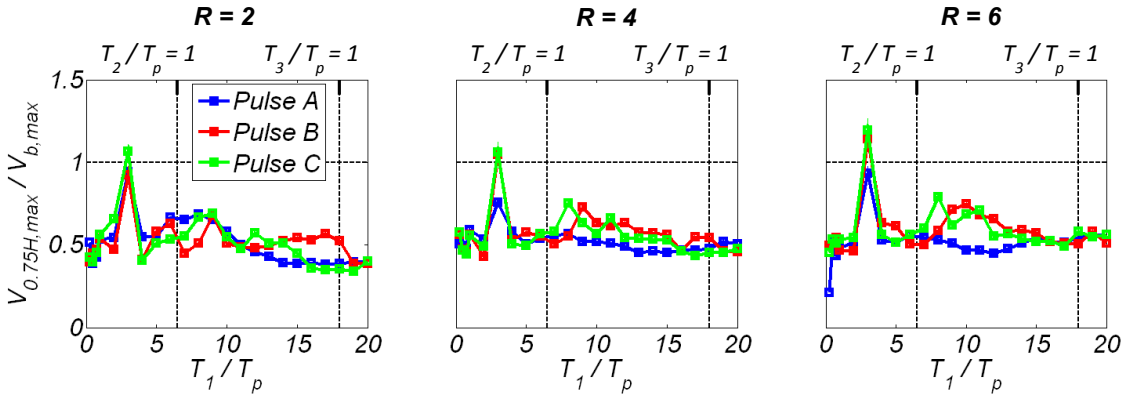

Figure 2-21. Peak shear force at 75% of the 20-story building's height computed with NDRHA.

2.5.4 *Effect of Damping Model*

The sensitivity of the building models to the choice of damping model was studied for the 20-story building. Caughey 2% constant damping in modes 1 through 6 was compared to Rayleigh 2% damping in modes 1 and 2, and in modes 1 and 4. Figure 2-22 and Table 2-3**Error! Reference source not found.** show how the Caughey and Rayleigh damping ratio values compare for the first four modes. In comparison with the Caughey damping model the Rayleigh 2% in modes 1 and 2 model results in at least 2.5 times larger damping ratios in modes three and above. In comparison with the Caughey damping model the Rayleigh damping model with 2% damping ratio in modes 1 and 4 results in 3.1 and 1.8 times lower damping ratio in modes 2, and 3, respectively.

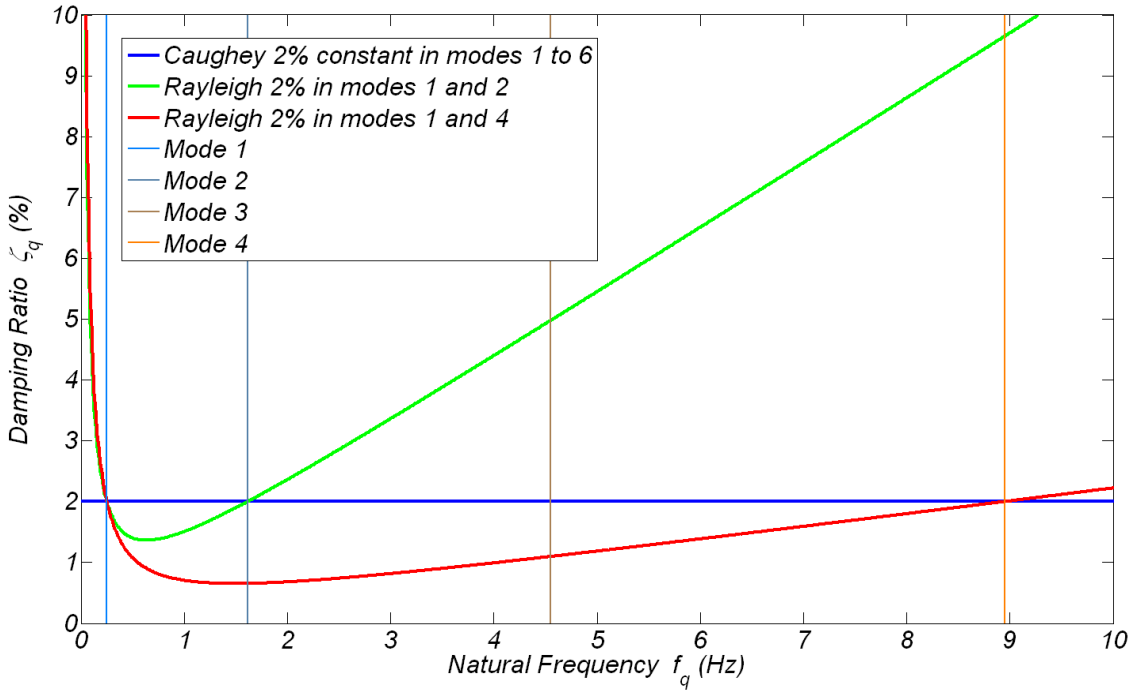

Figure 2-22. Caughey and Rayleigh damping comparison for the 20-story building.

Table 2-3. Caughey and Rayleigh damping comparison.

Mode	Mode 1 damping (%)	Mode 2 damping (%)	Mode 3 damping (%)	Mode 4 damping (%)
Caughey 2% in modes 1 through 6	2.00	2.00	2.00	2.00
Rayleigh 2% in modes 1 and 2	2.00	2.00	4.98	9.65
Rayleigh 2% in modes 1 and 4	2.00	0.65	1.10	2.00

Figure 2-23 compares the computed response in terms of four different response parameters (V_b, A_r, $M_{0.5H}$, and $\mu_{\varphi,b}$) for the three damping models for pulse B and R = 4. The larger damping ratios of the Rayleigh damping model with 2% damping ratio in modes 1 and 2, in comparison with the other two models, result in reduction of the different response quantities and especially base curvature ductility, base shear force, and roof acceleration. The effect of the damping model is less pronounced for the mid-height bending moment. The Rayleigh damping model with 2% damping ratio in modes 1 and 4 results in almost the same response with the Caughey damping model for all the T_1 / T_p values and all response parameters.

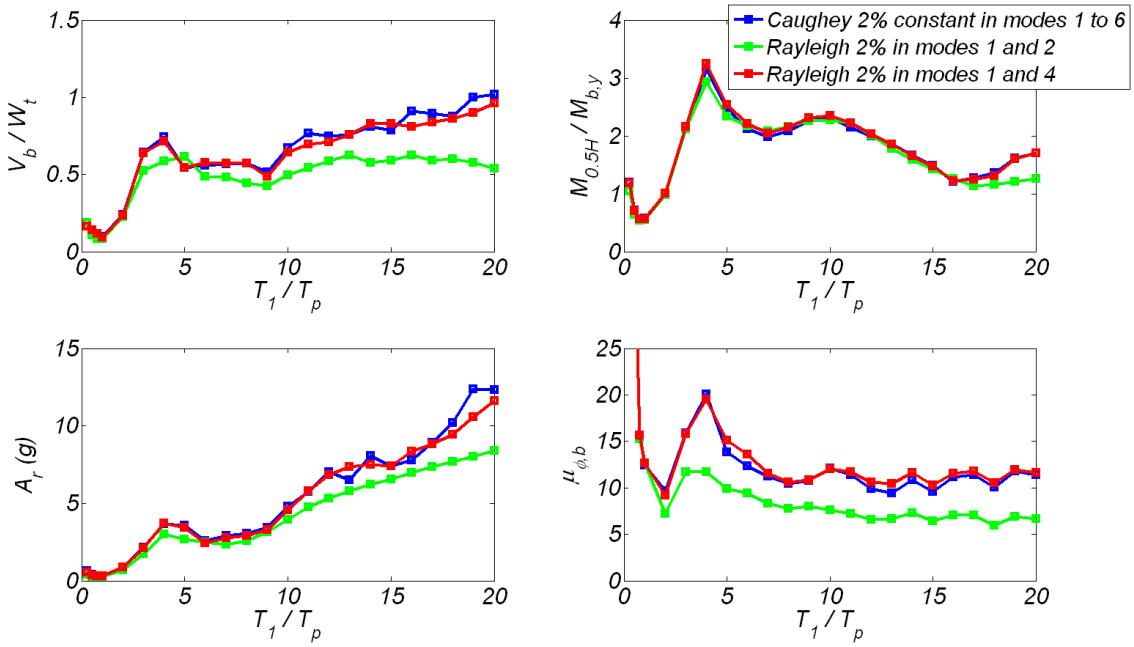

Figure 2-23. Damping sensitivity study for the 20-story building for pulse B and R = 4.

2.6 A Modified Modal Response Spectrum Analysis Method for RC Cantilever Walls with Base Inelasticity

Independent of the number of stories for the three pulse types and R values considered, MRSA, using effective flexural rigidities, significantly underestimated different response quantities, when used a uniform R factor in all the first four modes, and the SRSS combination rule. For T_1 / T_p smaller than one corresponding to low-frequency excitation, the response was first mode dominated. In this excitation period range, MRSA did not account for the post-yield base section hardening of the walls, resulting in an underestimation of the response; in addition section hardening was excessive for R = 4 and 6. For T_1 / T_p larger or equal than one, MRSA using the SSRS combination method and a uniform R factor in all the four modes significantly underestimated the response for all pulses and R values, because inelastic response at the base of cantilever wall buildings does not reduce the second and higher modes as much as the first mode of response.

A modified modal response spectrum analysis (MMRSA) method is presented that considers only the first three modes of response and uses a yield reduction factor R_1, and R_H for the first and higher (second and third) modes, respectively. Modal characteristics are computed using effective flexural rigidities. In this approach, the elastic response modal parameter Q^i (bending moment, shear force, floor acceleration) of interest at floor i can be computed as:

$$Q^i = \sqrt{\left[Q_1^i \cdot \frac{\Omega_{b,o}}{R_1}\right]^2 + \frac{\left[Q_2^i\right]^2 + \left[Q_3^i\right]^2}{\left(R_H\right)^2}} \tag{2.5}$$

where Q_q is the mode q elastic contribution to the response parameter considered. The base section over-strength factor $\Omega_{b,o}$ is the ratio of the peak expected base bending moment $M_{b,o}$ to $M_{b,y}$. Having determined the expected flexural yield strength of a wall, Equation 2.5 can be used to calculate floor accelerations and bending moments, above the base of the wall, and shear forces along its entire height. Once $M_{b,y}$, and $M_{b,q}$ are known, factor R_1 is computed based on Equation 2.6.

$$R_1 = \frac{m_t \cdot H \cdot \sqrt{\sum_{q=1}^{4}\left[r_{M,q,b} \cdot Sa\left(T_q\right)\right]^2}}{M_{b,y}} \tag{2.6}$$

As defined above for the three buildings considered, the modal parameters $r_{M,i}$, $r_{V,i}$, $r_{A,i}$ and thus Q_q^i are known from modal analysis; see Figure 2-8. For the analysis using the close-form pulses, factor R_1 is equal to R used for the MRSA (compare Equations 2.4 and 2.6). Also peak values of $M_{0.5H}$, V_b, A_r, and $\Omega_{b,o}$ were computed with NDRHA. Here, Equation 2.5 can be solved separately for the peak values of $M_{0.5H}$, V_b, A_r, in terms of R_H. Figure 2-24 plots the results of R_H for the 20-story building with $EI_e = 0.4EI_g$ for all the three pulses and T_1 / T_p between 0.75 and 20. Figure 2-24 shows that for all three response quantities, all pulses, and all R factors, R_H was significantly smaller than R_1 and smaller than 2.0, except Pulse C for base shear force and T_1 / T_p = 8. In some cases, especially for T_1 / T_p between 0.75 and 4, values of R_H smaller than one are computed. In these cases even considering the second and third mode elastic underestimates the response.

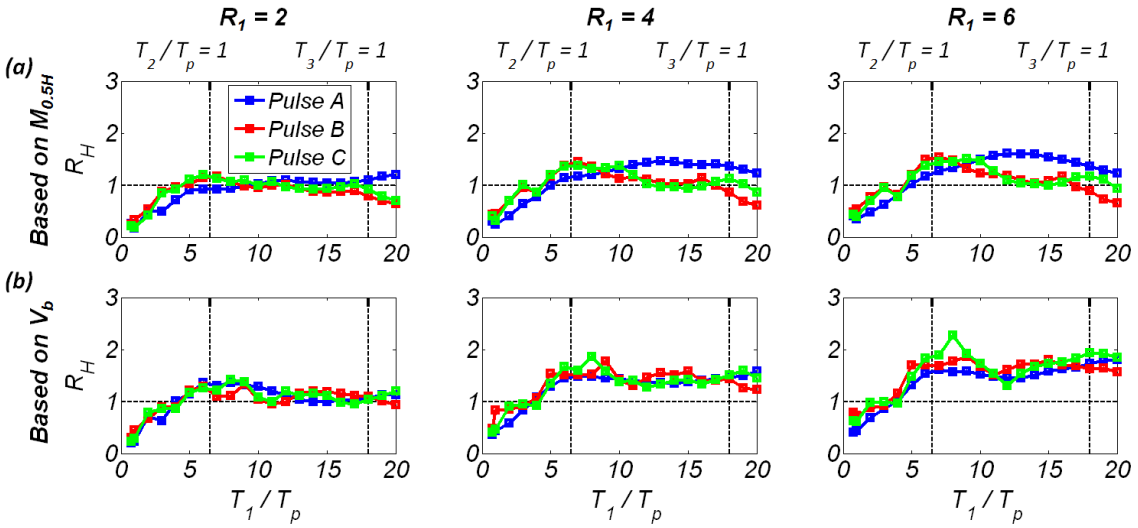

Figure 2-24. Yield reduction factor R_H for higher modes computed based on: (a) mid-height bending moment and (b) base shear force obtained from NDRHA of the 20-story building.

Comparison of MRSA and the MMRSA results for the three buildings subjected to near-fault records is shown in Figure 2-10. Results of MRSA with a uniform R factor in the first four modes and MMRSA as described in Equations 2.5 and 2.6, using $R_H = 1$, are presented. For the JFA292, RRS228, and PCD164 records, the $R_1 = R$ factors computed using Equation 2.6 for the 10-, 20-, and 40-story buildings are 5.97, 2.74, and 2.25, respectively. In all three cases, MRSA significantly underestimated the three response parameters along the height of the buildings. The MMRSA significantly improved the estimation of all response envelopes. The MMRSA significantly underestimated the floor accelerations at the bottom 25% of the height of the buildings. The total acceleration computed with modal response spectrum analysis, independent of the R values used, results in zero acceleration at the base of the fixed-base buildings.

2.7 Summary and Conclusions

This chapter of the dissertation investigated the inelastic response of tall cantilever wall buildings subjected to pulse-type ground motion, emphasizing the relationship between ground motion characteristics and higher modes of response, especially the second and third mode. Three 10-, 20-, and 40-story high cantilever wall buildings were designed to develop all nonlinear deformations at a flexural plastic hinge region located at their base. Nonlinear dynamic response history analyses (NDRHA) of these buildings was carried out. Initially, each building was subjected to both a near-fault record and a representation of this record using a close-form pulse. Then, an extensive parametric analytical study was conducted for each building subjected to three close-form pulses. Twenty three distinct pulse periods and three pulse amplitudes at each period were considered to study different levels of inelastic response. The following conclusions were drawn:

1. Strong pulse-type ground motions with the predominant pulse period in the range of the second structural modal period computed with effective flexural rigidities significantly excited the first, and second mode, causing highly inelastic response at the base of the walls for all buildings considered.
2. Simple close-form pulses provided fair approximations of the distinct pulses contained in near-fault records. Using the pulse approximations, the computed response in terms of section bending moment, shear force, and floor acceleration were similar to the corresponding response computed using near-fault records.
3. Strong pulse-type motion with a predominant pulse period close to or shorter than the second modal period excited significantly the second mode of response and resulted in bending moment demands at the intermediate wall height that far exceeded the base bending moment yield strength. Designing these regions to remain elastic requires large to excessive amounts of longitudinal reinforcement.
4. For any T_1 / T_p greater than one, the peak shear force at 75% of the height of the buildings, $V_{0.75H}$, approached or even exceeded 50% of the peak base shear force. For T_1 / T_p = 3, for all three pulses, $V_{0.75H}$ approached or even exceeded the peak base shear force.
5. Inelastic response at the base of cantilever wall buildings did not reduce the second and higher modes as much as the first mode of response.
6. Using a uniform yield reduction factor R in all the modes and the SRSS combination method, modal response spectrum analysis significantly underestimated the bending moments, shear forces, and floor accelerations along the height of the buildings for T_1 / T_p greater than one.
7. This underestimation increased with increasing R and with an increase of T_1 / T_p between 1 and 4. The level of underestimation was independent of the number of stories and showed small sensitivity to the pulse type and to the response parameter.
8. Modified modal response spectrum analysis that considered a yield reduction factor R_H factor in the second and higher modes equal to one (or much smaller than this used for the first mode), significantly improved the estimation of forces and accelerations along the height of cantilever wall buildings.

Chapter 2 References

1. Blakeley RWG, Cooney RC, Megget LM. Seismic shear loading at flexural capacity in cantilever wall structures. *Bulletin New Zealand National Society Earthquake Engineering* 1975; 8: 278–290.
2. Derecho AT, Iqbal M, Ghosh SK, Fintel M, Corley WG, Scanlon A. *Structural Walls in Earthquake-Resistant Buildings Dynamic Analysis of Isolated Structural Walls Development of Design Procedure – Design Force Levels*. Portland Cement Association, 1981.
3. Eibl J, Keintzel F. Seismic shear forces in RC cantilever shear walls. *Proceedings, 9th World Conference on Earthquake Engineering*, Tokyo/Kyoto, Japan 1988, Report 9-1-1.
4. Paulay T, Priestley MJN. *Seismic Design of Reinforced Concrete and Masonry Buildings*. Wiley: Hoboken, NJ, 1992.
5. Eberhard MO, Sozen MA. Member behavior-based method to determine design shear in earthquake-resistant walls. *Journal of Structural Engineering* 1993; 119(2):619–640.
6. Filiatrault A, D'Aronco D, Tinawi R. Seismic shear demand of ductile cantilever walls: a Canadian code perspective. *Canadian Journal of Civil Engineering* 1994; 21:363–376.
7. Panneton M, Léger P, Tremblay R. Inelastic analysis of a reinforced concrete shear wall building according to the National Building Code of Canada 2005. *Canadian Journal of Civil Engineering* 2006; 33:854-871.
8. Rutenberg A, Nsieri E. The seismic shear demand in ductile cantilever wall systems and the EC8 provisions. *Bulletin of Earthquake Engineering* 2006; 4:1–21.
9. Moehle JP, Sozen MA. Experiments to study earthquake response of R/C structures with stiffness interruptions (4th Ed.). *Civil Engineering Studies, Structural Research Studies No. 482*, University of Illinois, Urbana-Champaign, 1980.
10. Panagiotou, M., Restrepo, J.I., and Conte J.P. Shake Table Test of a 7-Story Full Scale Reinforced Concrete Wall Building Slice, Phase I: Rectangular Wall. *ASCE Journal of Structural Engineering*, Vol. 137, No. 6, 2011.
11. Panagiotou M. Seismic design, testing, and analysis of reinforced concrete wall buildings. Ph.D. Dissertation, University of California, San Diego, 2008.
12. Park R, Paulay T. *Reinforced Concrete Structures*. John Wiley & Sons, Inc., NJ, 1975.
13. ACI 318-08. *Building Code Requirements for Structural Concrete (ACI 318-08) and Commentary*. ACI Committee 318, Farmington Hills, 2008.
14. ASCE 7-05. *Minimum Design Loads for Buildings and Other Structures.* American Society of Civil Engineers, 2006.
15. CEN EC8: *Design of Structures for Earthquake Resistance*. European Committee for Standardisation: Brussels, Belgium, 2004.
16. NZS 3101. *New Zealand Standard, Part 1- The Design of Concrete Structures*, Standards New Zealand, Wellington, New Zealand, 2006.
17. CSA Standard A23.3-04. Design of Concrete Structures. *Canadian Standard Association*, Rexdale, Canada. 2005; 214pp.
18. Moehle J, Bozorgnia Y, Yang TY. The Tall Buildings Initiative. *Proceedings SEAOC Convention*. 2007; 315-324.
19. Priestley MJN, Calvi GM, Kowalsky MJ. *Displacement Based Seismic Design of Structures*. IUSS Press, Pavia, Italy. 2007.
20. Panagiotou M, Restrepo JI. Dual-plastic hinge design concept for reducing higher-mode effects on high-rise cantilever wall buildings, Vol. 38, Issue 12, pp 1359-1380, 2009.
21. Sullivan TJ, Priestley MJN, Calvi GM, Estimating the Higher-Mode Response of Ductile Structures. *Journal of Earthquake Engineering,* 2008; 12(4):456-472

22. Rodríguez ME, Restrepo JI, Carr AJ. Earthquake-induced floor horizontal accelerations in buildings. *Earthquake Engineering and Structural Dynamics* 2002; 31:693-718.
23. Goel RK, Chopra AK. Role of higher-"mode" pushover analyses in seismic analysis of buildings. *Earthquake Spectra* 2005; 21(4):1027-1041.
24. Chopra AK, Goel RK, Chintanapakdee R. Evaluation of a Modified MPA Procedure Assuming Higher Modes as Elastic to Estimate Seismic Demands. *Earthquake Spectra* 2004; 20(3):757–778.
25. Bertero VV, Mahin SA, Herrera RA. Aseismic design implications of San Fernando earthquake records. *Earthquake Engineering and Structural Dynamics* 1978; 6(1):31-42.
26. Anderson JC, Bertero VV, Uncertainties in Establishing Design Earthquakes. *ASCE Journal of Structural Engineering 1987*; Vol. 113; No. 8; 1709-1724.
27. Alavi B, Krawinkler H. Behavior of moment-resisting frame structures subjected to near-fault ground motions. *Earthquake Engineering and Structural Dynamics* 2004; 33:687–706.
28. Kalkan E, Kunnath SK. Effects of fling step and forward directivity on seismic response of buildings. *Earthquake Spectra* 2006; 22(2):367-390.
29. Krishnan S. Case studies of damage to 19-storey irregular steel moment-frame buildings under near-source ground motion. *Earthquake Engineering and Structural Dynamics* 2007; 36:861–885.
30. Dicleli M, Mehta A. Effect of near-fault ground motion and damper characteristics on the seismic performance of chevron braced steel frames. *Earthquake Engineering and Structural Dynamics* 2007; 36:927-948.
31. Hall JF, Heaton TH, Halling MW, Wald DJ. Near source ground motion and its effects on flexible buildings. *Earthquake Spectra* 1995; 11:569–606.
32. Akkar S, Yazgan U, Gulkan P. Drift estimates in frame buildings subjected to near-fault ground motions. *Journal of Structural Engineering* 2005; 131(7):1014-1024.
33. Liao W-I, Loh C-H, Wan S. Earthquake responses of RC moment frames subjected to near-fault ground motions. *Structural Design of Tall Buildings* 2001; 10:219-229.
34. Panagiotou M, Calugaru V, Visnjic T. Higher mode effects on the seismic response of tall cantilever wall buildings subjected to near fault ground motions. *Proceedings, Structural Engineers Association of California Convention*, San Diego, CA 2009; 345–357.
35. Somerville PG, Smith NF, Graves RW, Abrahamson NA. Modification of empirical strong ground motion attenuation relations to include the amplitude and duration effects of rupture directivity. *Seismological Research Letters* 1997; 68:199-222.
36. Iwan WD, Huang CT, Guyader AC. Evaluation of the effects of near-source ground motions. *Final Report on Research Conducted under PEER/PGE Research Program*, California Institute of Technology, 1998.
37. Sasani M, Bertero VV. Importance of severe pulse-type ground motions in performance-based engineering: historical and critical review. *Proceedings, 12th World Conference on Earthquake Engineering* 2000, Report No. 1302.
38. Makris N, Black JC. Dimensional analysis of bilinear oscillators under pulse-type excitations. *Journal of Engineering* Mechanics 2004; 130(9): 1019-1031.
39. Malhotra PK. Response of buildings to near-field pulse-like ground motions. *Earthquake Engineering and Structural Dynamics* 1999; 28:1309-1326.
40. MacRae GA, Morrow DV, Roeder CW. Near-fault ground motion effects on simple structures. *Journal of Structural Engineering* 2001; 127:996–1004.
41. Cuesta I, Aschheim MA. Isoductile strengths and strength reduction factors of elasto-plastic SDOF systems subjected to simple waveforms. *Earthquake Engineering and Structural Dynamics* 2001; 30:1043–1059.

42. Mylonakis G, Reinhorn AM. Yielding oscillator under triangular ground acceleration pulse. *Journal of Earthquake Engineering* 2001; 5:225–251.
43. Mavroeidis GP, Papageorgiou AS. A mathematical representation of near-fault ground motions. *Bulletin of the Seismological Society of America*, June 2003; 93(3):1099-1131.
44. Baker JW. Quantitative classification of near-fault ground motions using wavelet analysis. *Bulletin of the Seismological Society of America*, October 2007; 97(5):1486-1501.
45. Carr AJ. *Ruaumoko – A Program for Inelastic Time-History Analysis*. Department of Civil Engineering, University of Canterbury, New Zealand, 1998.
46. Chopra AK. *Dynamics of Structures: Theory and Applications to Earthquake Engineering*. Prentice Hall: Englewood Cliffs, NJ, 2001.

Chapter 3: Seismic Response of 20-Story Base-Isolated and Fixed-Base RC Core Wall Buildings at a Near-Fault Site

3.1 Introduction

Construction of buildings exceeding 50 m in height, referred herein as "tall" buildings, is increasing in earthquake-prone regions of the U.S. and worldwide. Common structural systems used in the seismic design of these buildings are reinforced concrete (RC) structural walls (for brevity referred to herein as "walls"), including non-planar core walls [1].

Considerable damage of tall RC wall buildings in previous earthquakes has been reported, including the 1985 M8.0 Mexico earthquake [2], the 2010 M8.8 Chile earthquake [3], and the 2011 M6.3 Christchurch, New Zealand, earthquake [4]. Note that these buildings were not designed according to the ACI 318-11 provisions considered here. In the 1999 M7.6 Chi-Chi, Taiwan, earthquake [5], tall RC frame buildings—the most common type of RC tall buildings close to the fault rupture (less than 10 km)—suffered severe damage or collapsed. In the Mexico and Chile subduction-zone earthquakes, severe damage and collapse of tall RC wall buildings occurred at 400 km [6] and 35 km [7], respectively, from the fault rupture due partly to amplification of the long-period content of the ground motions at soft-soil sites. Following the 2011 M6.3 Christchurch, New Zealand, earthquake out of the 50 tallest buildings taller than 35 m, 36 have been demolished or slated for demolition, 4 severely damaged with their fate still undecided at the time of this publication, and only 10 have reopened to occupants, most after 2 or more years of repair work [8]. Out of the 40 buildings demolished, slated for demolition, or severely damaged, 7 were built after year 2000.

Conventional tall RC wall buildings in the U.S. are designed to develop the majority of expected deformations in a single flexural plastic hinge, usually located near ground [1, 9–11]. Design forces are typically calculated using the code-prescribed design earthquake (DE) spectra with modal response spectrum analysis (MRSA) as prescribed in ASCE 7-10 [12], using a response modification factor, R, equal to 5; RC structural members are designed according to ACI 318-11 code provisions [13]. Minimum performance objectives of ASCE 7-10 require withstanding the maximum considered earthquake (MCE) with a low probability of either partial or total collapse, and withstanding the DE that is two-thirds that of the MCE, thereby ensuring life-safety. These requirements do not address post-earthquake structural or non-structural damage. In addition to code provisions, several groups have developed *ad hoc* procedures on performance, analysis, and design requirements for conventional tall buildings [14–17].

The seismic response of 20-story tall RC wall buildings designed according to Eurocode 8 has been studied numerically, demonstrating the significant contribution of higher modes to response [18]. Numerical studies have investigated the seismic response of 40- to 42-story tall RC core wall buildings located in California subjected to DE and MCE levels of shaking for sites of high seismicity [1, 9], as well as to pulse-type near-fault ground motions [10, 11].

These studies showed that for the MCE and near-fault ground shaking, these buildings develop significant inelastic deformations with 2% to 3% interstory drift ratios, large shear stresses in the walls that approach the upper limit allowed by ACI 318-11, and floor accelerations that approach or even exceed the peak ground acceleration (PGA). This magnitude of inelastic deformations and shear stresses can result in major structural and non-structural damage, requiring expensive repairs and loss of functionality. The response of 20-story tall RC core wall buildings to near-fault ground shaking has also been investigated [10, 11].

Seismic base isolation has been used as a design strategy for tall buildings to reduce accelerations, forces, and inelastic deformations in the superstructure (structure above the isolation system) and thus earthquake-induced structural and non-structural damage. This is achieved by concentrating the majority of deformations in robust isolation systems and by reducing higher mode response. A variety of seismic isolation devices are now available that have the force and displacement capacities required to isolate tall buildings. These devices include large (1.5 m-diameter) rubber bearings [19], large friction pendulum bearings [20], and large cross-linear bearings [21]. Friction pendulum bearings and cross-linear bearings with strength in tension up to 9 MN are also available [20–22]. Rubber bearings, linear bearings, friction pendulums, and fluid viscous dampers with more than 1 m horizontal displacement capacity are available and have been experimentally tested [19–26].

Japan is the leading proponent of using seismic isolation technology in tall buildings [27, 28]. Between 1990 and 2002, one-third of all the approved base-isolated (BI) buildings in Japan were taller than 40 m, and 40% of all BI buildings built in Japan after 1995 had a height-to-length ratio larger than two [27].

In the U.S., ASCE 7-10 permits the design of the structure above the isolation system of BI buildings for forces smaller than that required for elastic response at the DE; the isolation system is required to have force and displacement capacity larger than the expected demand at the MCE. Numerical studies have investigated the response of BI RC or steel frames using two degree-of-freedom (2DOF) models [29], or modeling 6 stories [30], 9 stories [31], 15 [32], 18 or 40 stories [25] of the superstructure. These studies show that the level of inelastic response of the superstructure depends on both the relative characteristics of the superstructure and isolation system, and ground motion characteristics. Oakland City Hall [33] is the only currently available study of the seismic response of a tall BI building with structural walls designed to resist most of the seismic forces along a part of the building height.

This chapter of the dissertation investigates numerically the seismic response of six simplified BI RC structural wall buildings with three stories below ground and twenty stories above ground, and compares their response to that of a fixed-base (FB) building with similar superstructure. All seven buildings are located at a site of high seismic hazard and are designed according to ASCE 7-10, except that one horizontal component of ground excitation is used in the two-dimensional (2-D) nonlinear response history analysis (NRHA). The NRHA is performed using a set of ground motions scaled to the DE and the MCE. The FB building and four of the BI buildings are also subjected to the unscaled fault-normal horizontal component of four historical near-fault ground motions that include strong long-period pulses.

This chapter of the dissertation addresses the following six questions: (1) what is the level of response (and possible damage of the structural and non-structural components) of the FB building at the DE and MCE level of shaking; (2) what are the characteristics of the base-isolated designs that result in nominally elastic response of the superstructure at the MCE level of shaking; (3) for these base-isolated designs, what is the level of reduction of floor accelerations and interstory drifts compared to that of the FB building; (4) what is the relation

between the flexural strength of the isolated superstructure, the characteristics of the isolation system, and the level of inelastic deformations the isolated superstructure developed at the DE and MCE; (5) what is the effect of the vertical component of the excitation; (6) what is the level of the response of the FB and BI buildings when subjected to four unscaled historical ground motion records with the largest linear spectral demands for periods longer than 5 s among all the historical records available.

3.2 Site and Ground Motions

The buildings are hypothetically located at a site in downtown Berkeley, California, with soil type C, 2 km from the Hayward fault. The site seismic hazard and corresponding smooth design spectra are in accordance with ASCE 7-10 at both DE and MCE levels; see Figure 3-1. Uni-axial horizontal as well as combination of horizontal and vertical excitation are used in this 2-D study. Two sets (Set 1 and Set 2) of fault-normal components for fourteen pulse-type ground motions each are linearly scaled such that their mean spectra for 5% damping ratio, ζ, match or exceed the smoothed DE and MCE design spectra over specific period ranges of interest. The fourteen motions of each of the two sets are presented in Table 3-1. Sets 1 and 2 are used for FB and BI buildings, respectively. The first set approximately matches the design spectra in the period range between 0.7 s ($0.35T_1$) to 4 s ($2T_1$), where T_1 = 2 s is the first-mode period of the FB building. For periods between 0.3 s and 0.7 s, the mean spectra of set 1 is 20% less on average than the design spectra. Set 2 matched the design spectra in the period range 1.9 s to 10.0 s, which includes the required range (per ASCE 7-10) of $0.5T_D$ to $1.25T_M$. Here, T_D = 3.7 s and T_M = 5.8 s is the effective period of the isolation system of the BI buildings (shortest T_D and longest T_M) at the design and maximum displacement, respectively. The mean scale factor at the MCE for Sets 1 and 2 is 1.43, and 1.55, respectively. The DE scale factors equal the MCE divided by 1.5. The same scale factor used to scale the horizontal FN and FP components was used to scale the vertical component of excitation. The mean acceleration spectra for the vertical component of excitation are shown in Figure 3-1.

To determine the principal direction of horizontal excitation, the following procedure was used: for each ground motion Sets 1 and 2 (corresponding to the FB and BI buildings, respectively), an equivalent three-dimensional (3-D) nonlinear 2DOF model was developed to represent the building; this model was subjected to bi-axial horizontal excitation for each pair of FN and FP components of every ground motion in the set. For each of these ground motion pairs, the direction of peak horizontal displacement was determined and defined as the principal direction of horizontal excitation.

For the FB building (Set 1), a nonlinear single degree-of-freedom (1DOF) oscillator was used in each of the X- and Y-axis of the model approximating the first-mode lateral force versus lateral displacement of the building. For the BI buildings (Set 2), a 3-D model of the isolation plane of building BI6a was used, described in Section 3, (assuming rigid in-plane stiffness and no rotation) with the total structural mass lumped at the centroid of the isolation plane. The flexibility of the superstructure was ignored in this model.

Figure 3-1 plots the mean spectra for the principal horizontal components for the Set 2 ground motions, which are 1.1 times on average that of the FN components between T = 4 s and 8 s. Figure 3-1 also plots the mean spectra for the components that are normal to the corresponding principal directions. The mean value of peak horizontal displacement of the 2DOF model of building BI6a, using the MCE-level bi-axial horizontal excitation was 1.15 m. This was in excellent agreement with that computed using the same model and the principal horizontal component of the motions as uni-axial excitation.

Table 3-1. Ground motions and scale factors at the DE- and MCE-levels of shaking.

Ground motions set	Station name	Earthquake			Scale factor	
		Location	Year	Magnitude	DE	MCE
Set 1 Fixed-base (FB) building	Duzce	Duzce, Turkey	1999	7.1	1.67	2.50
	Jensen Filter Plant				0.43	0.65
	Rinaldi Receiving	Northridge, CA	1994	6.7	0.97	1.45
	Sylmar Converter				0.93	1.39
	Los Gatos	Loma Prieta, CA	1989	6.9	1.00	1.50
	Meloland Overpass	Imperial Valley, CA	1979	6.5	0.85	1.28
	Mianzuqingping	Wenchuan, China	2008	7.9	1.66	2.50
	PRPC	Christchurch, NZ	2011	6.3	0.67	1.01
	Tabas	Tabas, Iran	1978	7.4	1.00	1.50
	Takatori	Kobe, Japan	1995	6.9	0.33	0.50
	TCU068				0.34	0.51
	TCU084	Chi-Chi, Taiwan	1999	7.6	0.36	0.54
	TCU102				1.44	2.16
	TCU129				1.67	2.50
Set 2 Base-isolated (BI) buildings	Duzce	Duzce, Turkey	1999	7.1	1.40	2.10
	El Centro Array #6	Imperial Valley, CA	1979	6.5	1.00	1.50
	Lucerne	Landers, CA	1992	7.3	0.60	0.90
	Mianzuqingping	Wenchuan, China	2008	7.9	1.39	2.08
	Tabas	Tabas, Iran	1978	7.4	0.37	0.55
	Takatori	Kobe, Japan	1995	6.9	0.87	1.30
	TCU52				0.63	0.95
	TCU67				1.67	2.50
	TCU068				0.50	0.74
	TCU87	Chi-Chi, Taiwan	1999	7.6	1.46	2.20
	TCU101				1.00	1.50
	TCU102				1.50	2.25
	TCU103				1.53	2.30
	Yarimca	Kocaeli, Turkey	1999	7.4	0.60	0.90

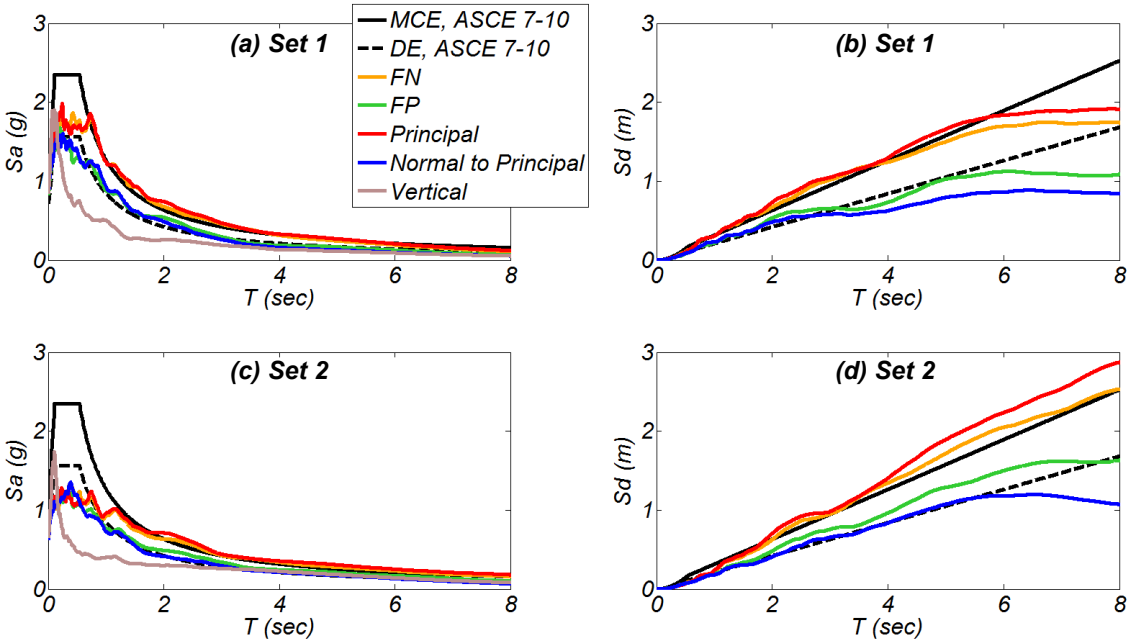

Figure 3-1. Mean linear acceleration and displacement response spectra of the FN, FP, principal, normal to principal, and vertical (only *Sa*) components for two sets of ground motions scaled to the MCE; DE, and MCE design spectra.

3.3 Description and Design of Buildings

Figure 3-2 shows the main features, and Table 3-2 lists the main properties of the FB and BI buildings. A core wall coupled through the floor slabs with columns in the perimeter of the buildings comprises the structural system above ground.

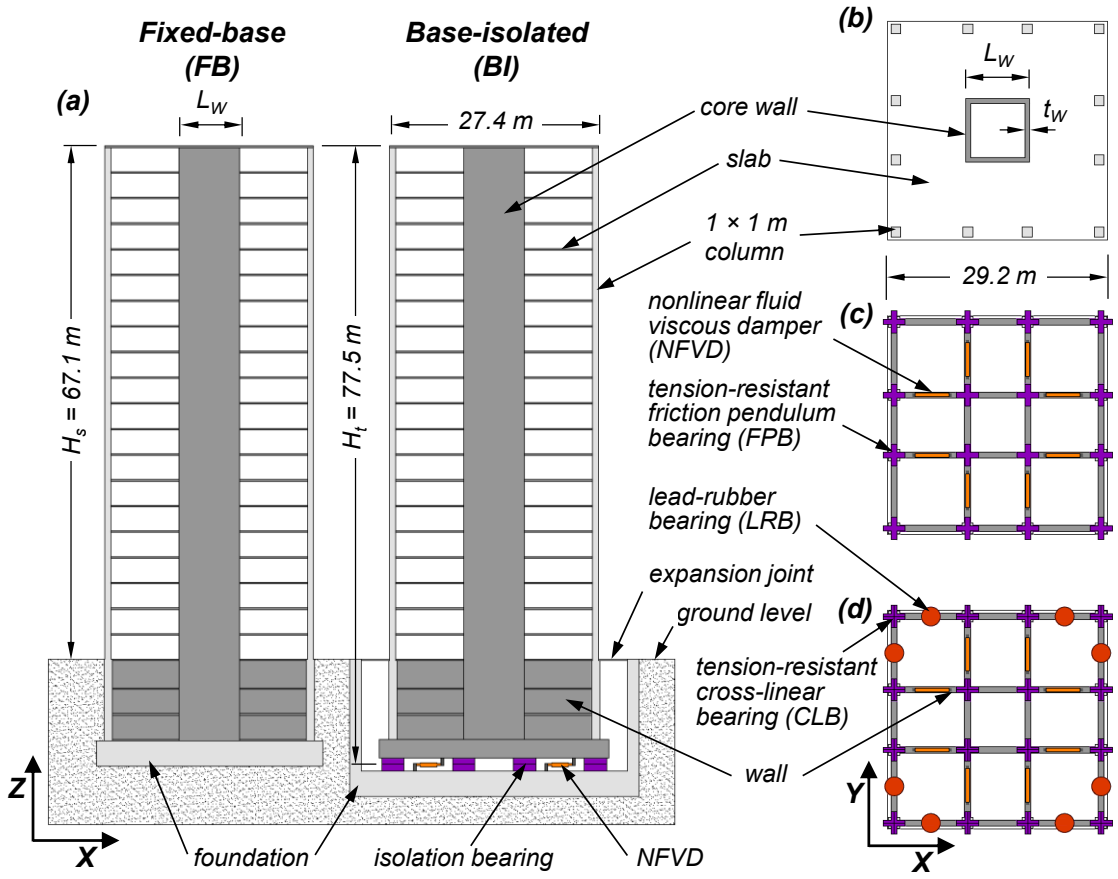

Figure 3-2. (a) Elevation of the 20-story buildings; (b) Floor plan-view above ground; (c) Plan-view of isolation system 1; and (d) Plan-view of isolation system 2.

Concrete with specified compressive strength $f_c^{'}$ = 48 MPa and steel with specified yield strength f_y = 414 MPa are used. The corresponding expected material properties used in the analysis are $f_{c,e}^{'}$ = 72 MPa and $f_{y,e}$ = 455 MPa. Table 3-2 lists the longitudinal reinforcement ratio, ρ_l, of the wall, the axial load of the wall at the ground level, P, divided by the cross-sectional area of the wall A_g times $f_{c,e}^{'}$ as well as the flexural strength (using expected material properties) of the wall section at the ground level, M_b, for bending about the Y-axis when the outer longitudinal reinforcement of the wall reaches 1% tensile strain. The 1 m x 1 m columns have a ρ_l equal to 1.0%. The slab reinforcement consists of #5 bars every 0.3 m in the two horizontal directions, both top and bottom. Below ground a grid of RC walls is used to distribute forces to the foundation and isolation system. The layout of the isolation systems of the BI buildings is shown in Figure 3-2(c) and (d). For the BI buildings, the seismic weight of each floor below ground is 1.5 times that of each floor above ground. A stiff diaphragm consisting of a RC slab and RC beams is assumed (above and below the isolation devices).

Uniaxial horizontal seismic excitation along the X-axis with or without concurrent vertical excitation is considered for all buildings.

Table 3-2. Characteristics of the seven buildings.

	Building type	**Fixed base**	**BI T_{is}=4 s**	**BI T_{is} = 5 s**		**BI T_{is} = 6 s**		
	Building name	**FB**	**BI4**	**BI5a**	**BI5b**	**BI6a**	**BI6b**	**BI6c**
	Type of isolation system	**N/A**	**Isolation system (IS) 1**					**IS2**
Superstructure	Total seismic weight, W_t (MN)	154*	200	207	200	206	200	206
	Core wall length, L_w (m)	9.1	9.1	10.4	9.1	9.1	9.1	9.1
	Core wall thickness, t_w (m)	0.51	0.51	0.61	0.51	0.61	0.51	0.51
	Wall long. reinf. ratio, ρ_l (%)	1.0	1.2	2.0	1.2	2.0	1.2	2.0
	Wall axial load ratio, $100P/\left(A_g f'_{c,e}\right)$	5.3	5.3	4.5	5.3	4.8	5.3	4.8
	M_b of wall at ground level (MN-m)	644	711	1438	711	1130	711	1130
Isolation system	Curv. radius of pend. bearing R_p (m)	N/A	4.0	6.2		9.0		N/A
	Diameter of LRBs (m)		N/A					1.5
	Numb. of 13 mm thick rubber layers							42
	Diameter of lead core (mm)							254
	Individual NFVD C_{ND} (MN-s$^{0.3}$/m$^{0.3}$)		N/A	1.68		2.10		2.85
	K_{is} (MN / m)		50	33.4	32.3	22.9	22.2	22.6

Notes *: For the FB building only the part above ground is considered (W_s=W_t) **

3.3.1 Fixed-base (FB) building

The majority of inelastic deformations for the FB building would typically be expected to be concentrated at a single flexural plastic hinge in the wall near ground level. Modal response spectrum analysis as prescribed in ASCE 7-10 with a response modification factor of R = 5, and the square root of sum of squares (SRSS) modal combination rule was used to obtain the design lateral forces. The design base shear force is V_u = 0.093W_t (W_t: the total seismic weight of the building – see Table 3-2). The wall was designed to resist the design moment, ignoring the contribution of framing action between the wall, the slab, and the columns.

3.3.2 Base-isolated (BI) buildings

Six BI buildings were studied. Five of the buildings (BI4, BI5a, BI5b, BI6a, and BI6b) were isolated with 16 tension-resistant friction pendulum bearings (FPBs) and 8 nonlinear fluid viscous dampers (NFVDs). Building BI6c used an isolation system that combines 12 very low-friction tension-resistant cross-linear bearings (CLBs), 12 lead-rubber bearings (LRBs), and 8 NFVDs. Both systems are described in more detail below. See Table 3-2 for the main characteristics of the isolation devices studied herein. The reader is referred to [19–23] for general characteristics of the isolation and damping devices used. It is assumed that both isolation systems are designed in such a way in order for the isolation devices to be replaceable.

The horizontal static force versus horizontal static displacement of both isolation systems was idealized with the bilinear relation shown in Figure 3-3(a). Three isolation periods, T_{is} = 4, 5, and 6 s, were investigated, where $T_{is}=2\pi\sqrt{m_t/K_{is}}$; m_t is the total mass of the building, and K_{is} the post-yield tangent stiffness of the isolation system; see Figure 3-3(a). The number after "BI" in the name of each of the six BI buildings describes the tangent isolation period, T_{is}, of the building; see Table 3-2. For all isolation systems considered, the amount of viscous damping was chosen in order for the isolation bearings to develop less than 0.9 m of horizontal displacement at the MCE level of shaking. The design of the wall above the ground level of the six BI buildings is described in Section 3.3.2.2.

3.3.2.1 Isolation systems

Isolation system 1: As shown in Figure 3-2(c), this isolation system combines 16 tension-resistant FPBs and 8 NFVDs. The FPBs consist of two orthogonal cylindrical rails interconnected by a housing slider assembly, which permits sliding in two orthogonal directions [20]. These bearings have significant displacement capacity (up to 1.5 m), a tension force capacity up to 9 MN, and a compression force capacity up to 133 MN [20]. Statically, the horizontal force versus horizontal displacement relation of this isolation system when loaded with vertical force F_V is shown in Figure 3-3(a), with the sliding stiffness K_{is} = $|F_V|$ / R_P, where R_P is the radius of curvature of the FPBs; see Table 3-2. Note that the relation between K_{is}, R_p, and F_V is maintained, both for compression and tension force F_V. A friction coefficient μ = 0.03 was used, resulting in $F_y = 0.03W_t$ which is more than the required resistance to wind equal to $0.017W_t$ according to ASCE 7-10. For all the FPBs, Δ_y = 2 mm. The force-velocity relation of each of the NFVDs used is $F_{ND} = \text{sgn}(V)C_{ND}|V|^{\alpha}$, where F_{ND} is the damper force, C_{ND} is the damper constant (see Table 3-2), V the velocity, and α=0.3 is the nonlinearity factor. Building BI4 did not require NFVDs, because at T_{is} = 4 s the peak isolator displacements did not exceed the isolator displacement capacity.

Isolation system 2. As shown in Figure 3-2(d), this isolation system combines 12 very low-friction (μ = 0.003) tension-resistant CLBs, 12 LRBs, and 8 NFVDs (α = 0.3). CLBs have been used in recent large-scale shake table tests [26] and have the following characteristics: (1) they consist of two orthogonal flat rails that permit sliding in two orthogonal directions; (2) they have a deformation capacity up to 1 m [21]; and (3) they are are capable of resisting large tension (up to 8.7 MN) and compression (up to 61 MN) forces.

1.5-m-diameter LRBs [19] have a horizontal displacement capacity of about 1 m (depends on the level of vertical force) and vertical compression force up to 40 MN. The lead core has a diameter equal to 254 mm and height h_L = 680 mm. The rubber layers are 13 mm thick. For this isolation system, $K_{is} = 12G_rA_r/t_r$, where G_r = 0.6 MPa is the shear modulus of the rubber, t_r is the total thickness of the rubber in each LRB, and A_r is the cross-sectional area of the rubber in each LRB. Also $K_0 = 12(G_LA_L/h_L + G_rA_r/t_r)$ and $\Delta_y = \tau_L h_L/G_L$, where G_L =150 MPa is the effective shear modulus of lead, τ_L = 10 MPa is the yield stress of lead, and A_L is the cross-sectional area of the lead core. For all the above, $K_0 = 6.9K_{is}$. The relations between material properties and stiffness properties of the bearings can vary based on the LRB manufacturer. The design of this isolation system assumes a loose-bolt connection between the LRBs and the RC slab, with beams comprising the diaphragm of the isolation system so as not to induce tension in the LRBs. The main difference in the horizontal force-horizontal displacement (see Figure 3-3(a)) of isolation systems 1 and 2 is that the latter has a smaller K_0; CLBs were used at the corners due their high vertical compression capacity.

3.3.2.2 Isolated superstructure

Three levels of flexural strength of the walls were studied in the six BI buildings. The design base shear force of the superstructure of all BI buildings exceeded $V_u = 0.098W_t$ as required per ASCE 7-10. Using the first-mode lateral force distribution computed with modal analysis to distribute V_u along the height of the building resulted in a design bending moment at the ground level that ranged between $M_{u,min} = 0.37H_tV_u$ and $M_{u,min} = 0.39H_tV_u$ for the six BI buildings, where H_t the building roof height from the isolation system; see Figure 3-2. The design of buildings BI4, BI5b, and BI6b incorporated a wall (see Table 3-2) with M_b that was 1.1 times $M_{u,min} / \varphi$, where $\varphi = 0.9$ is the strength reduction factor for flexure. The design of buildings BI6a and BI6c incorporated a wall with M_b equal to 1.8 times $M_{u,min} / \varphi$; while building BI5a was designed with a wall with M_b equal to 2.2 times $M_{u,min} / \varphi$.

3.4 Numerical Modeling

This 2-D numerical study used the Open System for Earthquake Engineering Simulation (OpenSees) software [36]. The numerical model is shown in Figure 3-3(b). Fiber-section force-based nonlinear beam-column-elements were used to model the RC wall and columns above ground. Material models *Concrete03* and *Steel02* were used. One element per story with four integration points was used for the walls and the columns. All slabs were modeled using beam-with-hinges elements, with a 0.9-m-long fiber-section plastic hinge at the ends of each element. The full width of the slab was considered effective in resisting bending. Horizontal rigid linear beam elements were used to model the length of the wall at each story. Linear beam elements of high rigidity were used to model the superstructure below ground. A P-delta geometric transformation was used in all beam elements. The model did not account for flexure-shear interaction, bar buckling, or bar fracture in the RC members. The FB building was modeled fixed at the ground level. Expected material properties (see Section 3) for concrete and steel were used in the analysis. The elastic modulus and the strain-hardening factor of steel were E_s = 200 GPa, and b = 0.02, respectively.

Uncoupled horizontal, vertical, and rotational zero-length spring elements were used to model the force-displacement behavior of the isolators in the corresponding directions. Modeling the dependence between sliding stiffness, K_{is}, of the FPBs and the vertical force acting on them was investigated and found to have a negligible effect on all the response quantities except the horizontal force of the individual FPBs and the horizontal force distribution in the diaphragm of the isolation system. For this reason, this interaction was not modeled in this study. The interaction between vertical force and horizontal stiffness in the LRBs was also ignored. A bilinear horizontal force-horizontal displacement relation was used to model the LRBs and the FPBs. The vertical stiffness in compression, and tension used for the tension-resistant friction pendulum bearings and the tension-resistant cross-linear bearings was $K_{v,c}$ = 12 MN/mm and $K_{v,t}$ = 1.2 MN/mm, respectively. The NFVDs were modeled as zero length elements, with an assigned viscous material with the force-velocity relationship $F_{ND} = \text{sgn}(V)C_{ND}|V|^{\alpha}$. Rayleigh initial stiffness and mass proportional damping with 2% damping ratio in the first and the third mode was used. Horizontal and vertical lumped masses were used at five nodes per floor – two column nodes, two mid-span slab nodes, and the central core wall node. Vertical forces due to gravity were applied at the same nodes.

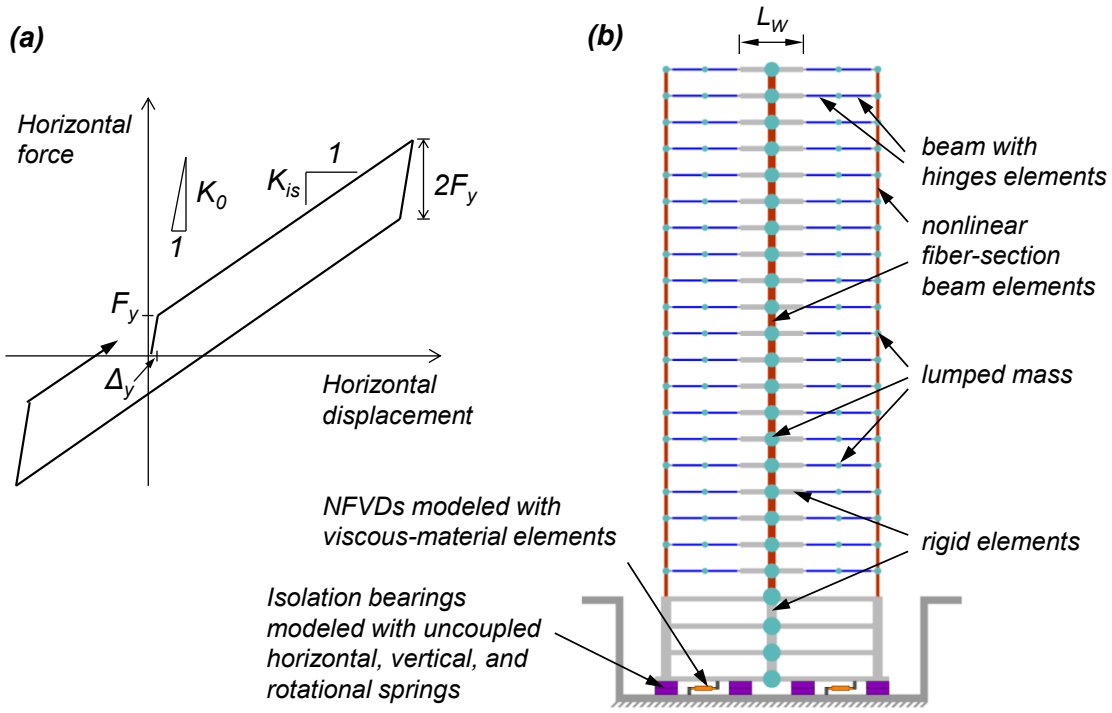

Figure 3-3. (a) Idealization of horizontal force (static) versus horizontal displacement of the two isolation systems; (b) schematic of the numerical model of the BI buildings.

3.5 Results of Numerical Analysis

3.5.1 Modal Analysis

Table 3-3 lists the first-mode period, T_1, and first-mode mass, m_1, divided by m_t. In all buildings cracked concrete material properties were used in the modal analysis with the following effective flexural rigidities: (1) E_cI_e=0.25E_cI_g for the base story of the wall and the columns; (2) E_cI_e=0.5E_cI_g for the walls and the columns above the base story; and (3) 0.35E_cI_g for the slabs, where I_g is the gross-section moment of inertia, and E_c = 40 GPa is the concrete elastic modulus. The modal analysis modeled the isolation systems using the stiffness K_{is}; see Figure 3-3(a). For the BI buildings, the first mode mass m_1 was 0.99M_t. Thus when the isolation system responds with the tangent stiffness K_{is}, the contribution of the higher modes of response is expected to be negligible. Table 3-3 also reports the first mode bending moment at the ground level, $M_{1,b}$, divided by the first mode shear force at the isolation level, $V_{1,iso}$. The ratio of $M_{1,b}$ / $V_{1,iso}$ ranged between 0.37H_t and 0.39H_t.

3.5.2 Response History Analysis using Sets of Motions Scaled to the DE and MCE

Arithmetic mean (for brevity referred to as mean) values of different response parameters of the seven buildings are summarized in Table 3-3 and shown in Figure 3-4 for the DE and MCE level of excitation. For each of the DE and MCE levels of excitation, the mean values obtained from the analysis using a set consisting of 14 ground motions, each of them rotated to the principal direction, are reported. This section presents the results of the analysis using only the horizontal component of excitation in the principal direction (without using the vertical component of excitation). The responses are presented in terms of height, h_i, of floor i from the ground level, divided by the roof height above the ground level, H_s. The presented responses are the horizontal displacement relative to the base of the building (considered the ground level for the fixed-base building and the base of isolation system for the BI buildings), D_i, divided by H_s, the interstory drift ratio, Θ_i, the shear force of the wall, V_i, divided by W_s (the seismic weight of the structure above ground), and the absolute floor acceleration A_i. Floor accelerations, shear forces, and vertical forces of the isolation bearings were filtered with a finite impulse response low-pass filter order 5000 and 20 Hz cut-off frequency to remove numerically induced spikes due to sudden changes in the tangent modulus of the materials used. To quantify variability, the coefficients of variation for selected response quantities at the MCE-level are presented in Table 3-4.

The FB building developed significant inelastic deformations in the wall at the DE and MCE levels where the roof drift ratio reached 1.29%, and 2.23%, respectively. The corresponding peak interstory drift ratios along the building height were 1.52% and 2.62%. The peak longitudinal reinforcement tensile strain in the wall (for brevity referred to as wall tensile strain) was computed at the bottom story and is 2.16% and 3.26% at the DE and MCE, respectively. At the MCE, low levels of inelastic deformations developed in the columns and the floor slabs (less than 0.51% tensile strain in the longitudinal reinforcement). For the above response parameters: the values at the MCE were 1.5 to 1.7 times the values at DE.

For the DE and MCE hazard levels, the shear force in the wall at the ground level was 0.36W_s, corresponding to a shear stress in the web of the wall, τ_w, of 0.088$f'_{c,e}$ and 0.086$f'_{c,e}$, respectively, which exceeded the maximum allowable stress of 0.078$f'_{c,e}$ ($8\sqrt{f'_{c,e}}$ in psi) prescribed in ACI 318-11. Such high level of shear stresses with concurrent significant inelastic deformations in the plastic hinge region of a wall resisting vertical force of P=0.053$f'_{c,e}A_g$ may cause major damage, including crushing of concrete and bar buckling

[39]. Note that the computed base shear force significantly exceeded the design base shear force. This is due to the significant contribution of higher modes in the response of tall RC wall buildings [39–11, 17, 18].

Results of experimental studies have shown that non-planar walls [37, 38, 39] subjected to cyclic static loading develop major damage for drift ratios of 1.5% to 2.5%. C-shape walls with ρ_l = 0.8% to 1.1%, and P = 0.059 $f_c^{'} A_g$ to 0.065 $f_c^{'} A_g$ experienced bar buckling at 2% drift ratio and vertical crushing of concrete at drift ratios of 2.25% to 2.5% [37]. T-shape wall specimens with ρ_l = 1.2%, P = 0.074 $f_c^{'} A_g$ to 0.087 $f_c^{'} A_g$ [38] experienced longitudinal bar buckling at drift ratios of 1.5% to 2.0%. A U-shape wall specimen with ρ_l = 1.0%, and P = 0.045 $f_c^{'} A_g$ [39] experienced web crushing at a drift ratio of 2.5%. The maximum shear stress of the web at crushing of this specimen was 0.06 $f_c^{'}$ ($f_c^{'}$ = 54.7 MPa), which is only 0.67 times the maximum shear stress allowed by ACI 318-11.

Considered as an average value along the height of the building, the FB building developed large floor accelerations of 0.58g (0.89 times peak ground acceleration, PGA) and 0.77g (0.79 times mean PGA) at the DE and MCE, respectively.

Presented next is the mean response of buildings BI5a and BI6a, which were designed with isolation system 1 and a wall with M_b equal to 2.2 and 1.8 times, respectively, the minimum required. The superstructure of these buildings experienced nominally elastic response at the MCE; the computed wall tensile strain was less than 0.32%. At the MCE, the interstory drift ratio for these buildings was only 0.36% to 0.51% (compared to 2.62% for the FB). For this level of interstory drift ratio, standard gypsum partitions remained undamaged [40]. The roof drift ratio of these buildings was 0.80% to 0.86% at DE (compared to 1.29% for the FB) and 1.57% to 1.62% at the MCE (compared to 2.23% for the FB).

Buildings BI5a and BI6a developed horizontal displacement of the isolation system of 0.84 m to 0.87 m at the MCE; this is within the displacement capacity of the bearings. At the MCE, the maximum compression force in an individual outer bearing was 26.4 MN (building BI5a), which is within the capacity of available FPBs. In terms of mean response at the MCE, these bearings approach but do not experience tension; this is why in Table 3-3 the minimum compression force is reported (1.16 MN for BI4).

The total force developed in the four NFVDs, $F_{ND,tot}$, for buildings BI5a and BI6a was 0.030W_t to 0.036W_t at DE and 0.035W_t to 0.043W_t at the MCE. For $F_{ND,tot}$ = 0.043W_t (building BI6a), the corresponding force in each of the NFVDs was F_{ND} = 2.2 MN.

At the DE, buildings BI5a and BI6a developed shear forces in the wall at the ground level that were 0.13W_s, and 0.11W_s, respectively, values that are less than 0.36 times that of the FB building. The corresponding shear forces at the MCE were 0.19W_s and 0.16W_s, respectively (compared to 0.36W_s for the FB). The same level of shear force reduction was observed along the entire height of buildings BI5a and BI6a.

For the same reason, these buildings developed average floor accelerations along the height at the DE (0.20g to 0.22g) and at the MCE (0.26g to 0.27g) that were less than 0.35 times the values computed for the FB building. Note the almost constant acceleration in the bottom 75% of the height of the BI buildings; see Figure 3-4.

Next the response of buildings BI4, BI5b, and BI6b that were designed with isolation system 1 and a wall of M_b equal to 1.1 times the minimum required according to ASCE 7-10 are considered. At the DE, building BI4 developed an interstory drift ratio of 0.82% and wall tensile strain of 1.1%. The superstructure of buildings BI5b and BI6b responded elastically to the DE with an interstory drift ratio of 0.38% to 0.43% and a wall tensile strain of 0.27% to 0.35%. The level of inelastic deformation of the superstructure of these three buildings at the MCE varied significantly, increasing with decreasing T_{is}.

The interstory drift ratio at the MCE of buildings BI6b, BI5b, and BI4 was 0.81%, 1.18%, and 2.62% (equal to that of the FB building), respectively. The corresponding values of wall tensile strain were 1.06%, 1.62%, and 3.20%. Note that building BI6b experienced nominally elastic response at the MCE. Building BI5b developed displacements and forces in the isolation system, shear forces in the wall, and floor accelerations similar to these of building BI5a.

Finally, the response of building BI6c is presented, which is the only building that was designed with isolation system 2. The superstructure of building BI6c experienced nominally elastic response at the MCE with an interstory drift ratio 0.58%. This building developed 0.86 m horizontal displacement of the isolation system; the total force in the 4 NFVDs was equal to $0.058W_t$ at the MCE, which is about 1.4 times that of building BI6a. This was the smallest floor accelerations among all six BI buildings ($0.18g$ at the DE and $0.24g$ at the MCE) with the smoothest shape along the height of the building among all the BI buildings. This is due to the less abrupt change in the horizontal stiffness in isolation system 2 compared to isolation system 1.

Table 3-3. Modal properties and mean response quantities computed using nonlinear response history analysis (NRHA).

	Building name (isolation system)	**FB**		**BI4 (IS1)**		**BI5a (IS1)**		**BI5b (IS1)**		**BI6a (IS1)**		**BI6b (IS1)**		**BI6c (IS2)**	
Modal properties	First mode period, T_1 (s)	2.0		4.3		5.2		5.2		6.2		6.2		6.2	
	First mode mass m_1 divided by m_t	0.66		0.99		0.99		0.99		0.99		0.99		0.99	
	First mode bending moment at ground level, $M_{1,b}$, divided by $V_{1,iso}$*	N/A		$0.39H_t$		$0.37H_t$		$0.38H_t$		$0.37H_t$		$0.37H_t$		$0.37H_t$	
	Excitation level	DE	MCE	DE	MCE	DE	MCE	DE	MCE	DE	MCE	DE	MCE	DE	MCE
Superstructure above ground	Roof drift ratio, D_r / H_s, (%)	1.29	2.23	1.36	2.94	0.80	1.57	0.98	2.08	0.86	1.62	0.90	1.80	0.88	1.72
	Interstory drift ratio, Θ_i, (%)	1.52	2.62	0.82	2.62	0.15	0.36	0.43	1.18	0.28	0.51	0.38	0.81	0.29	0.58
	Average floor acceleration, A_{ave} (g)	0.58	0.77	0.23	0.32	0.20	0.27	0.22	0.27	0.22	0.26	0.23	0.27	0.18	0.24
	Wall shear force, ground level, V_b / W_s	0.36	0.36	0.15	0.30	0.13	0.19	0.14	0.21	0.11	0.16	0.12	0.18	0.12	0.17
	Web shear stress of wall, τ_w / $f'_{c,e}$	0.088	0.086	0.037	0.072	0.024	0.034	0.034	0.052	0.024	0.033	0.030	0.044	0.025	0.035
	Wall long. reinf. tensile strain (%)	2.16	3.26	1.10	3.20	0.07	0.25	0.35	1.62	0.11	0.32	0.27	1.06	0.12	0.45
	Column long. reinf. tensile strain (%)	0.16	0.28	0.09	0.31	0.02	0.03	0.04	0.14	0.03	0.04	0.03	0.08	0.03	0.05
	Slab long. reinf. tensile strain (%)	0.30	0.51	0.16	0.51	0.03	0.08	0.08	0.23	0.06	0.10	0.08	0.16	0.06	0.11
Isolation system	Horizontal displacement, D_{is}, (m)	N/A		0.52	0.78	0.47	0.87	0.44	0.76	0.45	0.84	0.43	0.79	0.46	0.86
	Maximum compressive force of individual bearing (MN)			21.5	24.8	21.8	26.4	20.3	22.6	21.0	23.7	19.8	21.7	21.1	24.2
	Minimum compression force of individual bearing (MN)			3.58	1.16	4.17	1.59	4.64	2.59	4.70	2.48	5.12	3.31	4.62	2.23
	Total force of the 4 NFVDs, $F_{ND,tot}$ / W_t			N/A		0.030	0.035	0.031	0.035	0.036	0.043	0.037	0.044	0.050	0.058
	Total horizontal force, $F_{is,tot}$ / W_t			0.16	0.23	0.12	0.19	0.12	0.17	0.10	0.15	0.10	0.15	0.11	0.16

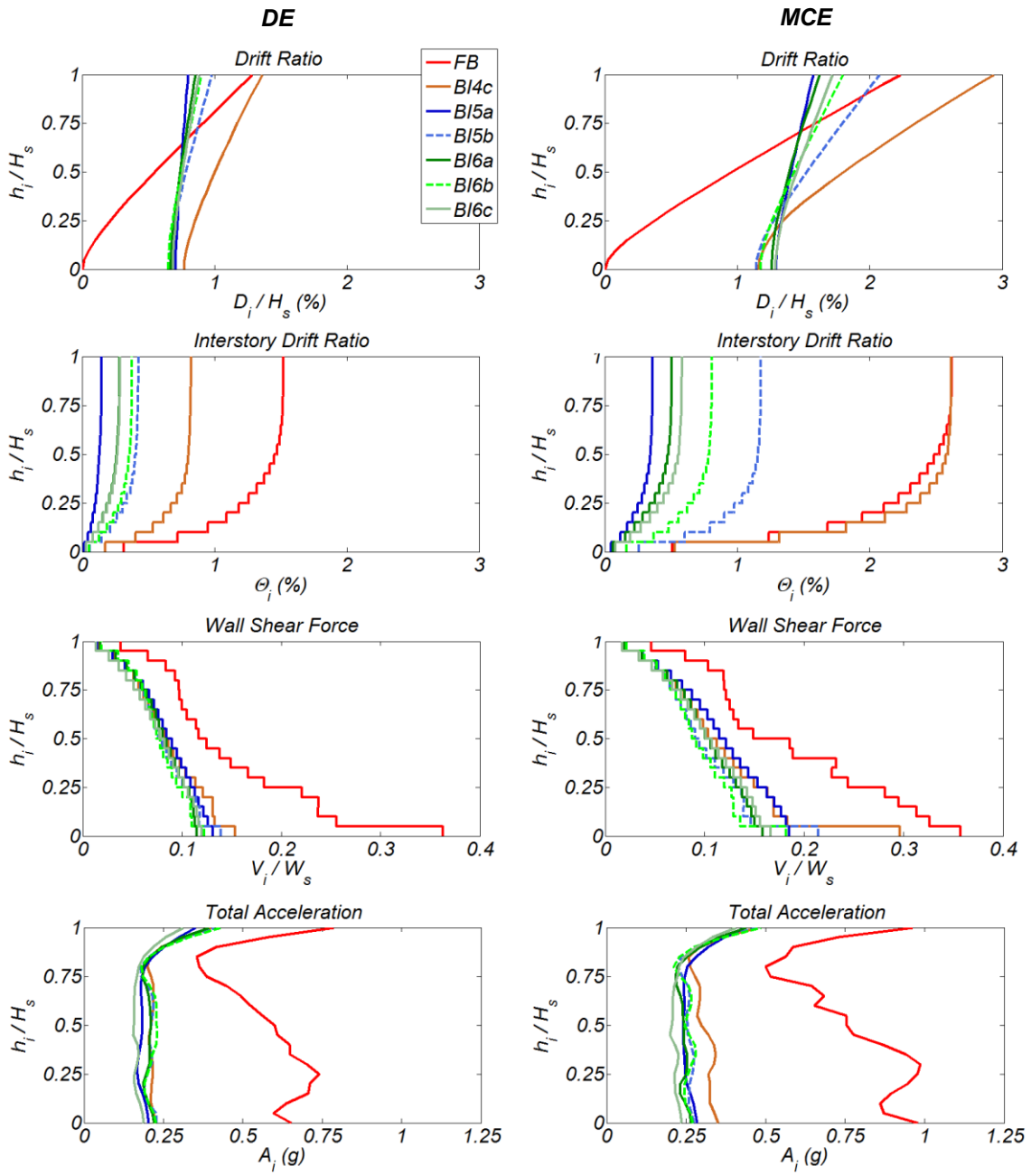

Figure 3-4. Mean responses along the building height at DE and MCE hazard level using the principal direction horizontal components of Set 1 and Set 2 ground motions.

Table 3-4. Coefficients of variation of mean responses for the MCE-level of shaking.

	Building name	FB	BI4	BI5a	BI5b	BI6a	BI6b	BI6c
Above ground	Interstory drift ratio, Θ_i, (%)	0.52	0.82	0.77	0.85	0.67	0.71	0.72
	Average floor acceleration, A_{ave} (g)	0.45	0.33	0.28	0.34	0.25	0.34	0.38
	Wall shear force, ground level, V_b / W_s	0.20	0.52	0.33	0.48	0.32	0.51	0.32
Isolation system	Horizontal displacement, D_{is}, (m)	N/A	0.37	0.52	0.46	0.54	0.50	0.54
	Maximum compressive force of individual bearing (MN)		0.12	0.20	0.13	0.14	0.11	0.16
	Minimum compression force of individual bearing (MN)		1.73	1.84	1.04	1.16	0.73	1.36

3.5.3 Effect of Vertical Ground Motion Component Excitation

The effect of vertical component of ground motion is studied next. The analysis described in Section 5.2 (using only the horizontal component of the motions) was repeated for buildings FB, BI4, and BI6a using concurrent horizontal and vertical excitation. Mean values of selected response parameters, summarized in Table 3-5, clearly indicate that the vertical component of excitation affects significantly only the peak tension force (or the smallest value of compression force for the case where tension is not developed). The only building that resulted in vertical tension force in the bearings (mean value for fourteen ground motions) was building BI4. The 0.19 MN of tension force that the bearings of this building developed is much smaller than the tension force capacity of the bearings (9 MN). The peak compression force the bearings experience increased by less than 18%. For the response parameters of the superstructure, there was a maximum 15% increase observed for wall base shear force for the FB building and average floor acceleration for building BI4.

Table 3-5. Mean response quantities for analysis with and without vertical ground motions components scaled at the MCE-level.

	Building name	FB		BI4		BI6a	
	Excitation Components: horizontal only (X); horizontal and vertical (X+Z)	X	X+Z	X	X+Z	X	X+Z
Superstructure above ground	Roof drift ratio, D_r / H_s, (%)	2.23	2.23	2.94	2.94	1.62	1.63
	Interstory drift ratio, Θ_i, (%)	2.62	2.63	2.62	2.62	0.51	0.51
	Average floor acceleration, A_{ave} (g)	0.77	0.80	0.32	0.37	0.26	0.30
	Wall shear force, ground level, V_b / W_s	0.36	0.41	0.30	0.30	0.16	0.16
	Wall long. reinf. tensile strain (%)	3.26	3.25	3.20	3.18	0.32	0.33
Isolation system	Horizontal displacement, D_{is}, (m)	N/A		0.78	0.77	0.84	0.85
	Maximum compressive force of individual bearing (MN)			24.8	27.5	23.7	28.0
	Minimum compression force of individual bearing (MN)			1.17	-0.19	2.48	0.71

3.5.4 *Response History Analysis to Unscaled Near-Fault Pulse-Type Ground Motions*

The response of buildings FB, BI5a, BI6a, BI6b, and BI6c to four unscaled historical pulse-type near-fault ground motions is considered next. Depending on the site location with respect to the fault rupture, near-fault ground motions may include strong acceleration, velocity, and displacement pulses as a result of directivity effects, with the predominant period, T_p, that generally increases with increasing earthquake magnitude [41, 42]. Motions that include strong long-period pulses may impose large demands in long-period FB and BI tall buildings that may exceed those expected at the MCE.

Table 3-6 summarizes the available ground motion records for those earthquakes of magnitude larger than M7 that are less than 10 km from the fault rupture, R_{rup}. The number of records with R_{rup} < 10 km for each of these earthquakes is also listed in this Table. All ground motions included in the PEER database [43] were considered. Note that not all of the 47 motions included in Table 3-6 were affected by forward directivity. More than two-thirds of these 47 records were recorded during the 1999 M7.6 Chi-Chi, Taiwan, earthquake and only five in the U.S. The small number of near-fault records from large magnitude (M > 7.0) earthquakes results in large uncertainty in determining the seismic hazard close to fault rupture and makes problematic the selection of pulse-type near-fault motions with specific combination of characteristics such as earthquake magnitude, source mechanism, R_{rup}, and site class.

The main characteristics of the four pulse-type near-fault ground motions used in the analysis of the FB and the four BI buildings are listed in Table 3-7. The ground velocity time series and the linear SDOF spectra of the four motions (horizontal component in the principal direction) are shown in Figure 3-5 and Figure 3-6, respectively. The principal horizontal components are obtained for all four motions using the two-node-3 DOF model of buildings BI6a as described in Section 2. The characteristics summarized in Table 3-7 are the peak ground velocity (PGV) of the principal, FN, and FP components, the average shear wave velocity in the top 30 m, $\overline{v_s}$, and the predominant period, T_p, of the pulse contained in the ground velocity time history. The T_p as computed using wavelet analysis [41] is reported here. For all these four motions R_{rup} < 2.1 km. The linear spectral displacements, *Sd*, of the four motions exceed the MCE design spectrum over different period ranges for the site considered herein, with R_{rup} = 2 km from the Hayward fault, which has the potential to produce an M7.2 earthquake [44]. For T = 5 s FN components of motions TCU 52, 68 and Tabas result in *Sd* equal to about 1.5 times that of the MCE design spectrum. For T = 6 s, FN components of motions TCU 52, 68 result in *Sd* equal to about 1.5 times that of the MCE design spectrum. At 6 s, the spectral demand of the principal component of TCU 68 is 1.6 times that of the FN component.

Table 3-6. Available near-fault records with R_{rup}<10 km for earthquakes with $M \geq 7.0$.

	Cape Mend. U.S.	Duzce Turkey	Landers U.S.	Tabas Iran	Kocaeli Turkey	Chi-Chi Taiwan	Wechuan China	Denali Alaska
Year	1992	1999	1992	1978	1999	1999	2008	2002
Magnitude	7.0	7.1	7.4	7.4	7.5	7.6	7.9	7.9
Number of records	2	6	1	1	2	32	2*	1

Notes: *PEER database does not include the motions from the 2008 M7.9 Wenchuan, China earthquake.

Table 3-7. Characteristics of the four near-fault ground motions used.

Station	Earthquake name, year and magnitude	Source mechanism	$\overline{v_s}$ (m/sec)	PGV(m/s)			T_p (sec)
				FN	FP	Prin-cipal	
El Centro Array #6 (ElCen6)	Imperial Valley, 1979, M6.5	Strike slip	206	1.12	0.65	1.17	3.9
Tabas	Tabas, Iran, 1978, M7.4	Reverse	767	1.21	0.98	1.21	5.3
TCU52	Chi-Chi, Taiwan, 1999, M7.6	Reverse	579	1.65	1.13	1.75	12.7
TCU68			487	1.85	2.51	2.96	12.2

These four motions were selected because they include very strong long-period pulses that result in large demands, exceeding those at the MCE for the buildings studied here. Note that one or more of their key characteristics (see Table 3-7) are not consistent with the site studied for the following reasons: (1) the number of historically recorded near-fault motions affected by forward directivity with all their key characteristics consistent with the site studied here is practically zero; and (2) because this investigation aims to study how the FB and the selected BI buildings would respond in some of the most severe near-fault motions ever recorded.

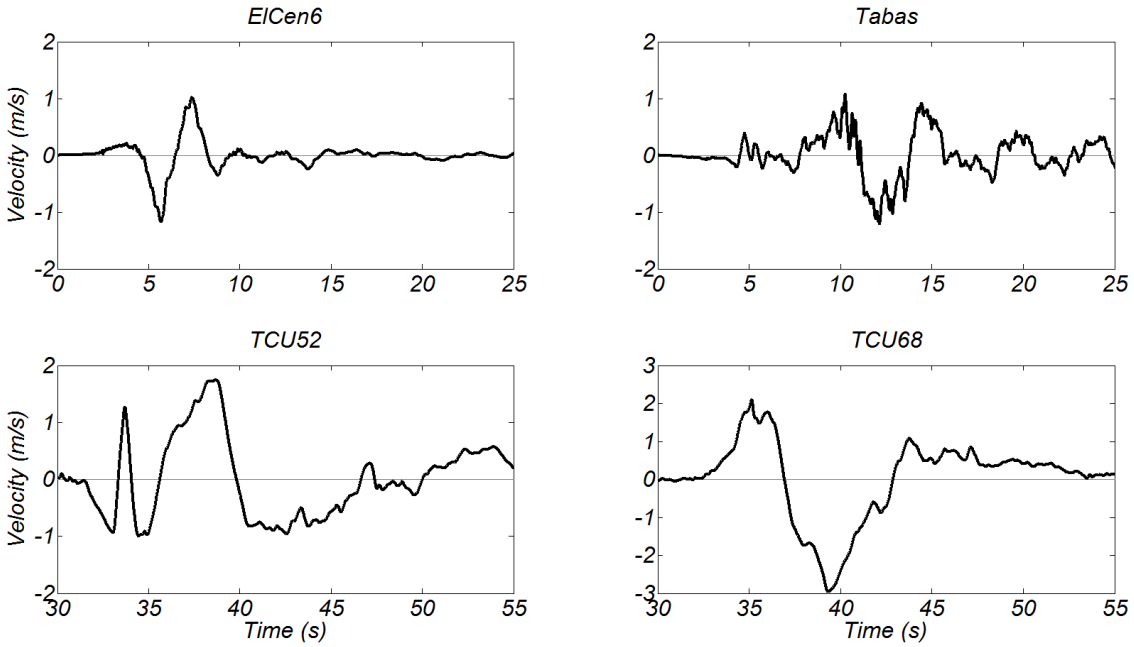

Figure 3-5. Ground velocity time history of the four near-fault ground motions in the principal horizontal direction.

Among all the motions currently available in the PEER database, the TCU68 motion results in the largest *Sd* in the period range of 6 to 10 s. The TCU52 and Tabas motions result in the third largest *Sd* at T = 5 s (after the TCU68 and TCU65 motions recorded in Chi-Chi earthquake); ElCen6 results in the fourth largest *Sd* at T= 3 s (after TCU52, 65, and 68 motions), all for ζ=5%. Note also that motions TCU52 and TCU68 also include some distinct pulses of period about 2.5 s in addition to the 12.7 s and 12.2 s periods described above, resulting in local peaks in *Sd* for T = 2.5 s. Motions TCU52 and TCU68 result in the largest *Sd* for T = 2.2 to 2.5 s (T_1 = 2 s for the FB building) among all motions included in the PEER database.

Figure 3-7 shows the NRHA results of the five buildings studied when subjected to the horizontal principal component of the four unscaled motions. The vertical component of excitation is not used here. The FB building reached roof drift ratios ranging between 1.6% and 3.5% (2.23% at the MCE), interstory drift ratios ranging between 1.8% and 3.9% (2.62% at the MCE), shear force in the wall ranging between $0.36W_s$ and $0.48W_s$ ($0.36W_s$ at the MCE), floor accelerations (average along the height of the building) ranging between $0.4g$ and $0.9g$ ($0.77g$ at the MCE), and wall tensile strain ranging between 2.8% and 5.1% (3.26% at the MCE).

The four BI buildings experienced less than 0.5% interstory drift when subjected to the ElCen6 and Tabas ground motions. Buildings BI5a, BI6a, and BI6c experienced less than 0.6% and 1.2% interstory drift when subjected to the TCU52 and TCU68 motions, respectively. Building BI6b reached 1.2% interstory drift for the TCU52 motion and 2.2% for the TCU68 motion.

The four BI buildings experienced less than 0.5 times the shear force compared to the FB building for the ElCen6, Tabas, and TCU52 motions, and 0.7 times the shear force compared to the FB building for TCU68 motion. Building BI5a (due to the higher stiffness of the isolation plane) experienced in the largest shear force in the wall among the four BI buildings for all four motions. All four BI buildings experienced less than 0.7 times the average (along the height of the building) floor acceleration compared to that which developed in the FB building for all four motions, and just 0.33 times that of the FB building for the Tabas motion.

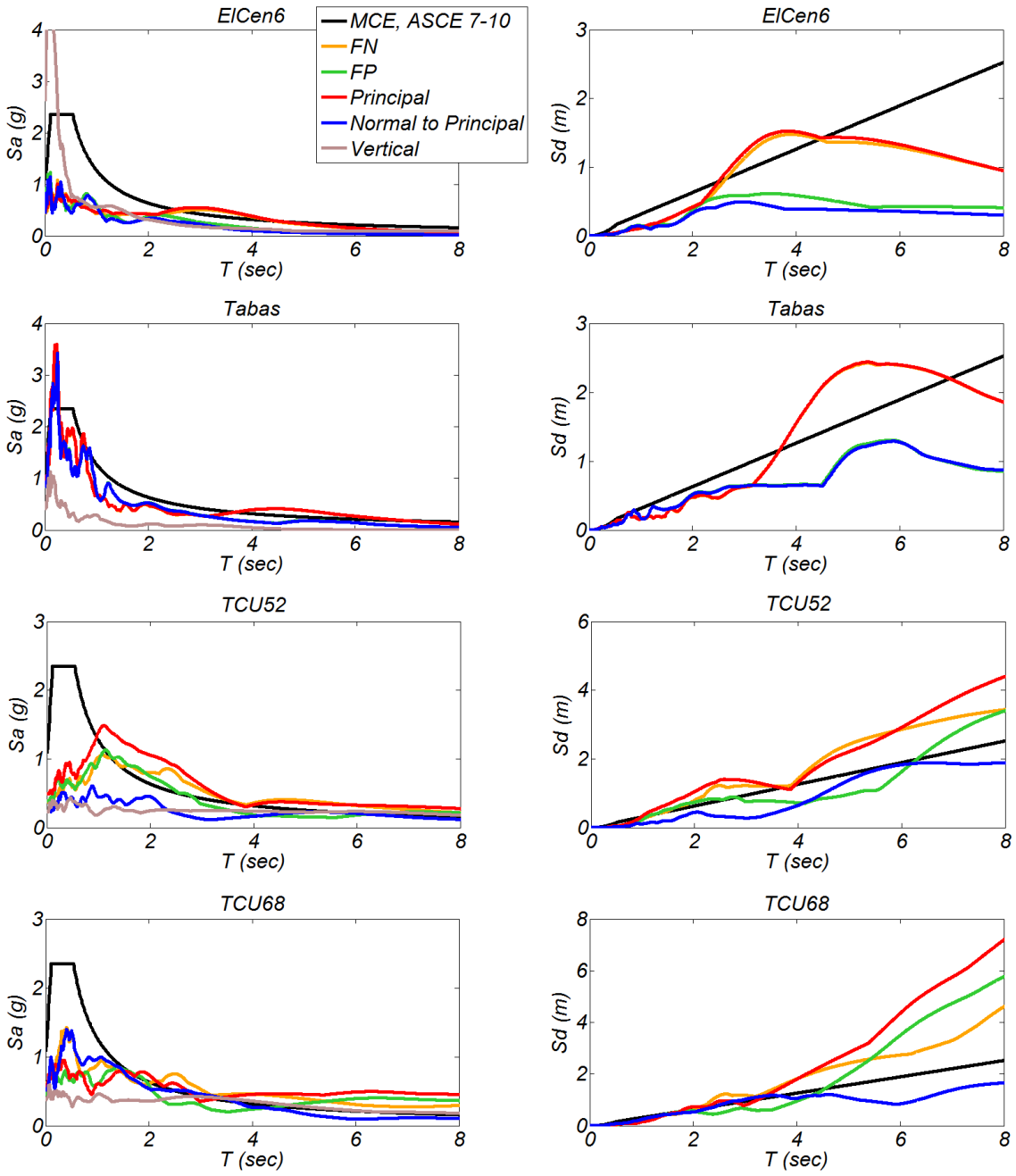

Figure 3-6. Acceleration and displacement linear response spectra for FN, FP, principal, normal to principal, and vertical (*Sa* only) components of the four near-fault historical records compared to the design spectra for the Berkeley, California, site; ζ=5%.

The horizontal displacement of the isolation system of the four BI buildings ranged between 0.65 m and 0.73 m for motion ElCen6, which was 0.82 times on average the corresponding displacement at the MCE. For the Tabas motion, D_{is} ranged between 0.72 m to 0.81 m, which is about 0.91 times that at the MCE. The corresponding range of D_{is} for motion TCU52 was between 1.12 to 1.24 m for building BI6a. Motion TCU68 resulted in the largest D_{is} = 1.54 m to 1.72 m. The level of D_{is} reached for TCU68 exceeded significantly the displacement capacity of the bearings used here as well as the displacement capacity of available LRBs. To design for such an extreme case would require FPBs with a larger displacement capacity than studied herein or a larger amount of viscous damping. For building BI6a, if the amount of viscous damping of the isolation plane increases to 3.2 MN-$s^{0.3}/m^{0.3}$ and 4.2 MN-$s^{0.3}/m^{0.3}$ then the computed peak displacement of the bearings for the TCU68 motion is 1.47 m, and 1.28 m, respectively.

Subjecting these five buildings to the combined horizontal principal and the vertical component of the ground motions resulted in less than 6% difference (compared to the case of excluding the vertical component) for all response parameters except the vertical forces in the bearings. The peak increase of the vertical compression force of the bearings computed for building BI6b subjected to ElCen6 motion was 30%, and the tension force computed in the bearings was equal to 2.3 MN.

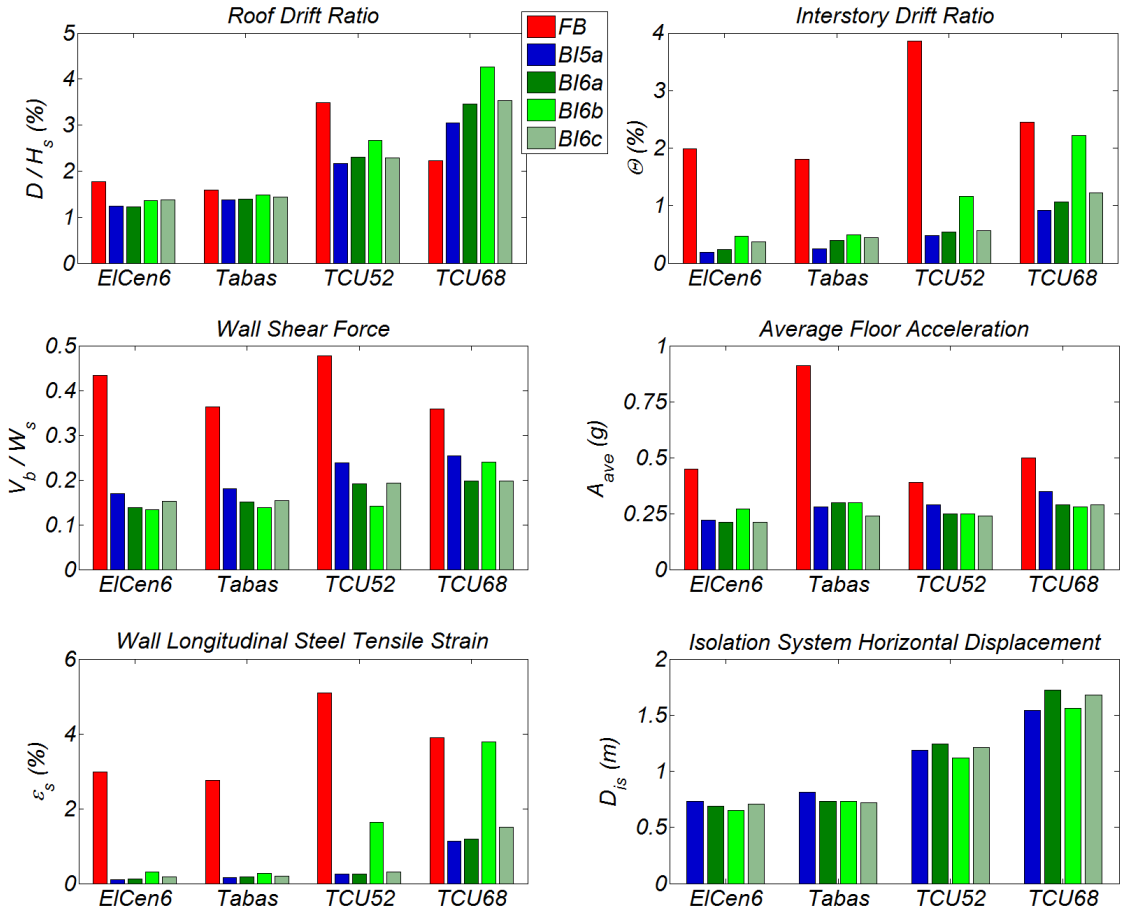

Figure 3-7. Response of the FB building and the four BI buildings to the four historical near-fault ground motions.

3.6 Summary and Conclusions

This chapter of the dissertation investigated the seismic response of six base-isolated (BI) buildings with three stories below ground and twenty stories above ground, and compared it to that of a similar fixed-base (FB) building. All buildings were hypothetically located in downtown Berkeley, California, 2 km from the Hayward fault, and were designed with a core wall to provide most of the lateral force resistance above ground. All buildings were designed to meet or exceed ASCE 7-10 design requirements. The design base shear force of the FB building was $0.098W_s$ (W_s: the seismic weight of the building above ground). Buildings BI4, BI5a, BI5b, BI6a, and BI6b used isolation system 1 that combined 16 tension-resistant friction pendulum bearings (FPBs) and 8 nonlinear fluid viscous dampers (NFVDs). Building BI6c used isolation system 2 that combined 12 very low-friction (μ=0.3%) tension-resistant cross-linear bearings (CLBs), 12 lead-rubber bearings (LRBs), and 8 NFVDs. Isolation periods T_{is} equal to 4 s (building BI4a), 5 s (buildings BI5a, and BI5b), and 6 s (buildings BI6a, BI6b, and BI6c) were studied. Building BI5a incorporated a wall design with flexural strength 2.2 times the minimum required by ASCE 7-10. Buildings BI6a and BI6c incorporated a wall design with M_b equal to 1.8 times the minimum required; for buildings BI4a, BI5b, and BI6b, M_b was equal to 1.1 times the minimum required.

Numerical models of all seven buildings were subjected to sets of 14 ground motions, the horizontal components rotated to the principal direction as defined by the angle to peak vector displacement of a biaxial two-node model of building BI6a subjected to FN and FP components simultaneously, and scaled to match the DE and the MCE design spectra. To study the effect of vertical ground motion components, buildings FB, BI4, and BI6a were subjected to both the principal direction horizontal and the vertical ground motion components. A representative subset of the studied buildings (FB, BI5a, BI6a, BI6b, BI6c) was also subjected to four unscaled historical near-fault ground motions, which include strong long-period pulses. The unscaled ground motions were also rotated to the principal direction based on the angle-to-peak vector displacement of a biaxial two-node model of building BI6a. The linear single DOF displacement spectra values for these motions were up to 1.5 times these of the MCE-level design spectrum for periods 5 s to 6 s. Based on the results of the analysis for the specific characteristics of the superstructure studied here, the following conclusions are drawn:

1. The FB building developed significant inelastic deformations at both the DE and MCE level of shaking. The mean roof drift ratio at the DE and MCE levels was 1.29% and 2.23%, respectively, while the corresponding peak interstory drift ratio along the height of the building was 1.52% and 2.62%, respectively. The damage potential of the core wall of the FB building increased in response to the concurrent large shear stresses and inelastic deformations. The shear force in the core wall at the ground level at the DE and MCE level was $0.36W_s$. The level of shear stresses in the web of the wall at the DE and MCE was $0.088\,f'_{c,e}$ and $0.086\,f'_{c,e}$ respectively, which exceeded the maximum allowed stress by ACI 318-11 ($0.078\,f'_{c,e}$). Tests of non-planar walls with longitudinal steel ratios and axial load ratios 0.8 to 1.2 times and 0.8 to 1.6 times, respectively, compared to the wall considered herein experienced significant damage, including bar buckling, and crushing of concrete at drift ratios of 1.5% to 2.5%.
2. Base-isolated buildings BI5a, BI6a, BI6b, and BI6c remained nominally elastic at the MCE [tension strain in the longitudinal reinforcement ranged between 0.25% (BI5a) and 1.06% (BI6b)] without exceeding the displacement and the force capacities of the isolation devices. These buildings developed less than 0.87 m of horizontal displacement of the isolation system while requiring a total force of the 4 NFVDS that ranged between $0.035W_t$ (BI5a) to $0.058W_t$ (BI6c) [$0.36W_s$ for the FB building]. In the case when the

vertical component of excitation was not included in the analysis, the peak compression force an individual FPB experienced was 26.4 MN for building BI5a and 21.7 MN for BI6b. The bearings did not undergo tension. The wall shear force at the ground level ranged from $0.16W_s$ (BI6b) to $0.19W_s$ (BI5a). The amount of longitudinal reinforcement in the wall of these buildings was 2.4 (BI5a) to 1.2 (BI6b) times that used in the FB building. Building BI6b was found to perform optimally, with a nominally elastic response at the MCE level of shaking and required the smallest amount of wall reinforcement. A comparison of buildings BI6a and BI6c found that isolation system 2 required about 1.35 times the amount of viscous dampers to obtain a similar horizontal displacement compared to isolation system 1, a result of the smaller initial stiffness characterizing the horizontal force-horizontal displacement behavior of LRBs (BI6c) compared to that of FPBs (BI6a).

3. Buildings BI5a, BI6a, BI6b, and BI6c developed less than 0.81% interstory drift compared to 2.62% for the FB building at the MCE; floor accelerations (averaged along the building height) were less than $0.27g$ at the MCE compared to $0.77g$ for the FB building.
4. The level of inelastic deformations of the core wall that buildings BI6b, BI5b, BI4 (all three had a wall with flexural strength, M_b, 1.1 times the minimum required by ASCE 7-10) developed at the MCE increased abruptly with decrease of T_{is}. Interstory drifts developed at the MCE increase from 0.81% in building BI6b to 1.18% in building BI5b and to 2.62% in building BI4 (2.62% also for the FB building). In cases where the provided flexural strength of the wall is less than that required to remain nominally elastic (buildings BI4, BI5b) inelastic deformations increase abruptly with decrease of T_{is} because upon plastic hinging of the wall the tangent stiffness of the superstructure is significantly smaller than that of the isolation system, resulting in concentration of lateral deformations in the plastic hinge.
5. Inclusion of the vertical component of ground motion in the analysis resulted in negligible difference in the displacement response parameters of the superstructure and in less than 15% increase of floor accelerations and shear forces, and less than 18% increase of the maximum compression force an individual FPB developed. The peak compressive force of FPBs for building BI6a was 28 MN; the bearings did not experience tension (in terms of average response to the 14 ground motions scaled at the MCE), even when the vertical component of excitation was considered. The peak tension computed in an individual FPB was 0.19 MN for building BI4.
6. In response to the four unscaled near-fault ground motions, the FB building developed significant to excessive inelastic deformations with interstory drift ratios that ranged from 1.8% to 3.9%; the corresponding range of tensile strain of the longitudinal reinforcement in the wall was 2.8% to 5.1%. All four BI buildings developed less than 1.2% interstory drift ratio for all ground motions, except building BI6b subjected to motion TCU68, which developed 2.2% interstory drift. The horizontal displacements of the isolation systems were 0.65 m to 1.24 m for motions ElCen6, Tabas, and TCU52. For the TCU68 (with the largest linear spectral demands among all historical ground motion records), the D_{is} of the four BI buildings ranged from 1.54 m (BI5a) to 1.72 m (BI6a). Doubling the amount of NFVDs in building BI6a resulted in a D_{is} = 1.28 m for TCU68.

Chapter 3 References

1. Klemencic R, Fry A, Hooper JD, Morgen BG. Performance-based design of ductile concrete core wall buildings – issues to consider before detailed analysis. *Structural Design of Tall and Special Buildings*, 2007; **16**:599–614.
2. Aguilar J, Juarez H, Ortega R, Iglesias J. The Mexico earthquake of September 19, 1985 – statistics of damage and of retrofitting techniques in reinforced concrete buildings affected by the 1985 earthquake. *Earthquake Spectra*, 1989; **5**(1):145-151.
3. Westenenk B, et al. Response of reinforced concrete buildings in Concepcion during the Maule earthquake. *Earthquake Spectra*, 2012; **28**(S1):S257-S280.
4. Elwood KJ, Pampanin S, Kam WY. NZ 22 February 2011 Christchurch Earthquake and Implications for the Design of Concrete Structures. *Proceedings, International Symposium on Engineering Lessons Learned from the 2011 Great East Japan Earthquake,* Tokyo, Japan, 2011. p.1157-1158.
5. Tsai KC, Hsiao CP, Bruneau M. Overview of building damages in 921 Chi-Chi earthquake. *Earth. Engineering and Engineering Seismology*, 2000; **2**(1):93–108.
6. Seed HB, Romo MP, Sun JI, Jaime A, Lysmer J. The Mexico earthquake of September 19, 1985 – relationships between soil conditions and earthquake ground motions. *Earthquake Spectra*, 1988; **4**(4):687-729.
7. Boroschek RL, Contreras V, Kwak DY, Stewart JP. Strong ground motion attributes of the 2010 Mw 8.8 Maule, Chile, earthquake. *Earthquake Spectra*, 2012; **28**(S1):S19-S38.
8. List of tallest buildings in Christchurch. http://en.wikipedia.org/wiki/List_of_tallest_buildings_in_Christchurch [accessed September 2013].
9. Moehle J, Bozorgnia Y, et al. Case studies of the seismic performance of tall buildings designed by alternative means. Task 12 Report for the Tall Buildings Initiative. *Pacific Earthquake Engineering Research Center*, PEER Report 2011/05.
10. Panagiotou M, Restrepo JI. Dual-plastic hinge design concept for reducing higher-mode effects on high-rise cantilever wall buildings. *Earthquake Engineering and Structural Dynamics*, 2009; **38**(12):1359–1380.
11. Calugaru V, Panagiotou M. Response of tall cantilever wall buildings to strong pulse-type seismic excitation. *Earthquake Engineering and Structural Dynamics* 2012; **41**(9):1301-1318.
12. American Society of Civil Engineers. *Minimum Design Loads for Buildings and Other Structures.* ASCE 7-10, Reston, VA, 2010.
13. American Concrete Institute. *Building Code Requirements for Structural Concrete (ACI 318-11) and Commentary*. ACI Committee 318, Farmington Hills, 2011.
14. Structural Engineers Association of Northern California. Seismic design and review of tall buildings using non-prescriptive procedures. *Recommended Administrative Bulletin, San Francisco*, 2007.
15. Willford M, Whittaker A, Klemencic R. Recommendations for the seismic design of high-rise buildings. *Council on Tall Buildings and the Urban Habitat, Draft for Comment*, February 21, 2008; 28.
16. Los Angeles Tall Buildings Structural Design Council. *An Alternative Procedure for Seismic Analysis and Design of Tall Buildings Located in the LA Region*, 2011.
17. Tall Buildings Initiative. Guidelines for Performance-Based Seismic Design of Tall Buildings. *Pacific Earthquake Engineering Research Center*, Report No. 2010/05.
18. Priestley MJN, Calvi GM, Kowalsky, MJ, *Displacement-Based Seismic Design of Structures*. Pavia, Italy, 2007.
19. Dynamic Isolation Systems (DIS). http://www.dis-inc.com/index.html [accessed June 2013].

20. Earthquake Protection Systems. http://www.earthquakeprotection.com/ [accessed June 2013].
21. THK. http://www.thk.com/?q=eng/node/260 [accessed June 2013].
22. Roussis PC, Constantinou MC. Experimental and analytical studies of structures seismically isolated with an uplift-restraining friction pendulum system. *Earthquake Engineering and Structural Dynamics*, 2006; **35**(5):595–611.
23. Taylor Devices Inc. http://www.taylordevices.com/dampers-seismic-protection.html [accessed September 2012].
24. Fujita T. Seismic isolation rubber bearings for nuclear facilities. *Nuclear Engineering Design*, 1991; **127**:379-391.
25. Komuro T, Nishikawa Y, Kimura Y, Isshiki Y. Development and realization of base isolation system for high-rise buildings. *Journal of Advanced Concrete Technology,* 2005; **3**(2):233–239.
26. Ryan KL, Dao ND, Sato E, Sasaki T, Okazaki T. Aspects of isolation device behavior observed from full-scale testing of an isolated building at E-Defense. *Proceedings, 20th Analysis & Computation Specialty Conference*, 2012; p. 25-36.
27. Pan P, Zamfirescu D, Nakashima M, Nakayasu N, Kashiwa H. Base-isolation design practice in Japan: introduction to the post-Kobe approach. *Journal of Earthquake Engineering*, 2005*;* **9**(1):147–171.
28. Kani N. Current state of seismic-isolation design. *Journal of Disaster Research*, 2009*;* **4**(3):175–181.
29. Sayani PJ, Ryan KL. Comparative evaluation of base-isolated and fixed-base buildings using a comprehensive response index. *ASCE Journal of Structural Engineering*, 2009; **135**(6):2952-2968.
30. Hall JF, Ryan KL, Isolated buildings and the 1997 UBC Near-Source Factors, *Earthquake Spectra*, 2000; **16**(2):393-411.
31. Morgan TA, Mahin SA. The use of base isolation systems to achieve complex seismic performance objectives. *Pacific Earthquake Engineering Research Center*, PEER Report 2011/06.
32. Kikuchi M, Black CJ, Aiken ID. On the response of yielding seismically isolated structures. *Earthquake Engineering and Structural Dynamics*, 2008; **37**(5):659-679.
33. Walters M. The seismic retrofit of the Oakland City Hall. *Proceedings, SMIP03 Seminar on Utilization of Strong-Motion Data,* 2003*;* p. 149-163.
34. Calugaru V, Panagiotou M. Seismic responses of 20-story base-isolated and fixed-base RC structural wall buildings subjected to near-fault ground shaking. *Dept. of Civil and Env. Eng., UC Berkeley,* Report No. UCB/SEMM-2012/03.
35. Kelly JM, Konstantinidis DA. *Mechanics of rubber bearings for seismic and vibration isolation*. United Kingdom, 2011.
36. Open System for Earthquake Engineering Simulation (OpenSees). opensees.berkeley.edu [accessed November 2012].
37. Sittipunt C, Wood S. Finite element analysis of reinforced concrete walls. *Report to the National Science Foundation*, University of Illinois at Urbana-Champaign, 1993.
38. Thomsen JH, Wallace JW. Displacement-based design of slender reinforced concrete structural walls - experimental verification. *Journal of Structural Engineering*, 2004; **130**(4): 618-630.
39. Beyer K, Dazio A, Priestley MJN. Quasi-static cyclic tests of two U-shaped Reinforced Concrete Walls. *Journal of Earthquake Engineering*, 2008; **12**(7):1023-1053.
40. Restrepo JI, Lang AF. Study of loading protocols in light-garage stud partition walls. *Earthquake Spectra*, 2011; **27**(4):1169-1185.
41. Mavroeidis GP, Papageorgiou AS. A Mathematical Representation of Near-Fault Ground

Motions. *Bulletin of the Seism. Society of America*, 2003; **93**:1099-1131.
42. Baker JW. Quantitative classification of near-fault ground motions using wavelet analysis. *Bulletin of the Seismological Society of America*, 2007; **97**(5):1486-1501.
43. Pacific Earthquake Engineering Research Center, Strong Motion Database, http://peer.berkeley.edu/peer_ground_motion_database [accessed 09/23/2012].
44. Aagard B, Graves RW, Schwartz DP, Ponce DA, Graymer RW. Ground-motion modeling of Hayward fault scenario earthquakes, Part I: Construction of the suite of scenarios, *Bulletin of the Seism. Society of America*, 2010; **100**(6):2927-2944.

Chapter 4: Earthquake Protection of Tall RC Buildings near the San Andreas Fault Using Base Isolation or Combination of Base Isolation and Rocking Core Walls

4.1 Introduction

Seismic base-isolation (BI) has been used as a design strategy for tall buildings to reduce accelerations, forces, and inelastic deformations in the superstructure (structure above the isolation system) and thus earthquake-induced structural and non-structural damage. This is achieved by concentrating the majority of deformations in robust isolation systems and by reducing higher mode response. The capabilities of currently commercially available seismic isolation devices allow the use of seismic isolation for tall buildings located even at near fault sites [1]. Numerical studies have investigated the response of base-isolated reinforced concrete or steel frame tall buildings modeling 15 [2], 18 or 40 stories [3] of the superstructure.

Another strategy to reduce post-earthquake damage due to plastic hinging in tall RC wall buildings, which has been studied numerically, is to use rocking walls without [4], or with unbonded steel and post-tensioning tendons [5]. The latter study proposed a design including multiple rocking planes along the height of a wall to reduce the contribution of second and higher modes of response. There has been no experimental study on rocking RC core (non-planar) walls. The behavior or rocking structures using un-bonded reinforcement and post-tensioning strands or bars has been studied numerically and experimentally extensively for low- and medium-rise structures [6–12], including designs where energy dissipation devices are externally attached to the RC rocking walls [10, 11]. The combination of base isolation and rocking has been investigated numerically for a rigid block subjected to pulse-type ground excitations [13]. The present study is the first to consider the combination of base isolation and a rocking core-wall for a tall building.

Numerical studies have investigated the seismic response to DE, MCE, and higher levels of shaking of 40- to 42-story tall RC core wall buildings both located hypothetically in downtown Los Angeles, California with S_{D1} = 0.73 g [14, 15, 16]. The authors are not aware of a study on the seismic response of a tall RC wall building located at less than 5 km from the San Andreas fault, at a site with S_{D1} = 1.07 g, like that studied here.

This chapter of the dissertation investigates the seismic design and response of four 20-story buildings hypothetically located in the San Francisco Bay Area, 0.5 km from the San Andreas fault. In all four buildings, a core wall provides the majority of lateral force resistance above ground. One of the four studied buildings is fixed-base (FB), two are base-isolated (BI), and one uses a combination of base isolation and a rocking core wall (BIRW).

Response history two-dimensional analysis is performed, including the vertical components of excitation, for a set of ground motions scaled to the design earthquake (DE) and to the maximum considered earthquake (MCE). The chapter of the dissertation also studies the response of the four buildings to two historical and two simulated near-fault ground motions, demonstrating that the BIRW building has the largest deformation capacity at the onset of structural damage.

This chapter of the dissertation addresses the following three questions: (1) how does a 20-story fixed-base building designed according to ASCE 7-10 [17] at a site 0.5 km from the San Andreas fault perform at the DE and MCE levels of excitation; (2) what are the base-isolation designs that can result in nominally elastic response of the superstructure at the MCE level of shaking, and what is the level of reduction of shear forces and floor accelerations compared to those of the FB building; (3) how and to what extent, can the performance, cost, and constructability of a base-isolated building be improved by incorporating a rocking core-wall in the design.

4.2 Site and Ground Motions

The buildings are hypothetically located at a site in Pacifica, California, with soil type C, 500 m from the San Andreas fault. The fourteen motions of each of the two sets are presented in Table 4-1. The site smooth design spectra according to ASCE 7-10 at both DE and MCE levels are shown in Figure 4-1. The S_{D1} = 1.07 g. Two components (one horizontal and one vertical) of excitation are used in the two-dimensional (2D) analysis. Two sets (Set 1 and Set 2) of fault-normal components for fourteen pulse-type ground motions each are linearly scaled such that their mean spectra for 5% damping ratio, ζ, match or exceed the smoothed DE and MCE design spectra over specific period ranges of interest. Sets 1 and 2 are used for FB and BI buildings, respectively. The first set approximately matches the design spectra in the period range between 0.7 s ($0.35T_1$) to 5.7 s ($2.9T_1$), where T_1 = 2 s is the first mode period of the FB building. For periods between 0.3 s and 0.7 s, the mean spectra of set 1 is 20% less on average than the design spectra. The second set matched the design spectra in the period range 2.3 s to 8.3 s, which includes the required range, per ASCE 7-10, of $0.5T_D$ to $1.25T_M$. Here, T_D = 5.6 s and T_M = 5.8 s is the effective period of the isolation system of the BI buildings (shortest T_D and longest T_M) at the design and maximum displacement, respectively. The mean scale factor at the MCE for Sets 1, and 2 of the motions is 1.87, and 1.94, respectively. For the vertical component of excitation the same scale factor used to scale the horizontal FN and FP components was used.

To determine the principal direction of horizontal excitation, the following procedure was used: for each ground motion Sets 1 and 2 (corresponding to the FB, and BI or BIRW buildings, respectively), a three-dimensional nonlinear two-degree-of-freedom model was developed to represent the building, and this model was subjected to bi-axial horizontal excitation for each pair (FN and FP components) of every ground motion in the set. For each of these ground motion pairs, the direction of peak horizontal displacement was determined and defined as the principal direction of horizontal excitation. For Set 1, intended for the FB building, a nonlinear single degree of freedom oscillator was used in each of the X- and Y-axis to approximate the first mode lateral response of the building. For Set 2, intended for the BI buildings, a three dimensional model of the isolation plane of building BI-1, described in Section 3, (assuming rigid in-plane stiffness and no rotation) with the total structural mass lumped at the centroid of the isolation plane was used. The flexibility of the superstructure was ignored in this model.

Figure 4-1 plots the mean spectra for the principal horizontal components for ground motions of Set1 and Set 2. This spectrum for Set 2 is 1.1 times on average that of the FN between T = 4 and 8 s. Figure 4-1 also plots the mean spectra for the components normal to the corresponding principal directions. The mean value of peak horizontal displacement of the 2DOF model of building BI-1, described above, using bi-axial horizontal excitation at the MCE level of shaking was 1.27 m and was in excellent agreement with that computed using the same model and the principal horizontal component of the motions as uni-axial excitation. For the 2-D analyses presented in Section 5.2, using ground motion Set 1 and ground motion Set 2, the scaled horizontal component of each motion rotated to the particular principal direction was used.

Table 4-1. Ground motions and scale factors at the DE- and MCE-levels of shaking.

Ground motions set	Station name	Earthquake			Scale factor	
		Location	Year	Magnitude	DE	MCE
Set 1 for FB building	Duzce	Duzce, Turkey	1999	7.1	2.33	3.50
	Jensen Filter Plant				0.50	0.75
	Rinaldi Receiving	Northridge, CA	1994	6.7	1.33	2.00
	Sylmar Converter				1.09	1.64
	Los Gatos	Loma Prieta, CA	1989	6.9	1.40	2.10
	Meloland Overpass	Imperial Valley, CA	1979	6.5	0.92	1.38
	Mianzuqingping	Wenchuan, China	2008	7.9	2.33	3.50
	PRPC	Christchurch, NZ	2011	6.3	0.67	1.00
	Tabas	Tabas, Iran	1978	7.4	1.67	2.50
	Takatori	Kobe, Japan	1995	6.9	0.50	0.75
	TCU068				0.50	0.75
	TCU084	Chi-Chi, Taiwan	1999	7.6	0.53	0.80
	TCU102				1.43	2.15
	TCU129				2.20	3.30
Set 2 for BI and BIRW buildings	El Centro Array #6	Imperial Valley, CA	1979	6.5	0.93	1.40
	Lucerne	Landers, CA	1992	7.3	0.73	1.10
	Mianzuqingping	Wenchuan, China	2008	7.9	1.40	2.10
	Tabas	Tabas, Iran	1978	7.4	0.67	1.00
	TCU52				0.67	1.00
	TCU65				0.67	1.00
	TCU67				2.13	3.20
	TCU68				0.67	1.00
	TCU75	Chi-Chi, Taiwan	1999	7.6	1.00	1.50
	TCU87				2.33	3.50
	TCU101				2.00	3.00
	TCU102				1.60	2.40
	TCU103				1.80	2.70
	Yarimca	Kocaeli, Turkey	1999	7.4	1.47	2.20

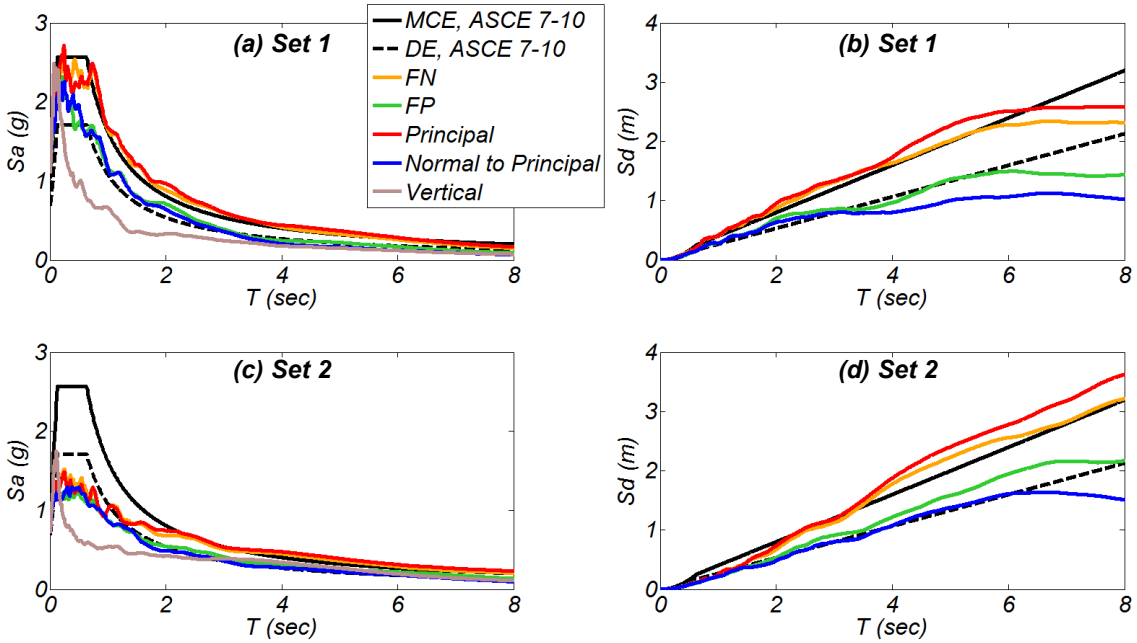

Figure 4-1. Mean linear acceleration and displacement response spectra of the FN, FP, principal, normal to principal, and vertical (only *Sa*) components for two sets of ground motions scaled to the MCE; DE and MCE design spectra.

4.3 Description and Design of Buildings

Figure 4-2 shows the main features, and Table 4-2 lists the main properties of the four buildings. A core wall coupled through the floor slabs with columns in the perimeter of the buildings comprises the structural system above ground in all four buildings. Concrete with specified compressive strength f_c' = 48 MPa and steel with specified yield strength f_y = 414 MPa are used. The corresponding expected material properties used in the analysis are $f_{c,e}'$ = 72 MPa and $f_{y,e}$ = 455 MPa. The 1 m x 1 m columns have ρ_l = 1.0%. The slab reinforcement consists of #5 bars every 0.3 m in the two horizontal directions, both top and bottom. Below ground a grid of RC walls is used to distribute forces to the foundation and isolation system. For the BI and BIRW buildings the seismic weight of each floor below ground is 1.5 times that of each floor above ground. A stiff diaphragm consisting of a RC slab and RC beams is used in the isolation systems above and below the isolation devices.

4.3.1 Fixed-base (FB) building

For this building, the majority of inelastic deformations would typically be expected to concentrate at a single flexural plastic hinge in the wall near ground level. Modal response spectrum analysis as prescribed in ASCE 7-10 with a response modification factor of R = 5, and the square root of sum of squares (SRSS) modal combination rule is used to obtain the design lateral forces. The design base shear force is $V_u = 0.093W_t$, where W_t is the total seismic weight of the building – see Figure 4-2. The wall is designed to resist the design moment ignoring the contribution of framing action between the wall, the slab, and the columns.

4.3.2 Base-isolated (BI) buildings

Two BI buildings are studied. Both use the same isolation system, which is described in Section 4.3.2.1. It is assumed that the isolation system is designed in such a way in order for the isolation devices to be replaceable. The main characteristics of the isolation devices used in the isolation systems are listed in Table 4-2. The horizontal static force versus horizontal static displacement of the isolation systems is idealized with the bilinear relation shown in Figure 4-3(a). The isolation period is T_{is} = 6 s, where $T_{is}=2\pi\sqrt{m_t/K_{is}}$, m_t is the total mass of the building and K_{is} the post-yield tangent stiffness of the isolation system.

4.3.2.1 Isolation system of BI buildings

As shown in Figure 4-2(c), this isolation system combines 16 tension-resistant friction pendulum bearings and 8 nonlinear fluid viscous dampers (NFVDs). Commercially available tension-resistant friction pendulum bearings consist of two orthogonal cylindrical rails interconnected by a housing slider assembly permitting sliding in two orthogonal directions [18]. The bearings used here have 1.2 m displacement capacity, a tension force capacity equal to 9.0 MN, and a compression force capacity 133 MN. Statically, the horizontal force versus horizontal displacement relation of this isolation system when loaded with vertical force F_V is shown in Figure 4-3(a) with the sliding stiffness $K_{is} = |F_V| / R_P$, where R_P is the radius of curvature of the pendulum bearings; see Table 4-2. Note that the relation between K_{is}, R_p, and F_V is maintained both for compression and tension force F_V. A friction coefficient μ = 0.03 is used resulting in $F_y = 0.03W_t$ which is more than the required resistance to wind equal to

0.017W_t according to ASCE 7-10. For all the pendulum bearings Δ_y = 2 mm. The force-velocity relation of each NFVD used is $F_{ND} = \text{sgn}(V)C_{ND}|V|^{\alpha}$, where F_{ND} is the damper force, C_{ND} is the damper constant, V is the velocity, and α=0.3 is the nonlinearity factor [19].

Table 4-2. Characteristics of the four studied buildings.

	Building name	**FB**	**BI-1**	**BI-2**	**BIRW**
Superstructure	Superstructure Weight, W_s (MN)	160	163	159	158
	Core wall length, L_w (m)	10.4	10.7	9.45	8.5
	Core wall thickness, t_w (m)	0.61	0.66	0.61	0.61
	Core wall area, A_w (m^2)	23.8	26.4	21.6	19.3
	Wall long. reinf. ratio, ρ_l (%)	1.2	1.2	1.2	0.6
	Wall axial load ratio, $100P/\left(A_g f'_{c,e}\right)$	4.5	4.3	4.8	5.1
	M_b of wall at ground level (MN-m)	962	1083	803	834
Rocking system	Post-tensioning steel ratio, ρ_{PT} (%)	N/A	N/A	N/A	0.5
	Initial PT stress, σ_{init} (GPa)				1.38
	Unbonded steel ratio, ρ_{UB} (%)				0.45
Isolation system	Curv. radius of pend. bearing R_p (m)	N/A	8.9	8.9	8.9
	NFVD constant C_{ND}, total for isolation plane (MN-$s^{0.3}/m^{0.3}$)		16.7	16.7	16.7
Total system	Total seismic weight, W_t (MN)	160	211	207	206
	Total core-wall long. steel mass (tonne)	175	194	158	138

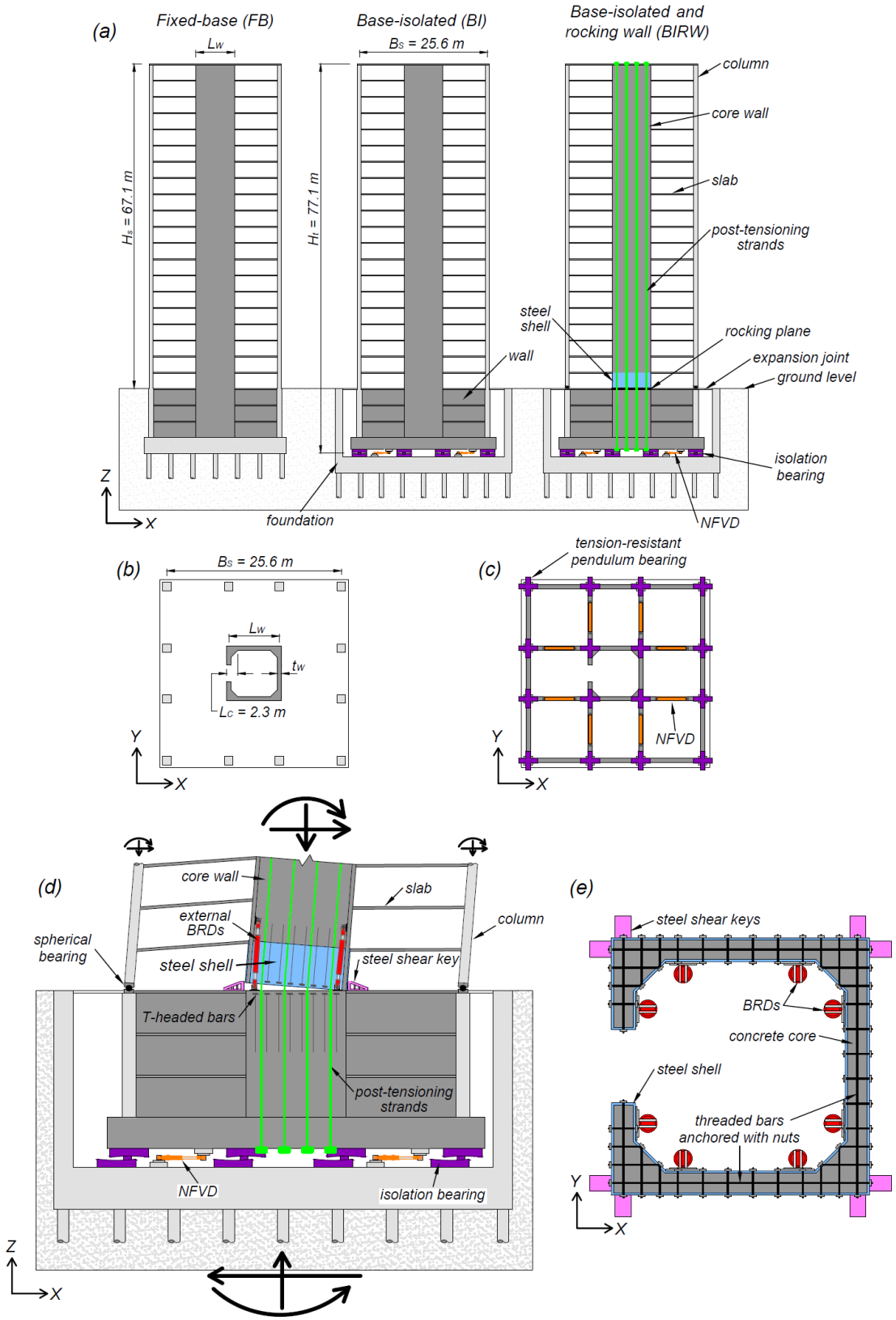

Figure 4-2. (a) elevation view of the FB, BI, and BIRW buildings; (b) plan view of the BIRW building above ground; (c) plan view of isolation system (BI and BIRW); (d) elevation view at deformed state of the bottom part of the BIRW building; (e) Plan view of the rocking plane of the BIRW building; reinforcement embedded in the section is not show for clarity.

4.3.2.2 Superstructure of BI buildings

Two levels of flexural strengths of the walls are studied with the two BI buildings. The wall characteristics were determined to results in 0.5% and 1.0% tension strain at the MCE level of shaking for the BI-1 and BI-2 buildings, respectively. The design base shear force of the superstructure of all BI buildings exceeds $V_u = 0.098W_t$ as required per ASCE 7-10. Using the first mode lateral force distribution, computed with modal analysis as described in Section 5.1, to distribute V_u along the height of the building results in a design bending moment at the ground level of about $M_{u,min} = 0.38H_tV_u$, where H_t the building roof height from the isolation system; see Figure 4-2. Buildings BI-1 and BI-2 use a wall with M_b equal to 2.2 and 1.8 times $M_{u,min} / \varphi$, respectively.

4.3.3 Base-isolated and rocking core-wall (BIRW) building

The BIRW building combines an isolation system identical to that used in the BI buildings and a post-tensioned core wall designed to rock at the ground level. Furthermore, pins or spherical bearings are used at the base of the columns of the base story above ground to prevent plastic hinging of the columns at this level. The expected lateral deformations in this system are distributed in deformations of the base isolation and rocking plane as well as elastic deformations of the wall. This system combines the advantages of seismic base isolation (significant reduction of second and higher modes of response and thus the significant reduction of floor accelerations, shear forces, and interstory drifts) with that of a rocking wall (larger displacement capacity at the onset of damage compared to fixed base walls). The BIRW system is a two-level-of-protection system: design of the relative characteristics of the base isolation and rocking plane ensures a specific distribution of lateral displacements in these two planes allowing this system to have a larger displacement capacity at the onset of structural damage compared to BI designs.

The first story height of the core wall is encased by a 25 mm thick steel shell; see Figure 4-2(a), (d), (e). The encasing steel shell serves as a stay-in-place form and is used only in the first story above ground to maximize the confinement of the concrete of the core and eliminate strength and stiffness degradation associated with damage of the concrete in compression during rocking of the core wall. To enhance constructability, structural integrity, and performance, threaded rods are used in the two directions of the core wall section to cross-connect the steel shell. The core wall section area is intentionally increased at the four corners [see Figure 4-2(b), (c), (e)] to reduce compression strain demands for the case of rocking about a single corner. To further enhance the behavior of the core wall in compression, T-headed bars, ρ_{TH} = 0.6%, are used as bonded reinforcement; see Figure 4-2(d). T-headed bars, with the head at the interface with the wall, are also used at the top of the foundation improving the compression force transfer to the foundation. To enhance shear force transfer between the rocking core wall and the foundation, steel shear keys are used at the corners of the wall; see Figure 4-2(d), (e).

Post-tensioning unbonded high-strength low-relaxation Grade 270 (1.86 GPa yield strength) strands are embedded in the core wall section to achieve specific lateral strength and stiffness and enhance the re-centering characteristics of the wall. The strands can be designed to be replaceable ensuring easy reparability and adaptability of the structural system. The amount of post-tensioning steel provided is ρ_{PT} = 0.5% and the initial tensile stress is 1.38 GPa.

Unbonded mild reinforcement embedded into the base story of the core wall, provides hysteretic energy dissipation at the rocking plane. An unbonded steel ratio ρ_{UB} = 0.45% is

used here. The unbonded rebars pass through steel pipes located near the rocking interface. These pipes are used to protect the unbonded rebars against plastic buckling. The steel pipes are wrapped with a neoprene sheet that allows the nearly free uplift of the wall with respect to them. The length of the unbonded part of these rebars is equal to the first story height, targeting ε_s = 2.0% for 1.0% rotation of the rocking plane. The use of unbonded rebars internal to the core wall prohibits post-earthquake repair or their replacement. Alternatively, buckling restrained devices (BRDs) can be externally fastened to the inner side of the core-wall to provide the required hysteretic energy dissipation and allow for post-earthquake replacement, making the system both repairable and adaptable over its service life.

From the second story and above, the core-wall has ρ_l = 0.6% bonded longitudinal reinforcement. The area of the core wall and the total amount of longitudinal reinforcement are 27% and 29% smaller, respectively, compared to the BI-1 building.

4.4 Numerical Modeling

This 2-D numerical study uses the Open System for Earthquake Engineering Simulation (OpenSees) software [20]. A schematic view of the numerical model is shown in Figure 4-3(b). Fiber-section force-based nonlinear beam-column-elements are used to model the RC wall and columns above ground. Material models *Concrete03* and *Steel02* are used. One element per story with four integration points is used, for the walls and the columns. All slabs are modeled using beam-with-hinges elements, with a 0.9-m-long fiber-section plastic hinge at the ends of each element. The full width of the slab is considered effective in resisting bending. Horizontal stiff linear beam elements are used to model the length of the wall at each story. Linear beam elements of high rigidity are used to model the superstructure below ground. P-delta geometric transformation is used in all beam elements. The model does not account for flexure-shear interaction, bar buckling, or bar fracture in the RC members. The FB building is modeled fixed at the ground level. Expected material properties (see Section 3) for concrete and steel are used in the analysis. The elastic modulus, and the strain-hardening factor of steel are E_s = 200 GPa, and b = 0.02, respectively.

Vertical and horizontal zero-length spring elements are used to model the force-displacement behavior of the isolators in the corresponding direction. Modeling the dependence between sliding stiffness, K_{is}, of the friction pendulum bearings and the vertical force acting on them was investigated and found to have a negligible effect on all the response quantities except the horizontal force of the individual pendulum bearings and the horizontal force distribution in the diaphragm of the isolation system. For this reason, this interaction is not modeled in this study. A bilinear horizontal force-horizontal displacement relation is used to model the tension-resistant friction pendulum bearings. The vertical stiffness in compression, and tension used for the tension-resistant pendulum bearings and the tension-resistant linear bearings is $K_{v,c}$ = 12 MN/mm and $K_{v,t}$ = 1.2 MN/mm, respectively. The NFVDs are modeled as zero length elements, with an assigned viscous material with the force-velocity relationship $F_{ND} = \text{sgn}(V)C_{ND}|V|^{\alpha}$.

At the rocking plane the contact/uplift behavior is modeled with 16 zero-length springs in the vertical direction with nonlinear behavior of confined concrete, and one zero-length spring in the horizontal direction with linear behavior and high stiffness. The stiffness of the contact springs is determined considering that each spring represents a region of the wall with height equal to 0.3 m, along which the compressive strain is assumed to remain constant. The tributary wall section area used in the evaluation of the stiffness of the 4 outer contact springs on both sides is $0.25t_wL_w$ = 1.30 m^2, and that of the 8 inner contact springs is $0.25t_w\left(L_w - 2t_w\right)$ = 1.11 m^2. The confined concrete material model (expected peak confined strength, $f'_{cc,e}$ = 101 MPa at $\varepsilon_{cc,e}$ = 0.4%, with constant stress at higher strains) with zero tensile strength is used in these contact springs. The un-bonded reinforcement are modeled with 9 truss elements spanning the first above ground story, using the steel material model described above. Post-tensioning steel is modeled with 9 truss elements spanning the full height of the building, including the three basement stories. The initial stress of the post-tensioning steel was modeling with an initial strain material, and the initial strain equal to 0.69%. Rayleigh initial stiffness and mass proportional damping with 2% damping ratio in the first and the third mode is used. Horizontal and vertical lumped masses are used at three nodes per floor. Vertical forces due to gravity are applied at the same nodes.

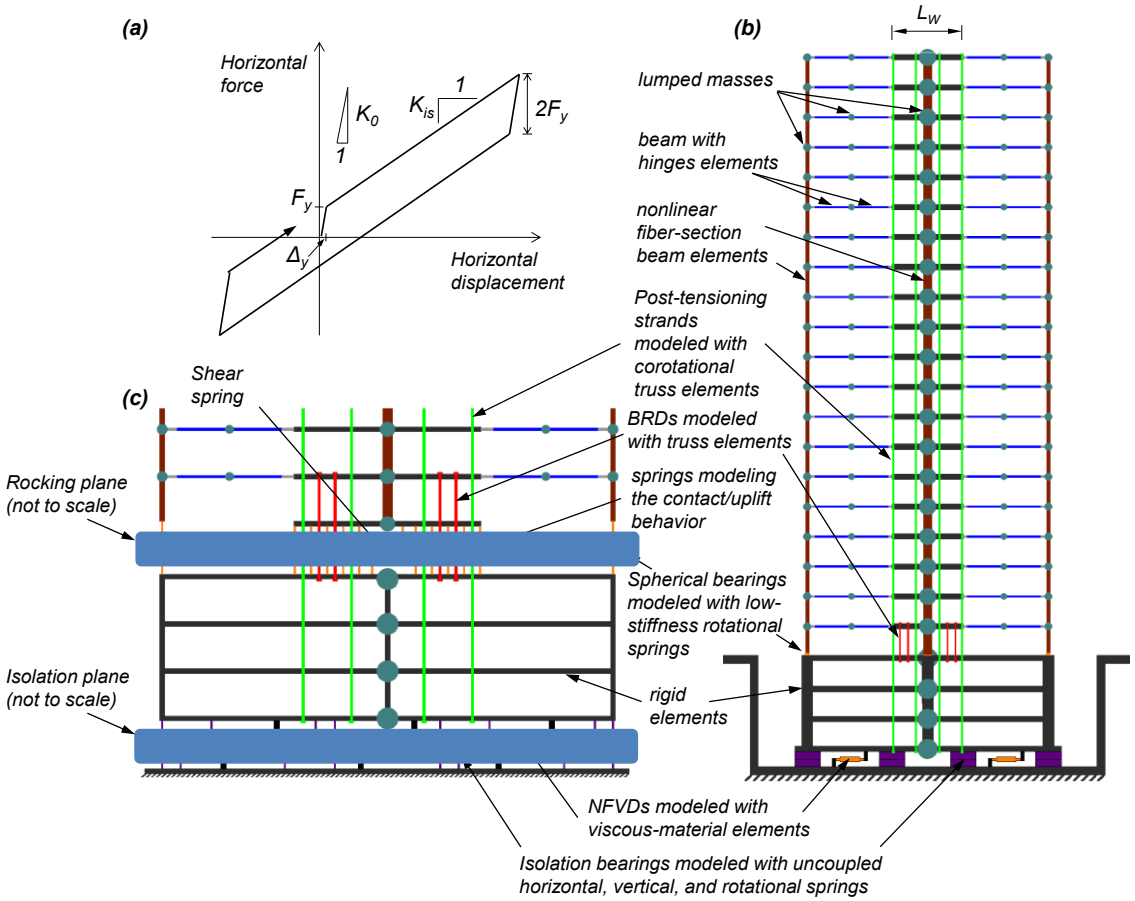

Figure 4-3. (a) Idealization of horizontal force (static) versus horizontal displacement of the two isolation systems; (b) Schematic of the numerical model of the BIRW buildings; (c) Schematic detail of isolation and rocking planes, not to scale.

4.5 Results of Numerical Analysis

4.5.1 Modal Analysis

In all buildings cracked concrete material properties are used in the modal analysis, with the following effective flexural rigidities: (1) E_cI_e=0.25E_cI_g for the base story of the wall and the columns; (2) E_cI_e=0.5E_cI_g for the walls and the columns above the base story; and (3) 0.35E_cI_g for the slabs where I_g is the gross-section moment of inertia and E_c = 40 GPa the concrete elastic modulus. In the modal analysis the isolation systems are modeled using the stiffness K_{is}; see Figure 4-3(a). For the BI and the BIRW buildings the first mode mass, m_1, is 0.99M_t. Thus when the isolation system responds with the tangent stiffness K_{is}, the contribution of the higher modes of response is expected to be negligible. The first mode of vibration periods for the buildings FB, BI-1, BI-2, and BIRW are 1.8, 6.2, 6.2, 6.4 s, respectively.

4.5.2 Response History Analysis using Sets of Motions Scaled to the DE and MCE

Arithmetic mean (for brevity referred to as mean) values of different response parameters of the four buildings are summarized in Table 4-3 and shown in Figure 4-4 for the DE and MCE level of excitation. For each of the DE and MCE level of excitation, the mean values obtained from the analysis using a set consisting of 14 ground motions are reported. The responses are presented in terms of height, h_i, of floor i from the ground level, divided by the roof height above the ground level, H_s. The presented responses are the horizontal displacement relative to the base of the building (ground level for the fixed-base, base of isolation system for the BI buildings, respectively), D_i, divided by H_s, the interstory drift ratio, Θ_i, the shear force of the wall, V_i, divided by W_s (the seismic weight of the structure above ground), and the absolute floor acceleration A_i. Floor accelerations and shear forces are filtered with a finite impulse response low-pass filter order 5000 and 10 Hz cut-off frequency, to remove numerically induced spikes due to sudden changes in the tangent modulus of the materials used.

The FB building develops significant inelastic deformations in the wall at the DE and MCE where the roof drift ratio reaches 1.32%, and 2.38%, respectively. The corresponding peak interstory drift ratios along the building height are 1.55% and 2.79%. The peak longitudinal reinforcement tensile strain in the wall (for brevity referred to as wall tensile strain) is computed at the bottom story and is 2.24% and 3.76% at the DE and MCE, respectively. At the MCE, low levels of inelastic deformations develop in the columns and the floor slabs (less than 0.67% tensile strain in the longitudinal reinforcement). For the above response parameters: the values at the MCE are 1.7 to 1.9 times the values at DE.

For the DE and MCE hazard level, the shear force in the wall at the ground level is 0.36W_s and 0.44W_s, respectively, corresponding to a shear stress in the web of the wall, τ_w, of $0.068f_{c,e}^{'}$ and $0.082f_{c,e}^{'}$ approaching and exceeding the maximum allowable stress of $0.078f_{c,e}^{'}$ ($8\sqrt{f_{c,e}^{'}}$ in psi) prescribed in ACI 318-11 [21]. Such high level of shear stresses with concurrent significant inelastic deformations in the plastic hinge region of a wall resisting large vertical force ($P = 0.045f_{c,e}^{'}A_g$) can result in major damage including crushing of concrete and bar buckling. Note that the computed base shear force significantly exceeds the design base shear force. This is due to the significant contribution of higher modes in the response of tall RC wall buildings [15–23, 24, 25].

Results of experimental studies have shown that non-planar walls [26, 27, 28] subjected to cyclic static loading develop major damage for drift ratios 1.5% to 2.5%. C-shape walls with

ρ_l = 0.8% to 1.1%, and $P = 0.059 f_c' A_g$ to $0.065 f_c' A_g$ experienced bar buckling at 2% drift ratio and vertical crushing of concrete at 2.25% to 2.5% drift ratio [26]. T-shape wall specimens with ρ_l = 1.2%, $P = 0.074 f_c' A_g$ to $0.087 f_c' A_g$ [27] experienced longitudinal bar buckling at 1.5% to 2.0% drift ratio. A U-shape wall specimen with ρ_l = 1.0%, and $P = 0.045 f_c' A_g$ [28] experienced web crushing at 2.5% drift ratio. The maximum shear stress of the web at crushing of this specimen was $0.06 f_c'$ (f_c' = 54.7 MPa), which is only 0.67 times the maximum shear stress allowed by ACI 318-11.

Considered as an average value along the height of the building, the FB building develops large floor accelerations of 0.67 g [1.37 times peak ground acceleration (PGA)] and 0.88 g (1.13 times PGA) at the DE and MCE, respectively.

Presented next is the mean response of the buildings BI-1 and BI-2, which are designed to remain practically elastic at the MCE, i.e. mean wall strains at the MCE not to exceed 0.5% and 1.0%, respectively, and have a wall with M_b equal to 2.2 and 1.8 times the minimum required. The computed wall tensile strains for BI-1 and BI-2 are 0.17% and 0.36% at the DE, and 0.45% and 1.04% at the MCE. The interstory drift ratio at the MCE for these buildings is 0.43% and 0.85%, as opposed to 2.79% for the FB. For this level of interstory drift ratio standard gypsum partitions remain undamaged [29]. The roof drift ratio of these buildings is 0.76% to 0.93% at DE (as opposed to 1.32% for the FB) and 1.59% to 1.95% at the MCE (as opposed to 2.38% for the FB).

Buildings BI-1 and BI-2 develop horizontal displacement of the isolation system of 0.87 m and 0.84 m at the MCE; this is within the displacement capacity of the bearings. At the MCE the maximum tension and compression forces in an individual outer bearing are 0.95 MN and 29.7 MN (building BI-1), respectively, which are within the capacity of commercially available tension-resistant pendulum bearings.

The total force developed in the four NFVDs, $F_{ND,tot}$, buildings BI-1 and BI-2 is around $0.07 W_t$ at the DE and around $0.09 W_t$ at the MCE. For $F_{ND,tot} = 0.09 W_t$ the corresponding force in each of the NFVDs is F_{ND} = 4.7 MN.

At the DE buildings BI-1 and BI-2 develop shear forces in the wall at the ground level that are $0.15 W_s$ and $0.16 W_s$, respectively, values that are less than 0.4 times that of the FB building. The corresponding shear forces at the MCE are $0.21 W_s$ and $0.20 W_s$, respectively (as opposed to $0.44 W_s$ for the FB). Compared to the FB building, the same level of shear force reduction is observed along the entire height of buildings BI-1 and BI-2. Buildings BI-1 and BI-2 achieve significant reduction of shear forces although they develop larger bending moments at the ground level than the FB building. This is because of the significant reduction of higher-mode response.

For the same reason, these buildings develop average floor accelerations along the height at the DE (0.26 to 0.27 g) and at the MCE (0.32 g to 0.34 g) that are less than 0.4 times the corresponding values computed for the FB building. Note the almost constant acceleration in the bottom 75% of the height of the BI buildings; see Figure 4-4.

The foundation shear forces for the BI-1 and BI-2 buildings at the DE are $0.13 W_t$ and $0.14 W_t$, respectively, and at the MCE are around $0.19 W_t$ for both BI buildings, while the corresponding values for the FB building are $0.26 W_t$ and $0.48 W_t$, indicating a reduction by a factor of around 2.5 for the BI buildings. The foundation moments for the BI-1 and BI-2 buildings at the DE are 1260 MN-m and 1168 MN-m, respectively, and at the MCE are 1624 MN-m and 1493 MN-m, while the corresponding foundation moment values for the FB building are 1638 MN-m and 1998 MN-m, indicating a 19–23% reduction for the BI-1 building and a 25–29% reduction for the BI-2 building.

The base isolation and rocking core-wall (BIRW) building at the DE and the MCE experiences roof drift ratios of 0.88% and 2.00%, interstory drift ratios of 0.39% and 0.90%, walls shear forces of $0.17W_s$ and $0.22W_s$, isolator displacements of 0.45 m and 0.83 m, isolator compression forces of 25.9 MN and 30.4 MN, total forces in the NFVDs of $0.08W_t$ and $0.09W_t$, foundation shear forces of $0.14W_t$ and $0.19W_t$, and foundation moments of 1249 MN-m and 1535 MN-m, respectively. These response values for the BIRW building are within 1–13% those of the BI-2 building. Average floor accelerations for the BIRW building at the DE and the MCE are 26% and 53% higher than for the BI-2, reaching 0.34 g and 0.48 g, respectively, while still being 48% and 45% lower than the corresponding average acceleration values for the FB building. At the MCE the BIRW reaches an isolator tensile force of 2.37 MN, which is up to 3.3 times higher than any of the two base-isolated buildings, yet is well within the capacity of commercially available tension-resistant pendulum bearings.

For the BIRW building at the MCE level of excitation, the rocking plane rotation is 0.55%, the tensile strain of unbonded steel is 1.39%, the tensile strain of the post-tensioning steel is 0.75%, and the compression strain of the outer fiber of the rocking wall is 0.35%. The 1.39% unbonded steel strain provides significant energy dissipation to the rocking system. The post-tensioning steel reaches 0.75% tensile strain, which is well within the elastic range for this high-strength steel. The steel shell around the base of the core wall provides sufficient confinement to safely accommodate the 0.35% peak compression strain of the outer fiber of the rocking wall.

Table 4-3 Mean response quantities computed using nonlinear response history analysis (NRHA).

		Design Earthquake (DE)				Maximum Considered Earthquake (MCE)			
	Building name	FB	BI-1	BI-2	BIRW	FB	BI-1	BI-2	BIRW
Superstructure above ground	Roof drift ratio, D_r / H_s, (%)	1.32	0.76	0.93	0.88	2.38	1.59	1.95	2.00
	Interstory drift ratio, Θ_i, (%)	1.55	0.23	0.45	0.39	2.79	0.43	0.85	0.90
	Average floor acceleration, A_{ave} (g)	0.67	0.26	0.27	0.34	0.88	0.34	0.32	0.48
	Wall shear force, ground level, V_b / W_s	0.36	0.15	0.16	0.17	0.44	0.21	0.20	0.22
	Web shear stress of wall, $100*\tau_w / f'_{c,e}$	0.068	0.026	0.032	0.037	0.082	0.035	0.040	0.049
	Wall long. reinf. ε_s (%)	2.24	0.17	0.39	0.04	3.76	0.45	1.04	0.07
	Column long. reinf. ε_s (%)	0.17	0.03	0.05	0.04	0.32	0.05	0.10	0.04
	Slab long. reinf. ε_s (%)	0.37	0.07	0.10	0.08	0.67	0.12	0.19	0.18
Rocking system	Rocking plane rotation (%)	N/A	N/A	N/A	0.12	N/A	N/A	N/A	0.55
	Unbonded steel ε_s (%)				0.34				1.39
	PT steel ε_s (%)				0.70				0.75
	Wall base ε_c (%)				0.16				0.35
Isolation system	Horizontal displacement, D_{is}, (m)	N/A	0.44	0.44	0.45	N/A	0.87	0.84	0.83
	Maximum bearing comp. force (MN)		25.4	24.5	25.9		29.7	29.4	30.4
	Minimum bearing comp. force bearing, negative value is tension (MN)		1.51	2.05	0.56		-0.95	-0.71	-2.37
	Total force of the 4 NFVDs, $F_{ND,tot} / W_t$		0.07	0.07	0.08		0.09	0.09	0.09
	Total horizontal force, $F_{is,tot} / W_t$		0.13	0.14	0.14		0.19	0.19	0.19
Found-ation	Total foundation shear force, V_f / W_t	0.36	0.13	0.14	0.14	0.48	0.19	0.19	0.19
	Total foundation moment, M_f (MN-m)	1638	1260	1168	1249	1998	1624	1493	1535

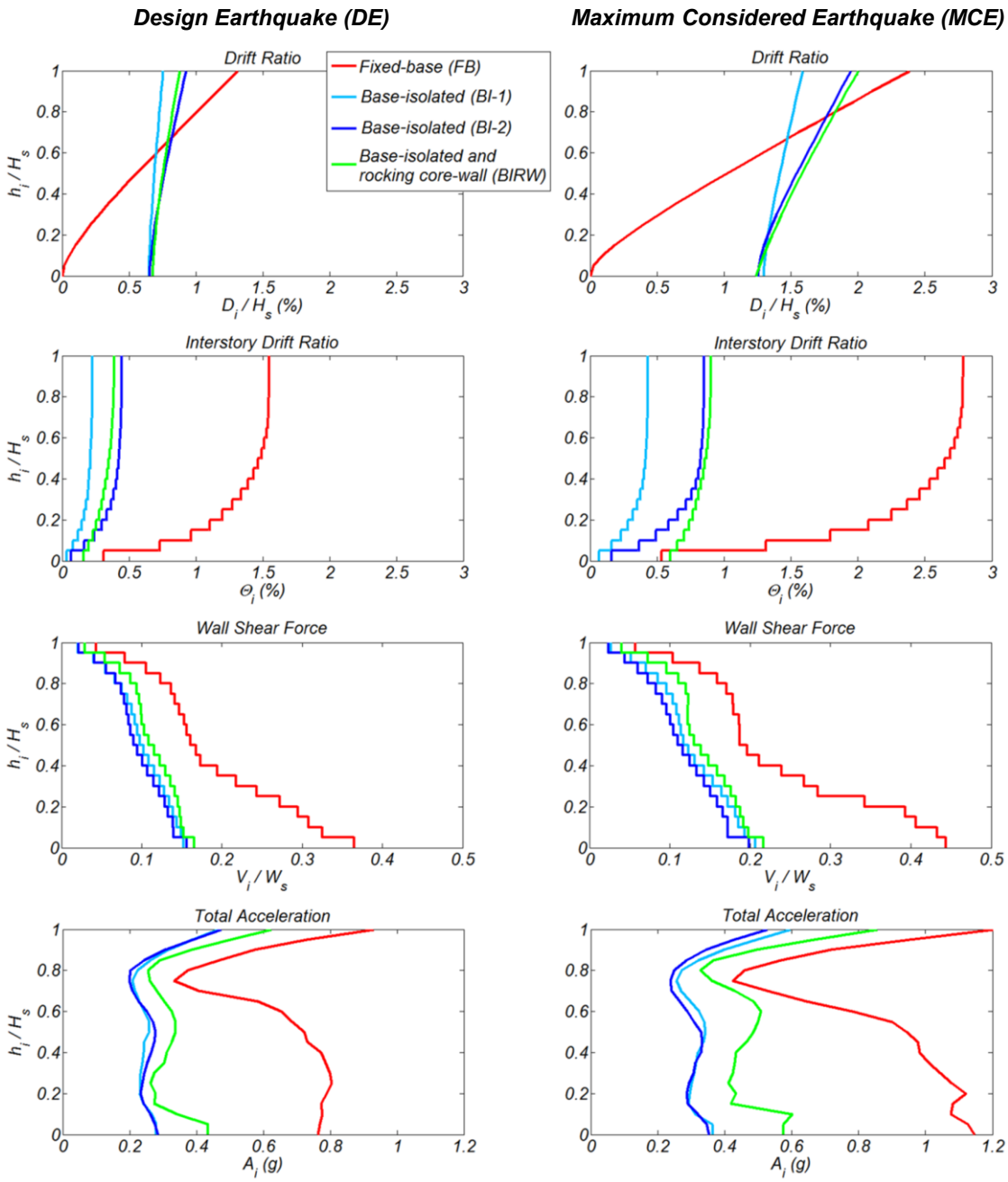

Figure 4-4. Mean response envelopes along the height of the buildings at the DE and MCE levels of shaking.

The coefficients of variation, c_v, for the critical responses to MCE-level scaled sets of 14 ground motions, defined as the sample standard deviation divided by the sample mean, are presented in Table 4-4, along with the MCE mean plus one standard deviation responses. For the BI-1 and BI-2 buildings, the wall tensile strain coefficient of variation are 0.86 and 0.80, respectively, and the MCE mean plus one standard deviation wall tensile strains are 0.84% and 1.87%, indicating that for the BI-2 building the formation of a plastic hinge for ground shaking that exceeds the MCE-level is likely. The BIRW system, on the other hand, is expected to maintain good performance at ground shaking exceeding MCE-level with MCE mean plus one standard deviation unbonded steel tensile strain, post-tensioning steel tensile strain, and base compression strain of 2.93%, 0.82%, and 0.60%, respectively.

Table 4-4 Coefficients of variation and mean plus one standard deviation responses for the MCE-level of shaking.

		Coefficients of variation, c_v				Mean plus one standard deviation			
	Building name	FB	BI-1	BI-2	BIRW	FB	BI-1	BI-2	BIRW
Superstructure above ground	Roof drift ratio, D_r / H_s, (%)	0.55	0.41	0.38	0.47	3.70	2.23	2.68	2.94
	Interstory drift ratio, Θ_i, (%)	0.53	0.60	0.49	0.78	4.27	0.69	1.28	1.61
	Average floor acceleration, A_{ave} (g)	0.51	0.22	0.16	0.36	1.33	0.41	0.37	0.66
	Wall shear force, ground level, V_b / W_s	0.45	0.27	0.26	0.15	0.64	0.26	0.25	0.25
	Web shear stress of wall, $100*\tau_w / f'_{c,e}$	0.45	0.27	0.26	0.15	0.12	0.04	0.05	0.06
	Wall long. reinf. ε_s (%)	0.45	0.86	0.80	0.38	5.46	0.84	1.87	0.10
	Column long. reinf. ε_s (%)	0.72	0.68	0.62	0.06	0.55	0.09	0.15	0.05
	Slab long. reinf. ε_s (%)	0.53	0.50	0.48	0.79	1.03	0.19	0.27	0.31
Rocking system	Rocking plane rotation (%)	N/A	N/A	N/A	1.14	N/A	N/A	N/A	1.17
	Unbonded steel ε_s (%)				1.11				2.93
	PT steel ε_s (%)				0.09				0.82
	Wall base ε_c (%)				0.69				0.60
Isolation system	Horizontal displacement, D_{is}, (m)	N/A	0.36	0.31	0.32	N/A	1.19	1.10	1.10
	Maximum bearing comp. force (MN)		0.14	0.18	0.06		33.90	34.72	32.3
	Minimum bearing comp. force bearing, negative value is tension (MN)		2.76	3.59	1.08		-3.57	-3.27	-4.94
	Total force of the 4 NFVDs, $F_{ND,tot} / W_t$		0.13	0.12	0.13		0.10	0.10	0.10
	Total horizontal force, $F_{is,tot} / W_t$		0.22	0.19	0.19		0.23	0.22	0.22
Found-ation	Total foundation shear force, V_f / W_t	0.40	0.22	0.19	0.18	0.67	0.23	0.22	0.22
	Total foundation moment, M_f (MN-m)	0.22	0.17	0.16	0.11	2444	1908	1728	1711

4.5.3 *Response History Analysis to Unscaled Near-Fault Pulse-Type Ground Motions*

The response of FB, BI-1, BI-2, and BIRW buildings to two unscaled historical and two simulated pulse-type near-fault ground motions is considered next. This investigation aims to study how the FB, the BI, and the BIRW buildings would respond in some of the most severe near-fault motions ever recorded. Depending on the site location with respect to the fault rupture, near-fault ground motions can include strong acceleration, velocity, and displacement pulses, as a result of directivity effects, with predominant period, T_p, that increases (in general) with increasing earthquake magnitude [30, 31]. Motions that include strong long-period pulses can impose large demands in long-period FB and BI tall buildings that may exceed these expected at the MCE.

The main characteristics of the four pulse-type near-fault ground motions used in the analysis of the FB and the four BI buildings are listed in Table 4-5. The simulated SF99 and SF519 motions are based on a source model that combines the available geodetic and seismic observations and recently constructed 3D geologic and seismic velocity models [32]. The ground velocity time series and the linear SDOF spectra of the four motions (horizontal component in the principal direction) are shown in Figure 4-5 and Figure 4-6, respectively. The principal horizontal components are obtained for all four motions using the 2 node-3 DOF model of buildings BI6a as described in Section 2. The characteristics summarized in Table 4-5 are the peak ground velocity (PGV) of the principal, FN and FP components, the average shear wave velocity in the top 30 m, $\overline{v_s}$, and the predominant period, T_p, of the pulse contained in the ground velocity time history. The T_p as computed using wavelet analysis [30] is reported here. For all these four motions R_{rup} < 2.1 km. The linear spectral displacements, *Sd*, of the four motions exceed the MCE design spectrum over different period ranges for the site considered herein, with R_{rup} = 2 km from the Hayward fault, which has the potential to produce an M7.2 earthquake [33]. For T = 5 and 6 s FN components of motions TCU52 and TCU68 in *Sd* equal to about 1.5 times that of the MCE design spectrum. The principal component for the TCU52 motion results in spectral demands similar to those of the FN component for periods up to 6 s, and exceeds those of the FN component for higher periods. At 6 s, the spectral demand of the principal component of TCU68 is 1.6 times that of the FN component. The principal components of the simulated SF99 and SF519 motions result in similar spectral demands to the corresponding FN components for all periods.

Table 4-5. Characteristics of the four near-fault ground motions used.

Station	Earthquake name, year and magnitude	Source mechanism	$\overline{v_s}$ (m/sec)	PGV(m/s)			T_p (sec)
				FN	FP	Prin-cipal	
TCU52	Chi-Chi, Taiwan, 1999, M7.6	Reverse	579	1.65	1.13	1.75	12.7
TCU68			487	1.85	2.51	2.96	12.2
SF99	San Francisco, CA, 1906, M7.8	Strike-slip	564	1.85	0.85	1.90	6.0
SF519			564	1.73	0.46	1.74	7.0

These four motions are selected because they include very strong long-period pulses that result in large demands, exceeding those at the MCE, in the response of the buildings studied here. Among all the motions currently available in the PEER database [34], TCU68 results in the largest *Sd* in the period range of 6 to 10 s, and TCU52 results in the third largest *Sd* at T = 5 s. Motions TCU52 and TCU68 include some distinct pulses of period about 2.5 s in addition to the 12.7 s, and 12.2 s periods described above, resulting in local peaks in *Sd* for T = 2.5 s. Motions TCU52 and TCU68 result in the largest *Sd* for T = 2.2 to 2.5 s (T_1 = 2 s for the FB building) among all motions included in the PEER database. The principal components of the simulated SF99 and SF519 motions exceed the MCE design spectrum from T = 4 s to T = 8 s on average by a factor of 1.5.

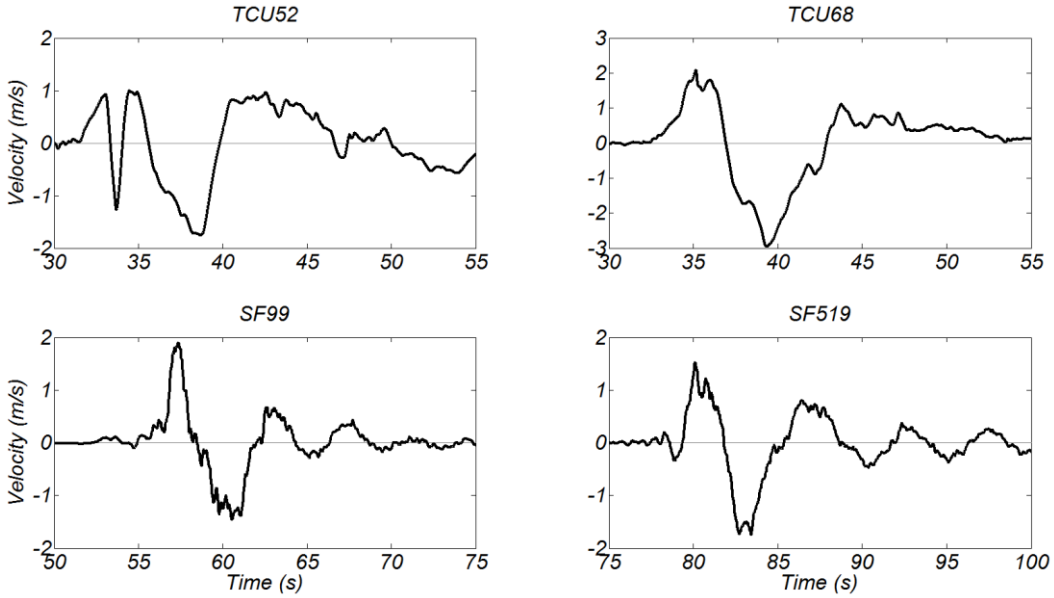

Figure 4-5. Ground velocity time history of the four near-fault ground motions in the principal horizontal direction.

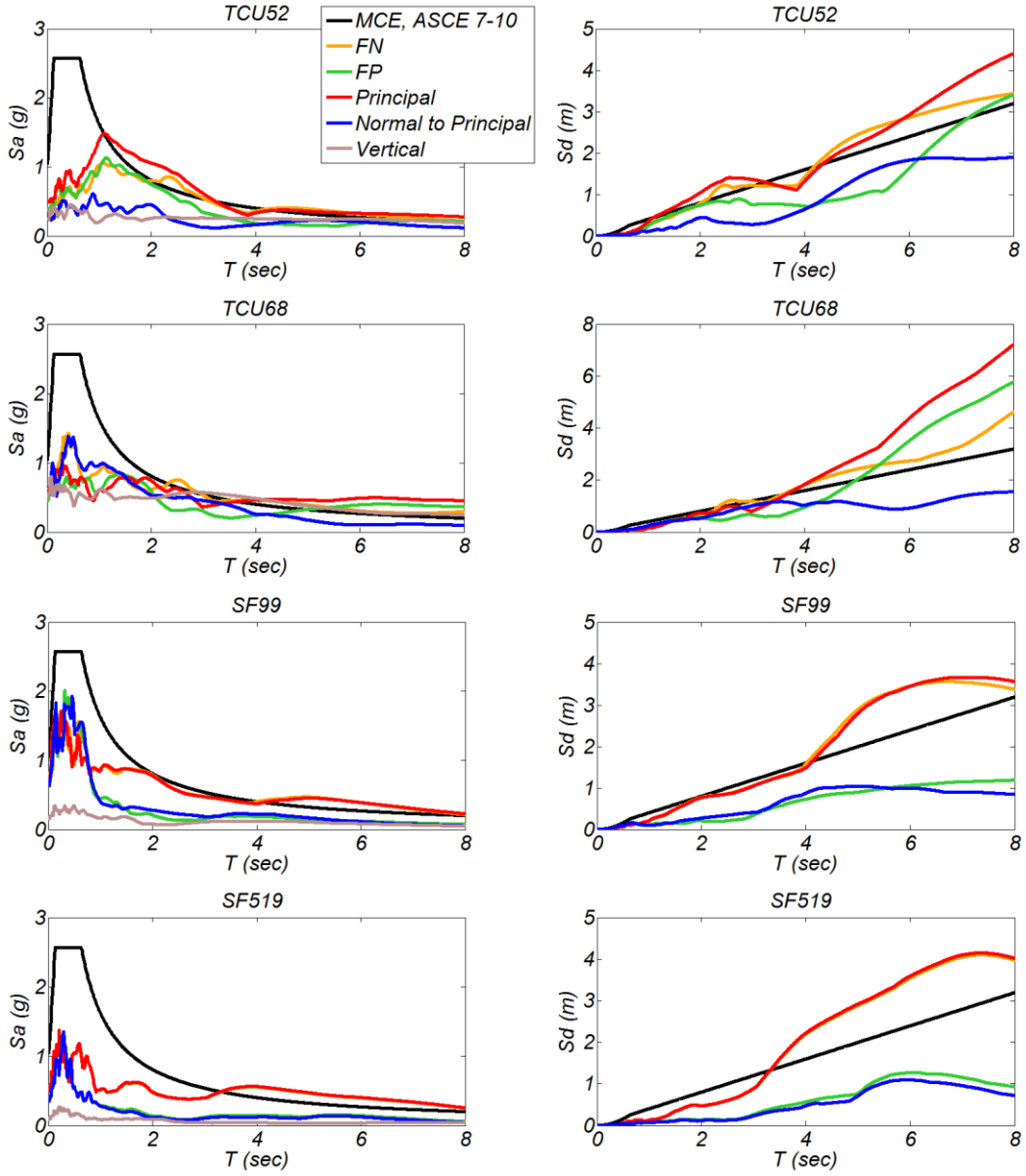

Figure 4-6. Acceleration and displacement linear response spectra for FN, FP, principal, normal to principal, and vertical (Sa only) components of the two near-fault historical records compared to the design spectra for the Berkeley, California, site; ζ=5%.

Figure 4-7 shows the NRHA results of the four buildings studied when subjected to the horizontal principal component and the vertical component of the four unscaled motions. The FB building reaches roof drift ratios ranging between 1.0% and 2.1% (2.38% at the MCE), interstory drift ratios ranging between 1.15% and 2.37% (2.79% at the MCE), shear force in the wall ranging between $0.25W_s$ and $0.33W_s$ ($0.44W_s$ at the MCE), floor accelerations (average along the height of the building) ranging between 0.44 g and 0.70 g (0.88 g at the MCE), and wall tensile strain ranging between 1.91% and 3.79% (3.76% at the MCE).

The two base-isolated and the BIRW buildings experience 0.5 to 0.9 times the base shear and 0.41 to 0.70 times the average floor accelerations as those of the FB building for all four ground motions, with the only exception of BIRW experiencing 1.05 times the FB acceleration for TCU68. In addition, the two base-isolated and the BIRW buildings experience less than 1% interstory drift ratio for all ground motions, except TCU68, for

which BI-2 reaches 1.21%, and BIRW reaches 1.39%, indicating possible damage to non-structural elements, such as standard gypsum partitions. However, for TCU68 the BIRW building experiences negligible structural damage with 1.0% rocking plane rotation, 2.53% unbonded steel strain, 0.90% post-tensioning steel strain, 0.54% wall toe compression strain, 0.09% wall steel strain, and less than 0.25% steel tensile strain in gravity columns and slabs. On the other hand, BI-2 for TCU68 forms a plastic hinge at the base of the wall with 1.74% steel strain. For TCU68 the BI-1, BI-2, and BIRW buildings experience 1.34, 1.23, and 1.22 m isolator displacement, respectively. For the other ground motions isolator displacement does not exceed 0.87 m. The results above demonstrate that the BIRW building has a significantly larger deformation capacity at the onset of structural damage than either of the base-isolated buildings, and especially the FB building.

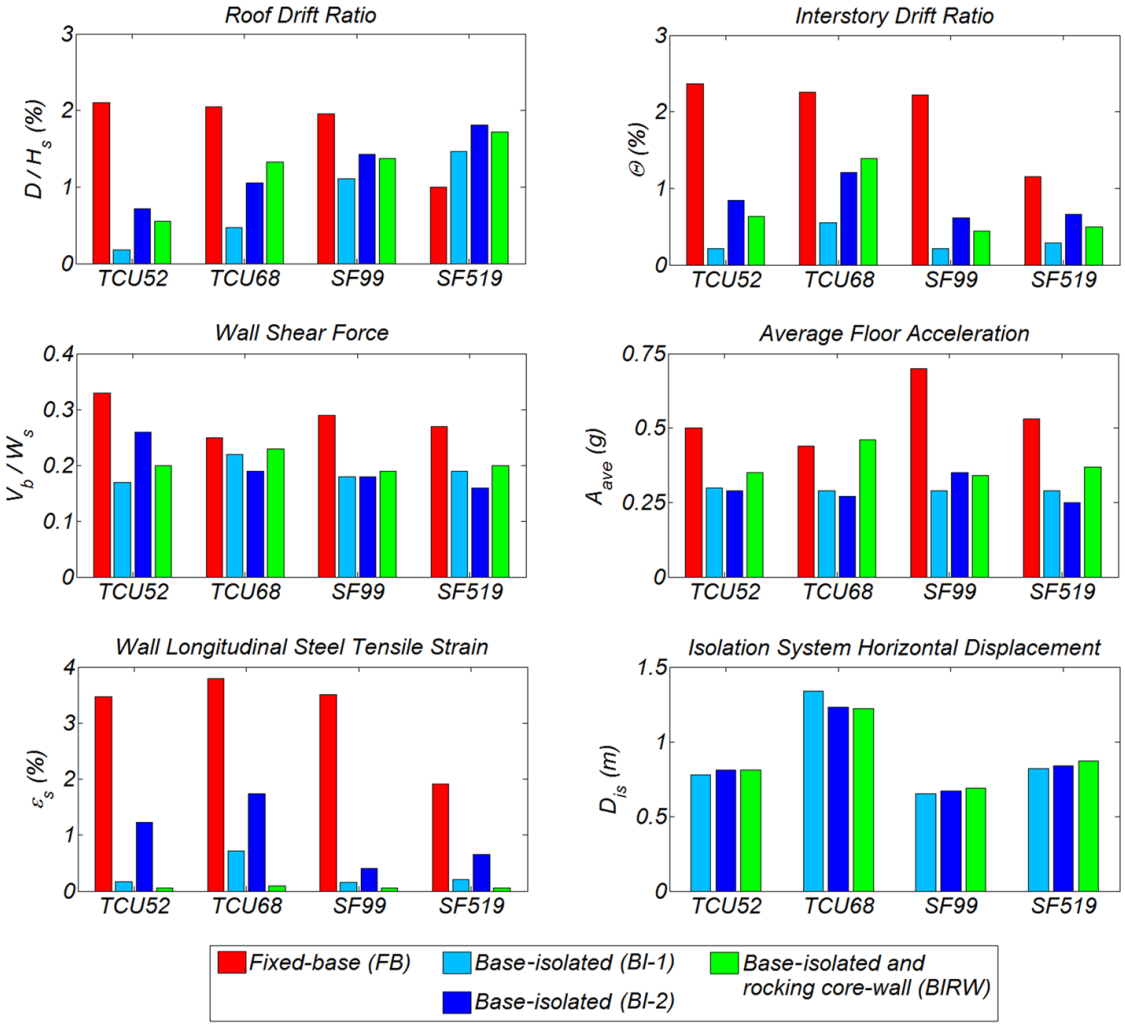

Figure 4-7. Response of the FB, BI-1, BI-2, and BIRW buildings to two historical and two simulated near-fault ground motions.

4.6 Summary and Conclusions

This chapter of the dissertation investigated the seismic design and response of four 20-story core-wall buildings hypothetically located in the San Francisco Bay Area, 500 m from the San Andreas fault. One of the four studied buildings was fixed-base (FB), two were base-isolated (BI-1 and BI-2), and one used a combination of base isolation and a rocking core wall (BIRW). The FB and the BI buildings satisfied requirements of ASCE 7-10. The BI and the BIRW buildings used the same 6 s period isolation system, which combines 16 tension-resistant friction pendulum bearings and 8 nonlinear fluid viscous dampers. Buildings BI-1 and BI-2 used walls with flexural strength 2.2 and 1.8 times, respectively, the minimum required by ASCE 7-10. The rocking core-wall included post-tensioning steel, buckling-restrained devices, and at its base was encased in a steel shell. The total amount of longitudinal steel in the wall of the BIRW building was 0.71 to 0.87 times that used in the BI buildings, and 0.79 times that used in the FB building. Response history two-dimensional analysis was performed, including the vertical components of excitation, for sets of 14 ground motions scaled to the design earthquake and to the maximum considered earthquake (MCE). This chapter of the dissertation also studied the response of the four buildings to two historical and two simulated near-fault ground motions, which included strong long-period pulses. The linear single degree of freedom displacement spectra values for these motions were up to 1.5 times these of the MCE-level design spectrum for periods 5 s to 6 s. Based on the results of the analysis the following conclusions are drawn:

1. The FB building developed significant inelastic deformations both at the DE and MCE level of shaking. The mean roof drift ratio at the DE and MCE levels was 1.32% and 2.38%, respectively, while the corresponding peak interstory drift ratio along the height of the building was 1.55% and 2.79%, respectively. The damage potential of the core wall of the FB building increases in response to the concurrent large shear stresses and inelastic deformations. The shear force in the core wall at the ground level at the DE and MCE level was $0.36W_s$ and $0.44W_s$, respectively. The level of shear stresses in the web of the wall at the DE and MCE was $0.068\,f'_{c,e}$ and $0.082\,f'_{c,e}$ respectively, where $f'_{c,e}$ = 72 MPa was the expected compressive strength of concrete. The maximum allowed stress by ACI 318-11 is $0.0078\,f'_{c,e}$. Tests of non-planar walls with longitudinal steel ratios and axial load ratios 0.8 to 1.2 times and 0.8 to 1.6 times, respectively, that of the wall considered herein experienced significant damage, including bar buckling, and crushing of concrete at drift ratios of 1.5% to 2.5%.
2. The FB building resulted in floor accelerations (average along the building height) equal to 0.67g (1.37 PGA) and 0.88g (1.13 PGA) at the DE and at the MCE, respectively.
3. Compared to the response of the FB building, commercially available isolation and viscous damping devices used in the design of the BI buildings resulted in an isolated superstructure for buildings BI-1 and BI-2 that remained practically elastic at the MCE, while reduced significantly interstory drifts, shear forces, and floors accelerations. Buildings BI-1 and BI-2 developed less than 0.87 m of horizontal displacement of the isolation system. The outer bearings of these buildings experienced up to 0.95 MN tension, which is well within the 9 MN capacity of the commercially available tension-capable pendulum bearings. At the MCE the BI-1 and the BI-2 buildings developed 0.43% and 0.85% interstory drift, respectively, and 0.45% and 1.04% tensile strain in the wall, while floor accelerations (average along the building height) were less than 0.34 g at the MCE, (0.88 g for the FB building). The shear force in the wall at the ground level at the MCE of these buildings was $0.20W_s$ to $0.21W_s$ ($0.44W_s$ for the FB building).

4. The BIRW building experienced elastic response of the wall at the MCE level of excitation, with floor accelerations and shear forces 0.5 times those experienced by the FB building. Inelastic deformation was concentrated in the unbonded steel, which reached tensile strains of 1.39% and provided energy dissipation for the rocking system. The high strength post-tensioning steel remained elastic, experiencing 0.75% tensile strain. The base of the rocking wall, encased in a steel shell, remained nominally elastic with the compression strain of 0.35%. The gravity columns, using spherical bearings at ground level, and the slabs also remained elastic with tensile strains of 0.04% and 0.18%, respectively.
5. The BIRW building is expected to remain elastic also for higher than MCE-level ground motions, as opposed to the base-isolated buildings, particularly the BI-2 building, which would likely form a plastic hinge at the wall base. This is evident from the 1.04% mean wall steel strain and the 0.80 coefficients of variation in the wall tensile strain for the BI-2 building for the MCE, and safe-level mean response and relatively low levels of variation in the critical components of the BIRW building.
6. In response to the four unscaled near-fault ground motions, the FB building developed significant inelastic deformations with interstory drift ratio that ranged from 1.2% to 2.4%. The corresponding range of tensile strain of the longitudinal reinforcement in the wall was 1.9% to 3.8%. Both BI and the BIRW buildings developed less than 1% interstory drift ratio for all ground motions, except TCU68, for which BI-2 reaches 1.21%, and BIRW reaches 1.39%. For both base-isolated and the BIRW building, the horizontal displacements of the isolation systems were less than 0.87 m for TCU52, SF99, and SF519, and reached 1.34, 1.23, and 1.22 m, for BI-1, BI-2, and BIRW, respectively. These results demonstrate that the BIRW building has a significantly larger deformation capacity at the onset of structural damage than either of the base-isolated buildings, and especially the FB building.

Chapter 4 References

1. Calugaru V, Panagiotou M. Seismic responses of 20-story base-isolated and fixed-base RC structural wall buildings at a near-fault site. *Earthquake Engineering and Structural Dynamics*, 2013, in review.
2. Kikuchi M, Black CJ, Aiken ID. On the response of yielding seismically isolated structures. *Earthquake Engineering and Structural Dynamics* 2008; **37**(5):659-679.
3. Komuro T, et al. Development and realization of base isolation system for high-rise buildings. *Journal of Advanced Concrete Technology* 2005; **3**(2):233–239.
4. Nielsen GM. Performance of rocking core walls in tall buildings subjected to severe seismic demands. *Master's Thesis*, University of California, Berkeley, CA, 2009.
5. Wiebe L, Christopoulos C. Mitigation of higher mode effects in base-rocking systems by using multiple rocking sections. *Journal of Earthquake Engineering* 2009; **13**(1):83–108.
6. Kurama Y, Sause R, Pessiki S, Lu LW. Lateral load behavior and seismic design of unbonded post-tensioned precast concrete walls. *American Concrete Institute, ACI Structural Journal* 1999; **96**:622-632.
7. Nakaki SD, Stanton JF, Sritharan S. An overview of the PRESSS five-story precast test building. *PCI Journal* 1999; **44**:26-39.
8. Seo C, Sause R. Ductility demands of self-centering systems under earthquake loading. *American Concrete Institute, ACI Structural Journal* 2005; **102**(2):275-285.
9. Restrepo JI, Rahman A. Seismic performance of self-centering structural walls incorporating energy dissipators. *Journal of Structural Engineering* 2007; **11**:1560-1570.
10. Marriott DJ, Pampanin S, Bull DK, Palermo A. Dynamic testing of precast, post-tensioned rocking wall systems with alternative dissipating solutions. *Bulletin of the New Zealand Society of Earthquake Engineering* 2008; **41**(2):90-102.
11. Marriot DJ, Pampanin S, Palermo A, Bull DK. Shake-table testing of hybrid post-tensioned precast wall systems with alternative dissipating solutions. *Proceedings of the 14th World Conference on Earthquake Engineering, Beijing, China,* 2008.
12. Kurama Y, Qiang S. Seismic design and response evaluation of unbonded post-tensioned hybrid coupled wall structures. *Earthquake Engineering and Structural Dynamics* 2008; **37**(14):1677-1702.
13. Vassiliou MF, Makris N. Analysis of the rocking response of rigid blocks standing free on a seismically isolated base. *Earthquake Engineering and Structural Dynamics* 2011; **41**(2):177-196.
14. Klemencic R, Fry A, Hooper JD, Morgen BG. Performance-based design of ductile concrete core wall buildings – issues to consider before detailed analysis. *Structural Design of Tall and Special Buildings* 2007; **16**:599–614.
15. Moehle J, Bozorgnia Y, et al. Case studies of the seismic performance of tall buildings designed by alternative means. Task 12 Report for the Tall Buildings Initiative. *PEER Report 2011/05*, University of California, Berkeley, CA, 2011.
16. Yang TY, Moehle JP, Bozorgnia Y, Zareian F, Wallace JW. Performance assessment of tall concrete core-wall building designed using two alternative approaches. *Earthquake Engineering and Structural Dynamics* 2012; **41**(11):1515–1531
17. American Society of Civil Engineers. *Minimum Design Loads for Buildings and Other Structures.* ASCE 7-10, Reston, VA, 2010.
18. Earthquake Protection Systems. http://www.earthquakeprotection.com/ [accessed September 2013].
19. Taylor Devices Inc. http://www.taylordevices.com/dampers-seismic-protection.html [accessed September 2013].
20. Open System for Earthquake Engineering Simulation (OpenSees). opensees.berkeley.edu

[accessed September 2013].
21. American Concrete Institute. *Building Code Requirements for Structural Concrete (ACI 318-11) and Commentary*. ACI 318-11, ACI Committee 318, Farmington Hills, 2011.
22. Panagiotou M, Restrepo JI. Dual-plastic hinge design concept for reducing higher-mode effects on high-rise cantilever wall buildings. *Earthquake Engineering and Structural Dynamics* 2009; **38**(12):1359–1380.
23. Calugaru V, Panagiotou M. Response of tall cantilever wall buildings to strong pulse-type seismic excitation. *Earthquake Engineering and Structural Dynamics* 2012; 41(9):1301-1318.
24. Tall Buildings Initiative, Guidelines for Performance-Based Seismic Design of Tall Buildings, *Pacific Earthquake Engineering Research Center*, *Report No. 2010/05*.
25. Priestley MJN, Calvi GM, Kowalsky, MJ, *Displacement-Based Seismic Design of Structures*, 2007, Pavia, Italy.
26. Sittipunt C, Wood S. Finite element analysis of reinforced concrete walls. *Report to the National Science Foundation, University of Illinois at Urbana-Champaign*, 1993.
27. Thomsen JH, Wallace JW. Displacement-based design of slender reinforced concrete structural walls - experimental verification. *Journal of Structural Engineering*, 2004; **130**(4): 618-630.
28. Beyer K, Dazio A, Priestley MJN. Quasi-static cyclic tests of two U-shaped reinforced concrete walls. *Journal of Earthquake Engineering* 2008; **12**(7):1023-1053.
29. Restrepo JI, Lang AF. Study of loading protocols in light-garage stud partition walls. *Earthquake Spectra* 2011; **27**(4):1169-1185.
30. Mavroeidis GP, Papageorgiou AS. A mathematical representation of near-fault ground motions. *Bulletin of the Seismological Society of America* 2003; **93**(3):1099-1131.
31. Baker JW. Quantitative classification of near-fault ground motions using wavelet analysis. *Bulletin of the Seismological Society of America*, 2007; **97**(5):1486-1501.
32. Aagard BT, et al. Ground-motion modeling of the 1906 San Francisco earthquake, Part II: Ground-motion estimates for the 1906 earthquake and scenario events. *Bulletin of the Seismological Society of America* 2008; **98**(2):1012–1046.
33. Aagard BT, et al. Ground-motion modeling of Hayward fault scenario earthquakes, Part I: Construction of the suite of scenarios. *Bulletin of the Seismological Society of America* 2010; **100**(6):2927-2944.
34. Pacific Earthquake Engineering Research Center, Strong Motion Database, http://peer.berkeley.edu/peer_ground_motion_database [accessed September 2013].

Chapter 5: Conclusions and Recommendations

5.1 Summary and Conclusions

This dissertation achieved three main objectives: (1) to investigate the seismic response of tall reinforced concrete core wall buildings, designed following current building codes, subjected to pulse type near-fault ground motion, with special focus on the relation between the characteristics of the ground motion and the higher-modes of response; (2) to determine the characteristics of a base isolation system that results in nominally elastic response of the superstructure of a tall reinforced concrete core wall building at the maximum considered earthquake level of shaking; and (3) to demonstrate that the seismic performance, cost, and constructability of a base-isolated tall reinforced concrete core wall building can be significantly improved by incorporating a rocking core-wall in the design.

5.1.1 Pulse-Type Excitation and Higher Mode Effects

First, this dissertation investigated the inelastic response of tall cantilever wall buildings subjected to pulse-type ground motion, emphasizing the relationship between ground motion characteristics and higher modes of response, especially the second and third mode. Three 10-, 20-, and 40-story high cantilever wall buildings were designed to develop all nonlinear deformations at a flexural plastic hinge region located at their base. Nonlinear dynamic response history analyses (NDRHA) of these buildings was carried out. Initially, each building was subjected to both a near-fault record and a representation of this record using a close-form pulse. Then, an extensive parametric analytical study was conducted for each building subjected to three close-form pulses. Twenty three distinct pulse periods and three pulse amplitudes at each period were considered to study different levels of inelastic response. The following conclusions were drawn:

1. Strong pulse type ground motions with the predominant pulse period in the range of the second structural modal period computed with effective flexural rigidities significantly excited the first, and second mode, causing highly inelastic response at the base of the walls for all buildings considered.
2. Simple close-form pulses provided good approximations of the distinct pulses contained in near-fault records. Using the pulse approximations, the computed response in terms of section bending moment, shear force, and floor acceleration were similar to the corresponding response computed using near-fault records.
3. Strong pulse type motion with a predominant pulse period close to or shorter than the second modal period excited significantly the second mode of response and resulted in bending moment demands at the intermediate wall height that far exceeded the base bending moment yield strength. Designing these regions to remain elastic requires large to excessive amounts of longitudinal reinforcement.
4. For any T_1 / T_p greater than one, the peak shear force at 75% of the height of the buildings, $V_{0.75H}$, approached or even exceeded 50% of the peak base shear force. For T_1 / T_p = 3, for all three pulses, $V_{0.75H}$ approached or even exceeded the peak base shear force.

5. Inelastic response at the base of cantilever wall buildings did not reduce the second and higher modes as much as the first mode of response.
6. Using a uniform yield reduction factor R in all the modes and the SRSS combination method, modal response spectrum analysis significantly underestimated the bending moments, and shear forces along the height of the buildings for T_1 / T_p greater than one.
7. This underestimation increased with increasing R and with an increase of T_1 / T_p between 1 and 4. The level of underestimation was independent of the number of stories and showed small sensitivity to the pulse type and to the response parameter.
8. Modified modal response spectrum analysis that considered a yield reduction factor R_H factor in the second and higher modes equal to one (or much smaller than this used for the first mode), significantly improved the estimation of bending moment, and shear force along the height of cantilever wall buildings.

5.1.2 Base Isolation of Tall RC Core Wall Buildings

Following the thorough analysis of tall RC core wall fixed-base buildings subjected to pulse type ground shaking, this dissertation went on to investigate the seismic response of six base-isolated (BI) buildings with three stories below ground and twenty stories above ground, and compared it to that of a similar fixed-base (FB) building. All buildings were hypothetically located in downtown Berkeley, California, 2 km from the Hayward fault, and were designed with a core wall to provide most of the lateral force resistance above ground. All buildings were designed to meet or exceed ASCE 7-10 design requirements. The design base shear force of the FB building was $0.098W_s$ (W_s: the seismic weight of the building above ground). Buildings BI4, BI5a, BI5b, BI6a, and BI6b used isolation system 1 that combined 16 tension-resistant friction pendulum bearings (FPBs) and 8 nonlinear fluid viscous dampers (NFVDs). Building BI6c used isolation system 2 that combined 12 very low-friction (μ=0.3%) tension-resistant cross-linear bearings (CLBs), 12 lead-rubber bearings (LRBs), and 8 NFVDs. Isolation periods T_{is} equal to 4 s (building BI4a), 5 s (buildings BI5a, and BI5b), and 6 s (buildings BI6a, BI6b, and BI6c) were studied. Building BI5a incorporated a wall design with flexural strength 2.2 times the minimum required by ASCE 7-10. Buildings BI6a and BI6c incorporated a wall design with M_b equal to 1.8 times the minimum required; for buildings BI4a, BI5b, and BI6b, M_b was equal to 1.1 times the minimum required.

Numerical models of all seven buildings were subjected to sets of 14 ground motions, the horizontal components rotated to the principal direction as defined by the angle to peak vector displacement of a biaxial two-node model of building BI6a subjected to FN and FP components simultaneously, and scaled to match the DE and the MCE design spectra. To study the effect of vertical ground motion components, buildings FB, BI4, and BI6a were subjected to both the principal direction horizontal and the vertical ground motion components. A representative subset of the studied buildings (FB, BI5a, BI6a, BI6b, BI6c) was also subjected to four unscaled historical near-fault ground motions, which include strong long-period pulses. The unscaled ground motions were also rotated to the principal direction based on the angle-to-peak vector displacement of a biaxial two-node model of building BI6a. The linear single DOF displacement spectra values for these motions were up to 1.5 times these of the MCE-level design spectrum for periods 5 s to 6 s. Based on the results of the analysis for the specific characteristics of the superstructure studied here, the following conclusions were drawn:

1. The FB building developed significant inelastic deformations at both the DE and MCE level of shaking. The mean roof drift ratio at the DE and MCE levels was 1.29% and 2.23%, respectively, while the corresponding peak interstory drift ratio along the height of the building was 1.52% and 2.62%, respectively. The damage potential of the core wall

of the FB building increased in response to the concurrent large shear stresses and inelastic deformations. The shear force in the core wall at the ground level at the DE and MCE level was $0.36W_s$. The level of shear stresses in the web of the wall at the DE and MCE was $0.088\,f'_{c,e}$ and $0.086\,f'_{c,e}$ respectively, which exceeded the maximum allowed stress by ACI 318-11 ($0.078\,f'_{c,e}$). Tests of non-planar walls with longitudinal steel ratios and axial load ratios 0.8 to 1.2 times and 0.8 to 1.6 times, respectively, compared to the wall considered herein experienced significant damage, including bar buckling, and crushing of concrete at drift ratios of 1.5% to 2.5%.

2. Base-isolated buildings BI5a, BI6a, BI6b, and BI6c remained nominally elastic at the MCE [tension strain in the longitudinal reinforcement ranged between 0.25% (BI5a) and 1.06% (BI6b)] without exceeding the displacement and the force capacities of the isolation devices. These buildings developed less than 0.87 m of horizontal displacement of the isolation system while requiring a total force of the 4 NFVDS that ranged between $0.035W_t$ (BI5a) to $0.058W_t$ (BI6c) [$0.36W_s$ for the FB building]. In the case when the vertical component of excitation was not included in the analysis, the peak compression force an individual FPB experienced was 26.4 MN for building BI5a and 21.7 MN for BI6b. The bearings did not undergo tension. The wall shear force at the ground level ranged from $0.16W_s$ (BI6b) to $0.19W_s$ (BI5a). The amount of longitudinal reinforcement in the wall of these buildings was 2.4 (BI5a) to 1.2 (BI6b) times that used in the FB building. Building BI6b was found to perform optimally, with a nominally elastic response at the MCE level of shaking and required the smallest amount of wall reinforcement. A comparison of buildings BI6a and BI6c found that isolation system 2 required about 1.35 times the amount of viscous dampers to obtain a similar horizontal displacement compared to isolation system 1, a result of the smaller initial stiffness characterizing the horizontal force-horizontal displacement behavior of LRBs (BI6c) compared to that of FPBs (BI6a).
3. Buildings BI5a, BI6a, BI6b, and BI6c developed less than 0.81% interstory drift compared to 2.62% for the FB building at the MCE; floor accelerations (averaged along the building height) were less than $0.27g$ at the MCE compared to $0.77g$ for the FB building.
4. The level of inelastic deformations of the core wall that buildings BI6b, BI5b, BI4 (all three had a wall with flexural strength, M_b, 1.1 times the minimum required by ASCE 7-10) developed at the MCE increased abruptly with decrease of T_{is}. Interstory drifts developed at the MCE increase from 0.81% in building BI6b to 1.18% in building BI5b and to 2.62% in building BI4 (2.62% also for the FB building). In cases where the provided flexural strength of the wall is less than that required to remain nominally elastic (buildings BI4, BI5b) inelastic deformations increase abruptly with decrease of T_{is} because upon plastic hinging of the wall the tangent stiffness of the superstructure is significantly smaller than that of the isolation system, resulting in concentration of lateral deformations in the plastic hinge.
5. Inclusion of the vertical component of ground motion in the analysis resulted in negligible difference in the displacement response parameters of the superstructure and in less than 15% increase of floor accelerations and shear forces, and less than 18% increase of the maximum compression force an individual FPB developed. The peak compressive force of FPBs for building BI6a was 28 MN; the bearings did not experience tension (in terms of average response to the 14 ground motions scaled at the MCE), even when the vertical component of excitation was considered. The peak tension computed in an individual FPB was 0.19 MN for building BI4.

6. In response to the four unscaled near-fault ground motions, the FB building developed significant to excessive inelastic deformations with interstory drift ratios that ranged from 1.8% to 3.9%; the corresponding range of tensile strain of the longitudinal reinforcement in the wall was 2.8% to 5.1%. All four BI buildings developed less than 1.2% interstory drift ratio for all ground motions, except building BI6b subjected to motion TCU68, which developed 2.2% interstory drift. The horizontal displacements of the isolation systems were 0.65 m to 1.24 m for motions ElCen6, Tabas, and TCU52. For the TCU68 (with the largest linear spectral demands among all historical ground motion records), the D_{is} of the four BI buildings ranged from 1.54 m (BI5a) to 1.72 m (BI6a). Doubling the amount of NFVDs in building BI6a resulted in a D_{is} = 1.28 m for TCU68.

5.1.3 Combination of Base Isolation and a Rocking Core Wall

Following the analysis of base-isolated buildings at a site 2 km from the Hayward fault, this dissertation took on even more challenging task of investigating the seismic design and response of four 20-story core-wall buildings hypothetically located in the San Francisco Bay Area, 500 m from the San Andreas fault. One of the four studied buildings was fixed-base (FB), two were base-isolated (BI-1 and BI-2), and one used a combination of base isolation and a rocking core wall (BIRW). The FB and the BI buildings satisfied requirements of ASCE 7-10. The BI and the BIRW buildings used the same 6 s period isolation system, which combines 16 tension-resistant friction pendulum bearings and 8 nonlinear fluid viscous dampers. Buildings BI-1 and BI-2 used walls with flexural strength 2.2 and 1.8 times, respectively, the minimum required by ASCE 7-10. The rocking core-wall included post-tensioning steel, buckling-restrained devices, and at its base was encased in a steel shell. The total amount of longitudinal steel in the wall of the BIRW building was 0.71 to 0.87 times that used in the BI buildings, and 0.79 times that used in the FB building. Response history two-dimensional analysis was performed, including the vertical components of excitation, for sets of 14 ground motions scaled to the design earthquake and to the maximum considered earthquake (MCE). This dissertation then also studied the response of the four buildings to two historical and two simulated near-fault ground motions, which included strong long-period pulses. The linear single degree of freedom displacement spectra values for these motions were up to 1.5 times these of the MCE-level design spectrum for periods 5 s to 6 s. Based on the results of the analysis the following conclusions are drawn:

1. The FB building developed significant inelastic deformations both at the DE and MCE level of shaking. The mean roof drift ratio at the DE and MCE levels was 1.32% and 2.38%, respectively, while the corresponding peak interstory drift ratio along the height of the building was 1.55% and 2.79%, respectively. The damage potential of the core wall of the FB building increases in response to the concurrent large shear stresses and inelastic deformations. The shear force in the core wall at the ground level at the DE and MCE level was $0.36W_s$ and $0.44W_s$, respectively. The level of shear stresses in the web of the wall at the DE and MCE was $0.068\,f'_{c,e}$ and $0.082\,f'_{c,e}$ respectively, where $f'_{c,e}$ = 72 MPa was the expected compressive strength of concrete. The maximum allowed stress by ACI 318-11 is $0.0078\,f'_{c,e}$. Tests of non-planar walls with longitudinal steel ratios and axial load ratios 0.8 to 1.2 times and 0.8 to 1.6 times, respectively, that of the wall considered herein experienced significant damage, including bar buckling, and crushing of concrete at drift ratios of 1.5% to 2.5%.
2. The FB building resulted in floor accelerations (average along the building height) equal to 0.67g (1.37 PGA) and 0.88g (1.13 PGA) at the DE and at the MCE, respectively.

3. Compared to the response of the FB building, commercially available isolation and viscous damping devices used in the design of the BI buildings resulted in an isolated superstructure for buildings BI-1 and BI-2 that remained practically elastic at the MCE, while reduced significantly interstory drifts, shear forces, and floors accelerations. Buildings BI-1 and BI-2 developed less than 0.87 m of horizontal displacement of the isolation system. The outer bearings of these buildings experienced up to 0.95 MN tension, which is well within the 9 MN capacity of the commercially available tension-capable pendulum bearings. At the MCE the BI-1 and the BI-2 buildings developed 0.43% and 0.85% interstory drift, respectively, and 0.45% and 1.04% tensile strain in the wall, while floor accelerations (average along the building height) were less than 0.34 g at the MCE, (0.88 g for the FB building). The shear force in the wall at the ground level at the MCE of these buildings was $0.20W_s$ to $0.21W_s$ ($0.44W_s$ for the FB building).
4. The BIRW building experienced elastic response of the wall at the MCE level of excitation, with floor accelerations and shear forces 0.5 times those experienced by the FB building. Inelastic deformation was concentrated in the unbonded steel, which reached tensile strains of 1.39% and provided energy dissipation for the rocking system. The high strength post-tensioning steel remained elastic, experiencing 0.75% tensile strain. The base of the rocking wall, encased in a steel shell, remained nominally elastic with the compression strain of 0.35%. The gravity columns, using spherical bearings at ground level, and the slabs also remained elastic with tensile strains of 0.04% and 0.18%, respectively.
5. The BIRW building is expected to remain elastic also for higher than MCE-level ground motions, as opposed to the base-isolated buildings, particularly the BI-2 building, which would likely form a plastic hinge at the wall base. This is evident from the 1.04% mean wall steel strain and the 0.80 coefficients of variation in the wall tensile strain for the BI-2 building for the MCE, and safe-level mean response and relatively low levels of variation in the critical components of the BIRW building.
6. In response to the four unscaled near-fault ground motions, the FB building developed significant inelastic deformations with interstory drift ratio that ranged from 1.2% to 2.4%. The corresponding range of tensile strain of the longitudinal reinforcement in the wall was 1.9% to 3.8%. Both BI and the BIRW buildings developed less than 1% interstory drift ratio for all ground motions, except TCU68, for which BI-2 reaches 1.21%, and BIRW reaches 1.39%. For both base-isolated and the BIRW building, the horizontal displacements of the isolation systems were less than 0.87 m for TCU52, SF99, and SF519, and reached 1.34, 1.23, and 1.22 m, for BI-1, BI-2, and BIRW, respectively. These results demonstrate that the BIRW building has a significantly larger deformation capacity at the onset of structural damage than either of the base-isolated buildings, and especially the FB building.

5.2 Recommendations for Further Research

Possible directions for continuing research on the topics addressed in this dissertation include conducting 3-D six degree-of-freedom model analysis to verify the conclusions and assumptions of the present 2-D model analysis-based work and conducting experimental verification of the base isolation and rocking core wall design concept.

5.2.1 3-D Modeling and Analysis

3-D modeling and analysis of the tall RC core wall buildings discussed in this dissertation would provide insight into the peak core wall, slab, and gravity column demands in response to three components of ground shaking. Peak response would be expected in the corner isolators and the corners of the core wall and gravity columns and is not available for direct numerical investigation with the current 2-D modeling and analysis. For the base-isolated buildings and the buildings combining base isolation and a rocking wall, the response of the seismic isolators and the viscous dampers could be studied in more detail with 3-D analysis. For the building combining base isolation and a rocking core wall, 3-D analysis would be particularly useful to study the peak compression demands on base of the rocking wall, as well as the interaction between the core wall, the slabs, and the gravity columns.

5.2.2 Experimental Verification of Numerical Analysis

A shaking table test program, investigating the response of scale models of the buildings discussed in this dissertation would provide invaluable insight and verification for the presented numerical analysis. The strong contrast between the highly inelastic response of the fixed-base buildings at even the design earthquake level of ground shaking, and the nominally elastic response of the base-isolated buildings and buildings combining base isolation and a rocking core wall at even the maximum considered earthquake level of ground shaking, would be effectively demonstrated with a side-by-side shaking table test. Furthermore, for the base-isolated buildings and the buildings combining base isolation and a rocking core wall, the experimental data from the test instruments measuring the deformations of the components that make up the isolation and the rocking systems, would provide valuable verification for the remarkable performance of these innovative structural components. Critical responses of particular interest to measure experimentally and demonstrate to be in an acceptable range include: tension and compression forces and deformations in the bearings, forces in the viscous dampers, deformations and forces in the post-tensioning steel and the energy dissipating devices, compression and tension strains in the core wall (particularly compression strains at the corners of the rocking core wall), slabs, and gravity columns.